

# Two distinct GRAS proteins control meristem formation and chloroplast maintenance in *Physcomitrella patens*



## Dissertation

zur Erlangung des Doktorgrades der Naturwissenschaften

an der Fakultät für Biologie

der Ludwig-Maximilians-Universität München

vorgelegt von

**Hossein Beheshti**

München 2020

Diese Dissertation wurde angefertigt unter der Leitung von Prof. Dr. Wolfgang Frank an der Fakultät für Biologie der Ludwig-Maximilians-Universität München.

Erstgutachter: Prof. Dr. Wolfgang Frank

Zweitgutachter: Prof. Dr. Herwig Stibor

Datum der Einreichung: 23.04.2020

Datum der mündlichen Prüfung: 13.07.2020

## **Eidesstattliche Erklärung**

Ich versichere hiermit an Eides statt, dass die vorgelegte Dissertation von mir selbstständig und ohne unerlaubte Hilfe angefertigt wurde. Des Weiteren erkläre ich, dass ich nicht anderweitig ohne Erfolg versucht habe, eine Dissertation einzureichen oder mich der Doktorprüfung zu unterziehen. Die folgende Dissertation liegt weder ganz, noch in wesentlichen Teilen einer anderen Prüfungskommission vor.

München, 20.04.2020

Hossein Beheshti

## **Statutory Declaration**

I declare that I have authored this thesis independently, that I have not used other than the declared sources/resources. As well I declare, that I have not submitted a dissertation without success and not passed the oral exam. The present dissertation (neither the entire dissertation nor parts) has not been presented to another examination board.

Munich, 20.04.2020

Hossein Beheshti

# TABLE OF CONTENTS

<b>SUMMARY</b> .....	<b>1</b>
<b>ZUSAMMENFASSUNG</b> .....	<b>2</b>
<b>ABBREVIATIONS</b> .....	<b>4</b>
<b>1 CHAPTER 1: INTRODUCTION</b> .....	<b>8</b>
1.1 The model organism <i>Physcomitrella patens</i> .....	8
1.2 GRAS transcription factors .....	10
1.3 Function and biogenesis of plant microRNAs .....	13
1.4 Chlorosis and chloroplast degradation .....	17
1.5 Transient starch degradation .....	19
1.6 Meristem regulation .....	21
1.7 Aim of the research.....	25
<b>2 CHAPTER 2: MATERIAL AND METHODS</b> .....	<b>26</b>
2.1 Chemicals and enzymes.....	26
2.2 Buffers and solutions .....	26
2.3 Culture media .....	31
2.4 Plant material, cell culture, and transformation.....	33
2.4.1 Plant materials and growth conditions .....	33
2.4.2 Transformation of <i>P. patens</i> protoplasts .....	33
2.4.2.1 Stable transformation.....	33
2.4.2.2 Transient transformation.....	33
2.4.3 Phenotypic analysis.....	34
2.5 Phylogenetic analysis.....	34
2.6 Identification of <i>P. patens</i> homologs.....	34
2.7 ROS detection .....	35
2.8 Cloning and bacterial transformation .....	35
2.8.1 Gateway pENTR/D-TOPO cloning .....	35
2.8.2 pJET1.2 cloning .....	35
2.8.3 Transformation of chemically competent <i>E. coli</i> cells.....	35
2.9 Plasmid DNA isolation .....	36
2.10 Genomic DNA isolation from <i>P. patens</i> .....	36
2.10.1 CTAB method .....	36
2.10.2 gDNA isolation for PCR-screening.....	37
2.11 Electrophoretic separation of nucleic acids .....	37

<b>2.12</b>	<b>Extraction and elution of DNA/RNA fragments from agarose gels .....</b>	<b>37</b>
<b>2.13</b>	<b>DNA sequencing .....</b>	<b>38</b>
<b>2.14</b>	<b>RNA isolation from <i>P. patens</i> .....</b>	<b>38</b>
<b>2.15</b>	<b>Spectrophotometric nucleic acid quantification.....</b>	<b>39</b>
<b>2.16</b>	<b>PCR.....</b>	<b>39</b>
2.16.1	Standard PCR .....	39
2.16.2	Reverse transcriptase PCR (RT-PCR).....	40
2.16.3	Quantitative RT-PCR (qRT-PCR).....	40
<b>2.17</b>	<b>RNA gel blot .....</b>	<b>41</b>
<b>2.18</b>	<b>Protein isolation and immunoblot analyses .....</b>	<b>42</b>
<b>2.19</b>	<b>Microscopy .....</b>	<b>42</b>
2.19.1	Subcellular localization and confocal microscopy .....	42
2.19.2	Transmission electron microscopy .....	43
2.19.3	Scanning electron microscopy.....	44
2.19.4	Binocular microscopy .....	44
<b>2.20</b>	<b>Generation of mutants.....</b>	<b>44</b>
2.20.1	<i>ΔPpGRAS 7</i> .....	44
2.20.2	<i>ΔPpGRAS 12</i> .....	45
2.20.3	<i>PpGRAS7</i> -iOE.....	45
2.20.4	<i>PpGRAS12</i> -iOE.....	46
2.20.5	<i>AtRGAL1</i> -iOE and <i>AtRGAL1</i> -iOE .....	46
2.20.6	<i>AtSCL6-II</i> -iOE, <i>At SCL6-III</i> -iOE, and <i>AtSCL6-IV</i> -iOE .....	46
2.20.7	<i>PpGRAS12::GUS</i> protein fusion.....	47
<b>2.21</b>	<b>PAM measurement .....</b>	<b>47</b>
<b>2.22</b>	<b>Extraction of pigments .....</b>	<b>48</b>
<b>2.23</b>	<b>Starch, maltose and sucrose quantification .....</b>	<b>48</b>
<b>2.24</b>	<b>Bioinformatics tools and other software .....</b>	<b>48</b>
2.24.1	Databases.....	48
2.24.2	Softwares.....	49
<b>3</b>	<b>CHAPTER 3: RESULTS.....</b>	<b>50</b>
<b>3.1</b>	<b>Phenotypical and functional analysis of <i>PpGRAS7</i> mutants.....</b>	<b>50</b>
3.1.1	<i>PpGRAS7</i> is not related to the 9 recognized GRAS subfamilies in <i>A. thaliana</i> .....	50
3.1.2	Loss of the nuclear-localized <i>PpGRAS7</i> protein results in a mild phenotypic deviation.....	52
3.1.3	<i>PpGRAS7</i> overexpression leads to chlorosis.....	54
3.1.4	<i>PpGRAS7</i> overexpression induces metabolic misbalances .....	57
3.1.5	Light triggers cell chlorosis in the <i>PpGRAS7</i> -iOE lines. ....	61

3.1.6	<i>PpGRAS7</i> overexpression lines display impaired photosynthesis.....	64
3.1.7	<i>PpGRAS7</i> overexpression affects pigment accumulation .....	66
<b>3.2</b>	<b>Phenotypical and functional analysis of <i>PpGRAS12</i> mutants .....</b>	<b>69</b>
3.2.1	The knockout of nuclear-localized <i>PpGRAS12</i> causes defects in sporophyte production .....	69
3.2.2	<i>PpGRAS12</i> overexpression leads to the formation of multiple apical meristems .....	71
3.2.3	MiR171 regulates <i>PpGRAS12</i> .....	76
<b>3.3</b>	<b>Overexpression of <i>AtRGA1</i>, <i>AtRGL1</i>, <i>AtSCL6-II</i>, <i>AtSCL6-III</i>, and <i>AtSCL6-IV</i> in <i>P. patens</i> .....</b>	<b>79</b>
3.3.1	<i>AtRGA1</i> and <i>AtRGL1</i> share the highest protein sequence similarities with <i>PpGRAS12</i> and <i>PpGRAS7</i> .....	79
3.3.2	Overexpression of the <i>ASCL6-II</i> in <i>P. patens</i> leads to chlorosis and the formation of multiple apical meristems .....	86
<b>4</b>	<b>DISCUSSION .....</b>	<b>90</b>
4.1	<i>PpGRAS7</i> is involved in chloroplast degradation and starch over-accumulation.....	90
4.2	<i>PpGRAS12</i> plays an important role in meristem regulation and maintenance .....	95
4.3	<i>AtRGL1</i> overexpression induces chlorosis in <i>P. patens</i> .....	97
4.4	Overexpression of miRNA171-targeted <i>AtSCL6-II</i> leads to the formation of multiple apical meristems and chlorosis in <i>P. patens</i> .....	98
<b>5</b>	<b>REFERENCES .....</b>	<b>99</b>
<b>6</b>	<b>APPENDIX .....</b>	<b>114</b>

## SUMMARY

Members of the plant-specific GRAS transcription factor family play important functions in plant growth and development. In *Physcomitrella patens*, two members of the GRAS family, (PpGRAS7 and PpGRAS12), are validated targets of miRNA171. It appeared that both nuclear genes harbor the conserved GRAS domain. Histochemical GUS staining revealed a stronger expression of the *PpGRAS12* gene in the miR171-resistant PpGRAS12::GUS protein fusion reporter lines compared to the miR171-sensitive PpGRAS12::GUS protein fusion reporter lines, which indicates a regulatory function of miR171 in the spatiotemporal expression of *PpGRAS12*. Mild phenotypic deviations were observed in both,  $\Delta PpGRAS12$  and  $\Delta PpGRAS7$  lines, at the gametophytic vegetative growth stage and prominent phenotypic aberrations were detected in the  $\Delta PpGRAS12$  lines at the sporophytic generation. Interestingly, highly specific and distinct growth arrests were observed in the inducible *PpGRAS7*-iOE and *PpGRAS12*-iOE lines. However, only *PpGRAS12*-iOE lines were able to recover after release to non-inducing conditions. While elevated levels of *PpGRAS12* caused the formation of multiple apical meristems, increased levels of *PpGRAS7* led to defects and the degradation of chloroplasts. Furthermore, an elevated *PpGRAS7* transcript level led to the plastid degradation and remarkable starch accumulation in *P. patens*. Based on these results key regulatory functions of *PpGRAS12* in the control of meristem identity and the requirement of *PpGRAS7* in the plastid maintenance and homeostasis are proposed. PpGRAS12 and PpGRAS7 share the highest protein sequence similarity with REPRESSOR OF GA (RGA1) and with RGA-LIKE 1 (RGL1) from *Arabidopsis thaliana*, respectively. The observed phenotype from the *AtRGA1*-iOE lines showed a partial similarity to *PpGRAS12*-iOE lines, while *AtRGL1*-iOE lines displayed a partial phenotypic similarity to *PpGRAS7*-iOE lines. For the functional comparison of *SCL6-II*, *SCL6-III*, and *SCL6-IV* as targets of miR171 in *A. thaliana* with *PpGRAS7* and *PpGRAS12* as targets of miR171 in *P. patens*, *AtSCL6-II*-iOE, *AtSCL6-III*-iOE, and *AtSCL6-IV*-iOE lines were generated in *P. patens*. The obtained *AtSCL6-II*-iOE lines displayed a strong chlorotic phenotype as well as the formation of multiple apical meristems. This supports the idea that *A. thaliana SCL6-II* might be a functional homolog of both *P. patens GRAS7* and *GRAS12* genes. Besides, it might indicate that *A. thaliana SCL6-II* has gained the functions of both *PpGRAS7* and *PpGRAS12* genes through the evolution of higher plants.

## ZUSAMMENFASSUNG

Mitglieder der Familie der pflanzenspezifischen GRAS-Transkriptionsfaktoren haben wichtige Funktionen für das Wachstum und die Entwicklung von Pflanzen. In *Physcomitrella patens* werden zwei Mitglieder der GRAS-Familie (*PpGRAS7* und *PpGRAS12*) durch die miRNA171 kontrolliert. Beide Gene kodieren konservierte Proteine mit einer GRAS-Domäne, die im Zellkern lokalisiert sind. Die histochemische GUS-Färbung ergab eine stärkere Expression des *PpGRAS12*-Gens in miR171-resistenten *PpGRAS12::GUS*-Linien im Vergleich zu miR171-sensitiven *PpGRAS12::GUS*-Linien. Dieser Befund weist auf die regulatorische Funktion der miR171 bei der Expression von *PpGRAS12* in Raum und Zeit hin. Erzeugte  $\Delta PpGRAS12$  und  $\Delta PpGRAS7$  Deletionsmutanten zeigten leichte phänotypische Änderungen während des vegetativen Wachstums. In den Gametophyten von  $\Delta PpGRAS12$  konnten nur geringfügige phänotypische Veränderungen festgestellt werden. Auffälliger waren hingegen die phänotypischen Veränderungen des Sporophyten in den  $\Delta PpGRAS12$ -Linien. Interessanterweise wurden in den induzierbaren *PpGRAS7*-iOE- und *PpGRAS12*-iOE-Linien hochspezifische und ausgeprägte Wachstumseinbußen beobachtet, wobei sich nur *PpGRAS12*-iOE-Linien in anschließender Kultivierung unter nicht induzierenden Bedingungen erholen konnten. Während erhöhte *PpGRAS12*-Spiegel die Bildung multipler, arretierter apikaler Meristeme verursachten, führten erhöhte *PpGRAS7*-Spiegel zu Defekten in den Chloroplasten auf Grund massiver Stärkeeinlagerungen. Basierend auf diesen Ergebnissen, werden *PpGRAS12* wichtige regulatorische Funktionen bei der Kontrolle der Meristemidentität und *PpGRAS7* eine Funktion als negativer Regulator des Stärkeabbaus zugeschrieben. *PpGRAS12* und *PpGRAS7* zeigen in *A. thaliana* ihre höchste Sequenzabdeckung mit REPRESSOR OF GA (*AtRGA1*) und mit RGA-LIKE 1 (*AtRGL1*). Induzierbare *AtRGA1*-iOE-Linien in *P. patens* besitzen phänotypische Ähnlichkeiten mit *PpGRAS12*-iOE-Linien, während der Phänotyp von induzierbaren *AtRGL1*-iOE-Linien in *P. patens* Ähnlichkeit zu *PpGRAS7*-iOE-Linien aufwies. Für den phänotypischen Vergleich von *AtSCL6-II*, *AtSCL6-III*, und *AtSCL6-IV*, die Zielgene der miR171 in *A. thaliana* sind, mit *PpGRAS7* und *PpGRAS12* als Ziele von miR171 in *P. patens*, wurden induzierbare Überexpressionslinien *AtSCL6-II*-iOE, *AtSCL6-III*-iOE und *AtSCL6-III*-iOE in *P. patens* generiert. Auffallend war, dass die *AtSCL6-II*-iOE-Linien einen starken Chlorosephänotyp sowie die Bildung mehrerer apikaler Meristeme aufwiesen. Dies unterstützt die Annahme, dass *AtSCL6-II* ein

funktionelles Homolog von *PpGRAS7*- und *PpGRAS12* ist. Außerdem könnte dies darauf hinweisen, dass *SCL6-II* in *A. thaliana* während der Evolution der Landpflanzen die Funktionen von *PpGRAS7* und *PpGRAS12* übernommen hat.

## ABBREVIATIONS

<i>A. thaliana</i>	<i>Arabidopsis thaliana</i>
AG	AGAMOUS
AGL1	AGAMOUS-LIKE 1
AP2	APETALA 2
AS2	ASYMMETRIC LEAVES 2
ATG5	AUTOPHAGY-RELATED PROTEIN 7
ATG7	AUTOPHAGY-RELATED PROTEIN 7
BAM	$\beta$ -AMYLASES
bp	base pair
CYCD	CYCLIN-D
cDNA	complementary DNA
CLV	CLAVATA
CV	Chloroplast vesiculation
CYT <sub>b6</sub>	Cytochrome <i>b<sub>6</sub>f</i> complex
DAB	3,3'-diaminobenzidine
DAPI	4',6-diamidin-2-phenylindol
DCL1	DICER-LIKE 1
DELLA	Aspartic acid (D), Glutamic acid (E), Leucine (L), Leucine (L), and Alanine (A)
DLT	DWARF AND LOW-TILLERING
DMSO	Dimethyl sulfoxide
DNA	Deoxyribonucleic acid
DPE1	DISPROPORTIONATING ENZYME 1
<i>Efl</i> $\alpha$	Elongation factor 1 $\alpha$
gDNA	genomic DNA
GUS	$\beta$ -Glucuronidase
GWD	GLUCAN WATER DIKINASE
h	hours
HAM	HAIRY MERISTEM
HCl	Hydrochloric acid

HSF3	HEAT SHOCK FACTOR PROTEIN 3
HSP70	HEAT SHOCK PROTEIN 70
iOE	inducible overexpression
ISA3	ISOAMYLASE 3
jba-1D	jabba-1D mutant
KAN1	KANADI 1
KAN2	KANADI 2
LAS	LATERAL SUPPRESSOR
LHCA	LIGHT-HARVESTING COMPLEX A
LHCB	LIGHT-HARVESTING COMPLEX B
LISCL	SCL from <i>Lilium longiflorum</i> L.
LOM	LOST MERISTEM
MEX1	MALTOSE EXCESS 1
min	minutes
miRNA	MicroRNA
mRNA	Messenger RNA
NBT	Nitrotetrazolium blue chloride
NCED	9-CIS-EPOXYCAROTENOID DIOXYGENASE
<i>nptII</i>	neomycin phosphotransferase
<i>P. patens</i>	<i>Physcomitrella patens</i>
PAM	Pulse amplitude modulation
PAT1	PHYTOCHROME A SIGNAL TRANSDUCTION 1
PCR	Polymerase chain reaction
PI3K	PHOSPHATIDYLINOSITOL 3-KINASE
PI3P	PHOSPATIDYLINOSITOL 3-PHOSPHATE
POR	PROTOCHLOROPHYLLIDE OXIDOREDUCTASE
<i>PpGRAS12</i>	<i>P. patens</i> GRAS domain transcription factor encoded on chromosome 12 (Pp1s205_1V6.1)
<i>PpGRAS7</i>	<i>P. patens</i> GRAS domain transcription factor encoded on chromosome 7 (Pp1S130_63V6.1)
PsaA	Photosystem I P700 chlorophyll a apoprotein A1
PsaB	Photosystem I P700 chlorophyll a apoprotein A2

PsaC	Photosystem I iron-sulfur center
PsaL	Photosystem I reaction center subunit XI
PsbA	Photosystem II protein D1
PsbD	Photosystem II protein D2
PsbM	Photosystem II reaction center protein M
PsbQ	Oxygen-evolving enhancer protein 3
PSI	Photosystem I
PSII	Photosystem II
PWD	PHOSPHOGLUCAN WATER DIKINASE
qRT-PCR	Quantitative real-time PCR
RGA1	REPRESSOR OF GA 1
RGL1	RGA-LIKE 1
RNA	Ribonucleic acid
ROS	Reactive oxygen species
rRNA	ribosomal RNA
RT	Room temperature
RT-PCR	Reverse transcriptase PCR
SAG	Senescence associated gene
SCL3	SCARECROW-LIKE 3
SCL4/7	SCARECROW-LIKE 4/7
SCL6-II	SCARECROW-LIKE 6-II
SCL6-III	SCARECROW-LIKE 6-III
SCL6-IV	SCARECROW-LIKE 6-IV
SCR	SCARECROW
SDS	Sodium dodecyl sulfate
sec	seconds
SEM	Scanning electron microscopy
SEX4	STARCH-EXCESS 4
$\beta$ -estradiol	Beta-estradiol
Ta	Annealing temperature
TE	Tris/EDTA buffer
TEM	Transmission electron microscopy

TIP2;2	TONOPLAST INTRINSIC PROTEIN 2;2
TPT	TRIOSE PHOSPHATE TRANSLOCATOR
TRI	Trizol (guanidinium thiocyanate)
Tris	Tris (hydroxymethyl) aminomethane
WT	Wild type
WUS	WUSCHEL
Y	Quantum yield of photosystem
YAB3	YABBY 3
YFP	Yellow fluorescent protein
Δ	Knockout

# 1 CHAPTER 1: INTRODUCTION

## 1.1 The model organism *Physcomitrella patens*

Mosses are characterized as the oldest living clade of land plants, which separated by approximately 450 million years of evolution from higher plants (Reski & Frank, 2005). From the evolutionary perspective, mosses possess a unique position among land plants, halfway between green algae and flowering plants, which make them an appropriate model organism for comparative studies of land plants evolution. *Physcomitrella* (= *Aphanorhegma*) *patens* (*P. patens*) is an ancient moss (bryophyte), which was adopted as a genetic tool in order to its unique features. In the course of the last few decades, *P. patens* has been utilized as a model to study various components of cell, developmental and evolutionary plant biology. The ability to use gene targeting through homologous recombination (HR) and the RNA interference methods to study gene function has turned *P. patens* into a useful model organism (Schaefer & Zryd, 1997). The gametophytic generation in *P. patens* is haploid, therefore altering or destroying a gene may directly result in altered molecular functions. The filamentous protonemal stage emerges after the germination of haploid spores (Fig. 1). The protonema is generally divided into two cell types: chloronema and caulonema cells (Fig. 1). Chloronema cells are chloroplast enriched type of cells with perpendicular cross-walls and extend by the sequential division of the apical cell and subapical cells branch to form new apices. Caulonema cells contain fewer and less-well-developed chloroplasts with oblique cross-walls (Strotbek *et al.*, 2013).

The subapical cells of caulonemal filaments branch to form more filaments and three-faced buds, which develop into leafy stems, called “gametophores” (Cove *et al.*, 2009) (Fig. 1). *P. patens* is monoecious; both male (antherozoids) and female (oogonia) gametes are produced on the same gametophore (Fig. 1). Male gametes are produced within antheridia and female gametes within archegonia. After fertilization (mostly self-fertilization), the fertilized zygotes develop into diploid sporophytes (Fig. 1). Within the sporophyte (2n), spore mother cells give rise to spores (n) mitotically. Since mosses have not shown vast changes to the last common ancestor of mosses and seed plants, which was living about 450 million years ago, they might be a proper model to study plant evolution and diversity (Cove *et al.*, 2009).

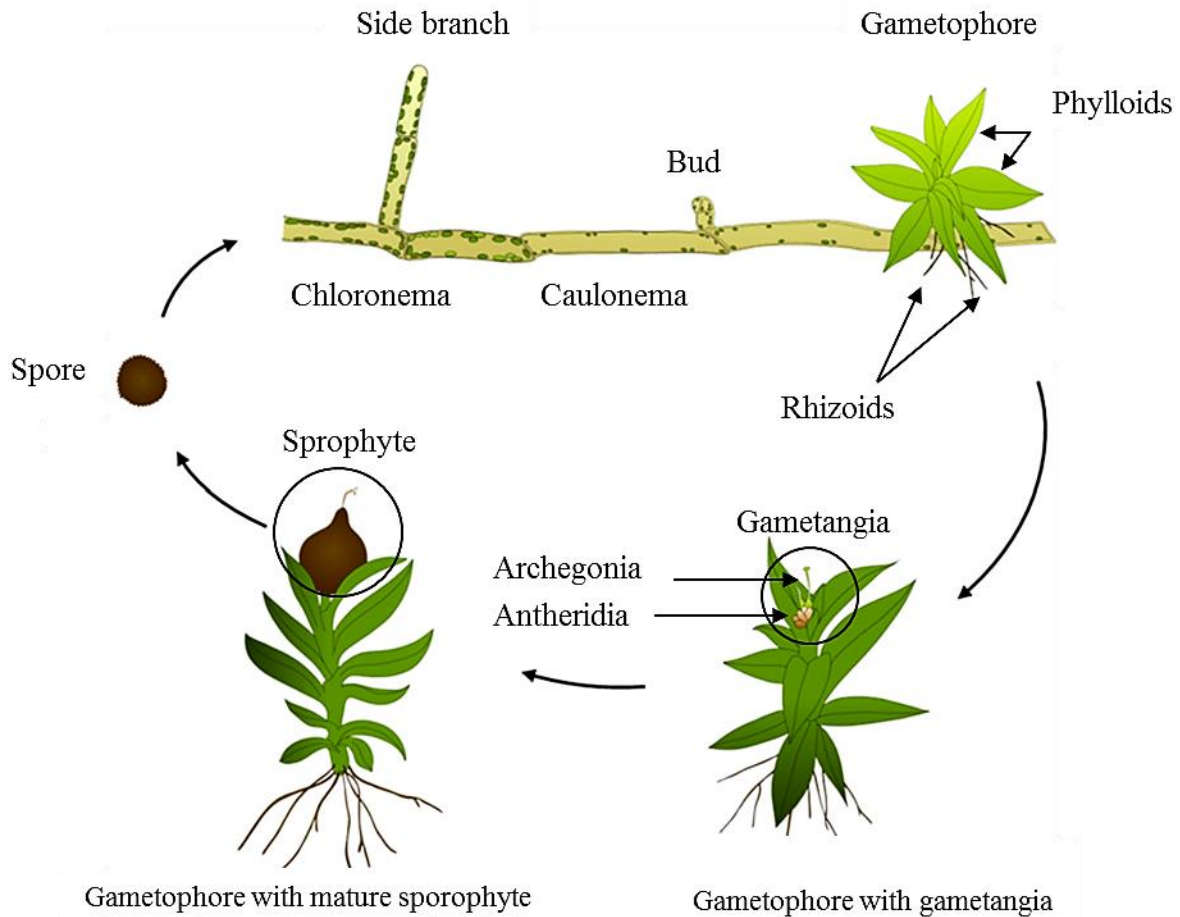


**Fig. 1. Scheme representing the *P. patens* life cycle.** Germination of haploid spores generates protonema cells. Protonema consists of chloronema cells (chloroplast-rich) and caulonema cells (longer, thinner and contain fewer chloroplasts). Meristematic buds with three-faced apical cells emerge from side branches to form the leafy stems, called “gametophores”. Gametangia develop on the gametophores and after the fertilization, the fertilized zygotes develop into sporophytes. Modified from Lang *et al.* (2018).

Apart from the high efficiency of homologous recombination, a simple structure and development, rapid colony-forming ability, totipotency, genetic diversity, a sequenced, well-annotated and assembled genome (Rensing *et al.*, 2008; Lang *et al.*, 2018), physical and genetic maps, and more than 250,000 expressed sequence tags, have made *P. patens* a suitable tool for genetic studies.

## 1.2 GRAS transcription factors

The plant-specific *GRAS* genes encode a family of transcription factors with key roles in plant growth and development. The GRAS protein family is named according to the first three GRAS proteins identified in *Arabidopsis thaliana* (*A. thaliana*), GIBBERELLIC ACID INSENSITIVE (GAI), REPRESSOR OF GAI (RGL) and SCARECROW (SCR) (Di Laurenzio *et al.*, 1996; Peng *et al.*, 1997; Silverstone *et al.*, 1998). To date, several studies have been dedicated to GRAS family characterization, functional analysis, and a remarkable number of GRAS proteins have been identified in almost 300 land plant species. In addition to plants, GRAS proteins with a higher degree of similarity to Rossmann-fold methyltransferase domains can be detected in several bacteria (Zhang *et al.*, 2012).

The size of GRAS proteins ranges from 400-770 amino acids with a highly conserved C-terminal region, the GRAS domain (Pysh *et al.*, 1999; Bolle, 2004). Several ordered motifs are present in the C-terminal region that is crucial for interactions between GRAS and other proteins. Two leucine-rich areas named leucine heptad repeat I (LHRI) and leucine heptad repeat II (LHRII) surrounding a conserved VHIID motif and followed by the PFYRE and SAW motifs are defined as the main components of GRAS domains (Pysh *et al.*, 1999; Tian *et al.*, 2004; Hirsch & Oldroyd, 2009). Based on the protein sequence, the GRAS protein family is divided into eleven subfamilies: DELLA, HAIRY MERISTEM (HAM), PHYTOCHROME A SIGNAL TRANSDUCTION 1 (PAT1), LATERAL SUPPRESSOR (LAS) & SCARECROW-LIKE 4/7 (SCL4/7), SCARECROW (SCR), SHORT ROOT (SHR), SCARECROW-LIKE 3 (SCL3), LISCL (LI SCL), *Clonorchis sinensis* (*C. sinensis*) GRAS34 (CsGRAS34), *Oryza sativa* 19 (Os19) and DWARF AND LOW-TILLERING (DLT) (Zhang *et al.*, 2019) (Fig. 2). Nine out of eleven subfamilies including DELLA, HAM, PAT1, LAS & SCL4/7, SCR, SHR, SCL3, LISCL, and DLT were reported in *A. thaliana*, *C. sinensis*, and *Oryza sativa* (*O. sativa*) (Fig. 2), whereas CsGRAS34 was only reported in *C. sinensis* (Fig. 2) and Os19 was reported in both *C. sinensis* and *O. sativa* (Fig. 2). However, in other studies in *A. thaliana* and *O. sativa*, poplar (*Populus trichocarpa*), bean (*Ricinus communis*), and tomato (*Solanum lycopersicum*), the number of distinct subfamilies ranged from 8 to 13 (Hirsch & Oldroyd, 2009; Liu & Widmer, 2014; Huang *et al.*, 2015; Xu *et al.*, 2016). GRAS protein subfamilies are known to be involved in various processes of plant growth and development such as gibberellin signal transduction (DELLA), radial root patterning and root growth (SCR and

SHR), initiation and formation of axillary meristems (LAS), shoot meristem maintenance (HAM), phytochrome A signal transduction (PAT1 and SCL21), and gametogenesis (LISCL) (Schumacher *et al.*, 1999; Bolle *et al.*, 2000; Helariutta *et al.*, 2000; Wysocka-Diller *et al.*, 2000; Greb *et al.*, 2003; Morohashi *et al.*, 2003; Engstrom, 2012; Park *et al.*, 2013; Torres-Galea *et al.*, 2013). *GRAS* genes also appeared to be involved in plant disease resistance and abiotic stress response (Mayrose *et al.*, 2006). *GRAS* transcription factors evolved after the split of Charophyceae or Coleochaetophyceae (Nishiyama *et al.*, 2018). Cheng *et al.*, (2019) showed that *GRAS* genes originated in the common ancestor of Zygnematophyceae and embryophytes, and were gained by horizontal gene transfer from soil bacteria.

DELLA proteins (GAI, RGA, RGA-LIKE 1 (RGL1), RGL2, and RGL3) were observed to act as repressors of gibberellin-responsive plant growth (Park *et al.*, 2013). The term DELLA was derived from the amino acid sequence DELLA that is located in the N-terminal region of the members of this subfamily. *P. patens* DELLA proteins lack the DELLA motif and do not interact with GA INSENSITIVE DWARF1s (GID1s) (Yasumura *et al.*, 2007; Wang & Deng, 2014). Gibberellic acid (GA) is not detected in *P. patens* and *PpDELLAs* are not sensitive to GAs when expressed in *A. thaliana* (Yasumura *et al.*, 2007). Exclusively, a part of the GA biosynthetic pathway, from geranylgeranyl diphosphate to *ent*-kaurenoic acid exists in *P. patens* (Miyazaki *et al.*, 2015). Consequently, the GID1/DELLA-mediated GA signaling emerged subsequent to the divergence of vascular plants from the moss lineage (Hirano *et al.*, 2007).

Members of SCLs are involved in several biological processes, e.g. *SCL6-II* (*At2g45160*), *SCL6-III* (*At3g60630*), and *SCL6-IV* (*At4g00150*) play a regulatory function in shoot branch production (Wang *et al.*, 2010) and chlorophyll biosynthesis (Ma *et al.*, 2014). Furthermore, in *A. thaliana* *SCL6-II*, *SCL6-III*, and *SCL6-IV* [also known as HAM (HAIRY MERISTEM) or LOM (LOST MERISTEM)] are reported as targets of miRNA171 (Llave *et al.*, 2002) and play an important role in the shoot apical meristem maintenance and axillary meristem formation, polar organization and chlorophyll synthesis (Schulze *et al.*, 2010; Wang *et al.*, 2010). In *A. thaliana*, *LOM1* and *LOM2* were shown to stimulate cell differentiation at the periphery of shoot meristems and to assist to maintain their polar organization (Schulze *et al.*, 2010). Furthermore, *AtHAM1*, *AtHAM2*, and *AtHAM3* genes not only are essential for shoot apical meristem maintenance, but

also play an important role in the maintenance of root indeterminacy (Engstrom *et al.*, 2011).

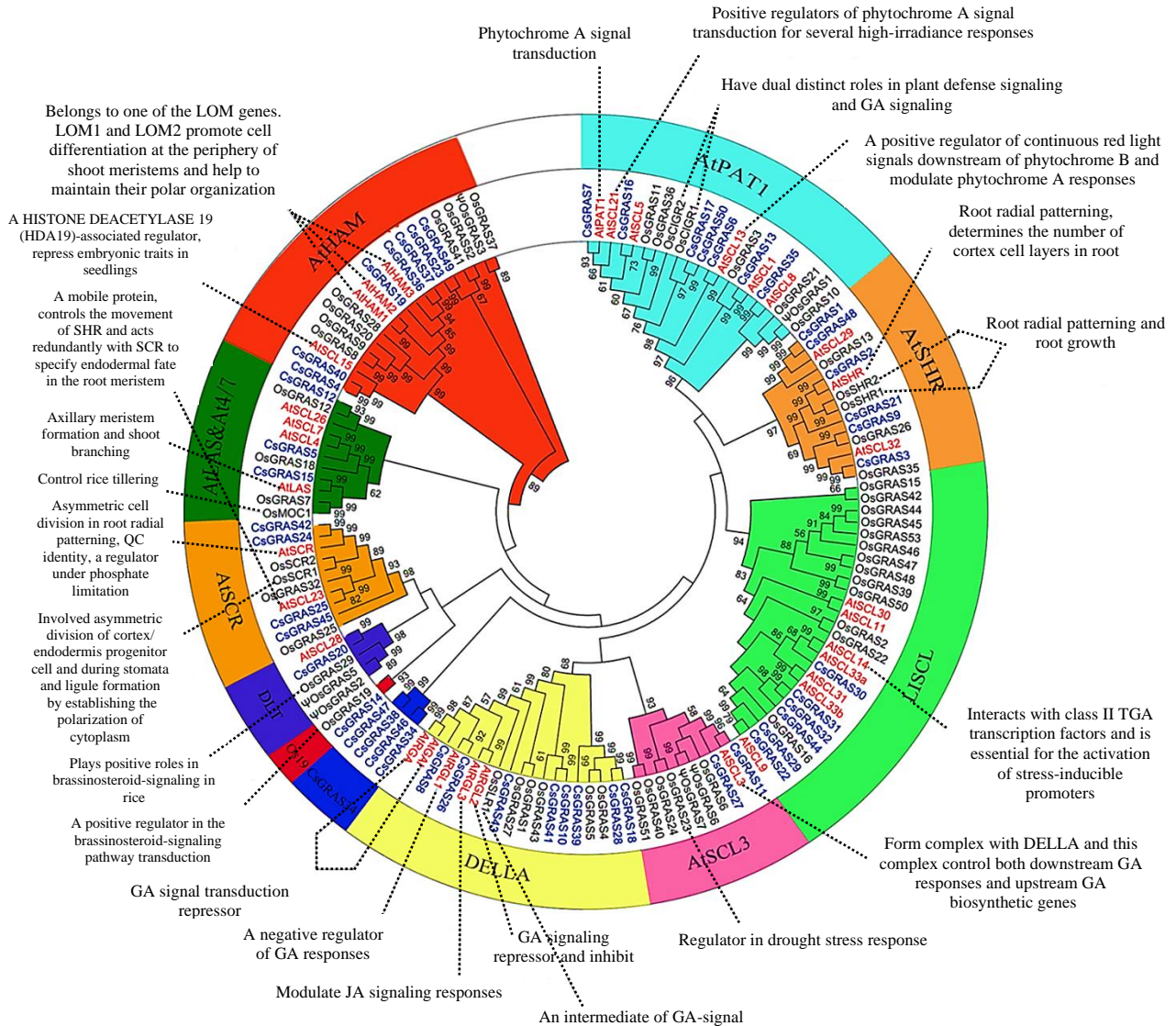


**Fig. 2. The phylogenetic analysis of GRAS proteins in *C. sinensis*, *A. thaliana*, and *O. sativa*.** The phylogenetic tree includes eleven GRAS subgroups. Different colors indicate individual subgroups. Nine out of eleven subfamilies including DELLA, AtHAM, PAT1, AtALS & SCL4/7, AtSCR, AtSHR, AtSCL3, LISCL, and DLT are present in all three organisms (*C. sinensis*, *A. thaliana*, and *O. sativa*), whereas CsGRAS34 is only present in *C. sinensis* and Os19 is present in both *C. sinensis* and *O. sativa*. Main biological functions of GRAS proteins, which were demonstrated by previous studies (Schumacher *et al.*, 1999; Bolle *et al.*, 2000; Helariutta *et al.*, 2000; Wysocka-Diller *et al.*, 2000; Greb *et al.*, 2003; Morohashi *et al.*, 2003; Engstrom, 2012; Park *et al.*, 2013; Torres-Galea *et al.*, 2013), are shown in the phylogenetic tree. The phylogenetic tree is from Zhang *et al.* (2019).

The *Petunia HAM* genes promote shoot indeterminacy by the undefined non-cell-autonomous signaling mechanism (Engstrom *et al.*, 2011). Tomato (*Solanum lycopersicum*) encodes three HAM homologs that are guided for cleavage by miR171 (Hendelman *et al.*, 2016) and their silencing led to over-proliferation of cells in the periphery of the meristems. *SIHAM* genes not only function in the meristem maintenance, but also play minor roles in the morphogenesis of a simple leaf in tomato (Hendelman *et al.*, 2016).

The very old diversification of GRAS proteins may have implications for understanding the evolution of GRAS protein function, including possible cellular level functions of HAM proteins (Engstrom, 2011). The presence of *HAM* homologs in the genomes of *P. patens* and *Selaginella moellendorffii* (*S. moellendorffii*), conservation of the domain structure and miR170/171-binding sequence among distantly related *HAM* genes suggest that the HAM function in flowering plants may be derived from a common ancestor of bryophytes (Engstrom *et al.*, 2011). HAM proteins are most closely related to DELLA proteins and both proteins are transcriptional repressors of growth-promoting proteins whose activity is negatively regulated by gibberellins via the ubiquitin-mediated degradation pathway (Rensing *et al.*, 2008). Both HAM and DELLA proteins possess strongly supported homologs in *S. moellendorffii* and *P. patens*, indicating that divergence of the HAM and DELLA subfamilies from a common ancestral protein occurred prior to the divergence of the moss and vascular plant lineages.

### **1.3 Function and biogenesis of plant microRNAs**

MicroRNAs are a class of non-coding RNA molecules and play key roles in the regulation of gene expression. A *MIR* gene is transcribed by RNA polymerase II as a long transcript, which is called primary miRNA (pri-miRNA) (Fig. 3) (Bartel, 2004; Lee *et al.*, 2004). Subsequently, the pri-miRNA is cleaved by a DICER-LIKE 1 (DCL1) enzyme to a stem-loop intermediate known as miRNA precursor (pre-miRNA) (Fig. 3) (Zhang *et al.*, 2006). In plants, DCL1 cleaves pre-miRNAs into the miRNA:miRNA\* duplex in the nucleus instead of the cytoplasm (Fig. 3) (Bartel, 2004). In addition to DCL1, HYPONASTIC LEAVES 1 (HYL1), a dsRNA binding protein, and SERRATE (SE), a C2H2-type zinc finger, are also essential for the processing of pri-miRNAs and the accumulation of mature miRNAs (Han *et al.*, 2004; Yang, L *et al.*, 2006; Zhu, 2008). Then

HASTY, the plant ortholog of exportin 5, transfers the duplex into the cytoplasm (Fig. 3) (Zhang *et al.*, 2006). The miRNAs are unwound into single-stranded mature miRNAs by helicases in the cytoplasm (Fig. 3). Lastly, mature miRNAs are incorporated into the RNA-induced silencing complex (RISC) and direct the translational repression or cleavage of their target mRNAs by base-pairing (Fig. 3) (Bartel, 2004; Dugas & Bartel, 2004). In addition to DCL1, HUA ENHANCER 1 (HEN1) that contains two dsRNA-binding domains and a nuclear localization signal, is required for the miRNA biogenesis and post-transcriptional gene silencing (PTGS) in plants (Park *et al.*, 2002; Boutet *et al.*, 2003). HEN1 specifically methylates miRNAs and siRNAs (Yang, Z *et al.*, 2006). Despite the close similarity of miRNA biogenesis and functional mechanism in both animals and plants, plant miRNAs display some differences. The stem-loop structures of plant pre-miRNAs are larger and more variable compared to animal pre-miRNAs (Yang *et al.*, 2007). Moreover, the mature plant miRNAs pair to their target sites with near-perfect complementarity, and unlike animal miRNAs they normally identify a single target site in the coding region and induce cleavage of the target mRNA (Yang *et al.*, 2007). miRNAs were first discovered in *Caenorhabditis elegans* (*C. elegans*) (Lee *et al.*, 1993), and so far many miRNAs have been discovered in diverse species of living organisms as well as plants. According to the miRBase (2019), 664 and 250 miRNAs were reported in *A. thaliana* and *P. patens*, respectively (<http://www.mirbase.org/>).

The functions of some miRNAs including miR156, which is responsible for floral organ identity and flowering time (Schwab *et al.*, 2005), miR160 that is responsible for auxin signaling and root development (Wang *et al.*, 2005) and miR164 that controls the boundary in the meristem, organ formation, separation, and petal number (Schwab *et al.*, 2005) were recognized and confirmed. In addition, miR172 play roles in flower organ identity and flowering time (Schwab *et al.*, 2005). Furthermore, miR399 has shown to be responsible for the phosphate-starvation response (Fujii *et al.*, 2005) and miR173 and 390 functions in directing ta-siRNA biogenesis (Allen *et al.*, 2005).

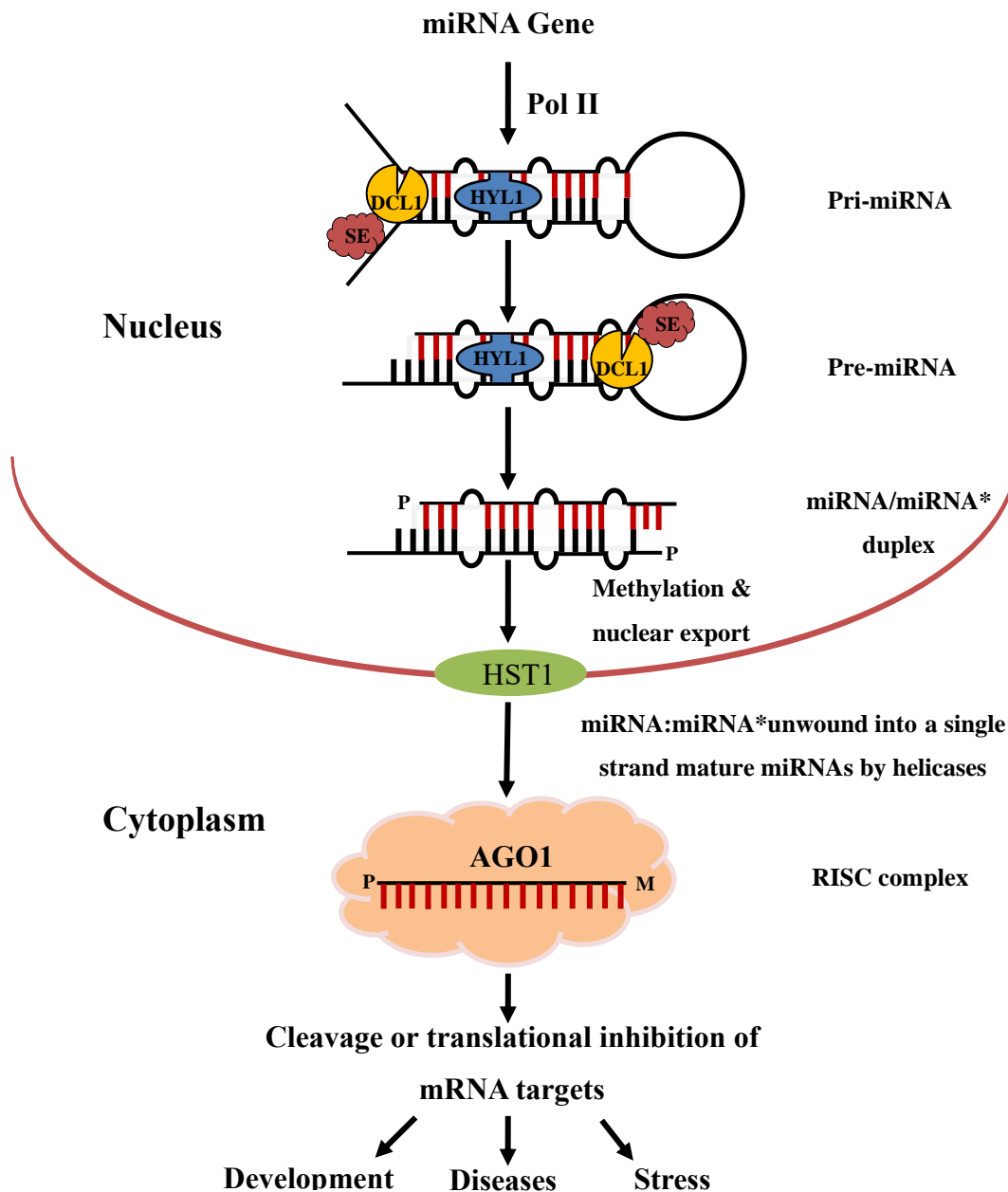


**Fig. 3. MiRNA biogenesis and its function in plants.** *MIR* genes are transcribed by RNA polymerase II enzymes. The primary miRNA is processed by the RNaseIII enzyme DCL1 and its associated RNA-binding cofactors, HYL1 (containing two double-stranded RNA-binding domains) and SE (a C2H2-type zinc finger) to generate a miRNA/miRNA\* duplex. The miRNA/miRNA\* duplex is then methylated and exported to the cytoplasm by HST1, unwound into a single strand mature miRNA by a helicase and incorporated into the RNA-induced silencing complex (RISC) to silence mRNA targets important for development, diseases, and stress responses. Modified from Zhu (2008).

The miR171 is a conserved miRNA family that exists in all major land plant groups, including bryophytes (Axtell & Bowman, 2008) and plays a critical role in regulating plant growth and development through repressing expression of SCARECROW-LIKE (SCL) transcription factors. In *A. thaliana*, the miR171-GRAS module has been elucidated as a key player in meristem maintenance (Huang *et al.*, 2017). Palatnik *et al.* (2003) reported the JAW locus in *A. thaliana*. JAW generates miR319 that is able to direct mRNA cleavage of a number of *TCP* genes (*TEOSINTE BRANCHED*, *CYCLOIDEA*, and *PCF1/2*) controlling leaf development. Overexpression of the wild type (WT) and microRNA-resistant *TCP* variants revealed that mRNA cleavage was adequate to minimize the *TCP* function. It was concluded that the existence of *TCP* genes with microRNA target sequences in a broad range of species demonstrates the control of leaf morphogenesis via miRNAs and is preserved in foliage with different leaf shapes. Through an activation-tagging approach, Aukerman and Sakai (2003) illustrated that overexpression of miRNA 172 (miR172) in *A. thaliana* caused early flowering and disorder in the floral organ identity specification. *APETALA 2* (*AP2*) and *AGAMOUS* (*AG*) are two floral homeotic genes that specify the identities of perianth and reproductive organs, respectively, for flower development in *A. thaliana* (Zhao *et al.*, 2007). MiR172 is normally expressed in a temporal manner, consistent with its proposed role in flowering time control (Aukerman & Sakai, 2003). The distinct functions of *AG* and miR172 in flower development and their independent role in the negative regulation of *AP2* were demonstrated by Zhao *et al.*, (2007). It was proposed that *AP2*, which is the target gene of miR172, was downregulated by miR172 via translational mechanisms rather than by RNA cleavage. Moreover, gain-of-function and loss-of-function analysis depicted that two of the *AP2*-like target genes function as floral repressors, and this strongly supports the idea that flowering time is regulated by the miR172 via downregulating *AP2*-like target genes. Sunkar and Zhu (2004) reported the identification of new miRNAs related to abiotic stresses in *A. thaliana*. It was explained how stresses such as cold, NaCl, dehydration, and ABA regulate miRNAs. According to their results, miR393 was strongly upregulated by all four (NaCl, dehydration, ABA, and cold) treatments. MiR397b and miR402 were slightly upregulated by all the stress treatments, whereas miR319c was upregulated only by the cold stress. Among miRNAs, which are regulated by stresses, only miR389a was downregulated by all of the stress treatments. MiR160 and miR397 are proved to respond to cold stress in rice, wheat, and *A. thaliana* (Sun *et al.*, 2019).

## 1.4 Chlorosis and chloroplast degradation

The chloroplast is an organelle, which provides energy by producing sugar throughout photosynthesis. Plants generally have established specific strategies to control chloroplast homeostasis in plant cells. These adaptive strategies are mainly used in plants to adapt to various environmental and developmental cues. The chloroplast degradation during leaf senescence and the transition of chloroplasts into other types of plastids during the day-night cycle are amongst the adaptive strategies (Zhuang & Jiang, 2019).

Several mechanisms are involved in chlorophyll and chloroplast degradation. Previous studies in *A. thaliana* showed that autophagy and senescence are two established cellular pathways involved in the degradation of chloroplast proteins (Martinez *et al.*, 2008; Liu & Bassham, 2012). Leaf senescence, which is defined as an ‘altruistic death’ causes the redistribution of degraded nutrients that are produced during the growth phase of the leaf to developing parts of the plant (Woo *et al.*, 2013). Senescence is considered as the final stage of leaf development and can be regulated by endogenous and environmental signals (Gan & Amasino, 1995; Yoshida, 2003; Chen *et al.*, 2017). Leaf senescence is characterized by leaf chlorosis, which is mainly due to the chlorophyll degradation and upregulation of senescence-associated genes (*SAGs*).

Two HD-ZipI transcription factors were previously reported to be engaged in flower senescence in *Petunia* (*Petunia hybrid*) and rose (*Rosa hybrid*) (Reiss, 2003). The independent downregulation of both transcription factors has resulted in a delay in flower senescence and a decrease in the expression of senescence-related genes, such as *SAG12* and *SAG29*. Martinez *et al.* (2008) showed the involvement of the senescence-associated vacuoles (SAV) in the degradation of the soluble photosynthetic proteins of the chloroplast stroma during senescence of leaves in tobacco (*Nicotiana tabacum* L.). According to their experiment in tobacco, detached leaves incubated in darkness, ethylene treatment leads to a 2-fold increase in the number of SAVs per cell and acceleration of the chloroplast degradation rate, compared to the untreated leaves.

Previous studies in *A. thaliana* revealed the involvement of autophagy in nutrient remobilization during leaf senescence (Diaz *et al.*, 2008; Masclaux-Daubresse & Chardon, 2011). Autophagy (self-eating) is a macromolecule degradation process and generally occurs under stress conditions or during developmental transitions. During autophagy, cells recycle cytoplasmic

contents in a process, which is conserved among eukaryotes (Baena-Gonzalez *et al.*, 2007; Yang & Klionsky, 2009; Mehrpour *et al.*, 2010; Liu & Bassham, 2012). Autophagy is involved in cellular development and differentiation, functions in tumor suppression, and plays an irrefutable role in the cellular response to stress and resistance to pathogens (Klionsky, 2005; Yang & Klionsky, 2009). There are three major types of autophagy in eukaryotic cells: macro-autophagy, micro-autophagy, and chaperone-mediated autophagy (Klionsky, 2005). Similar to macro-autophagy, micro-autophagy is also involved in dynamic membrane rearrangements to engulf portions of the cytoplasm. Both, macro- and micro-autophagy are able to sequester large structures, such as entire organelles. During macro-autophagy, portions of the cytoplasm are sequestered into an autophagosome, while micro-autophagy engages the direct engulfment of the cytoplasm at the lysosome surface (Yang & Klionsky, 2009). Chaperone-mediated autophagy is known to play a role in the translocation of unfolded, soluble proteins across the lysosome membrane (Yang & Klionsky, 2009).

Starvation is the most characteristic trigger of autophagy and lack of essential nutrients might induce autophagy. For instance, nitrogen starvation is the most effective stimulus in yeast, but the shortage of carbon, auxotrophic amino acids and nucleic acids, and even sulfate might induce autophagy (Takeshige *et al.*, 1992). In plants, autophagy can be induced by nitrogen or carbon deficits (Moriyasu & Ohsumi, 1996; Yoshimoto *et al.*, 2004). In mammals, a reduction of total amino acids intensely induces autophagy in many types of cultured cells, but the effects of individual amino acids are different (Mizushima, 2007). Autophagy-related (ATG) proteins are considered as the core of the autophagic machinery and function during the induction of autophagy and the formation of autophagosomes. ATG proteins are divided into four highly conserved groups in eukaryotes including plants (Chung *et al.*, 2009; Shin *et al.*, 2009; Yang & Klionsky, 2010). The four groups are namely, ATG1 kinase complex, the phosphatidylinositol 3-kinase complex (PI3K), transmembrane autophagy-related protein 9 (ATG9), and proteins involved in ATG8 and ATG12 conjugation. The ATG1 kinase complex contains ATG1, ATG13, FIP200, and ATG101, which are responsible for the induction of autophagy in response to the lack of nutrients (Kim *et al.*, 2012). The PI3K complex phosphorylates phosphatidylinositol that is essential for the production of phosphatidylinositol-3-phosphate (PI3P) (Marshall & Vierstra, 2018). PI3P is required to recruit proteins involved in autophagy. The PI3P complex contains VPS34 kinase, VPS15, ATG6, and

ATG14 (Kametaka *et al.*, 1998; Itakura *et al.*, 2008). ATG9 plays a crucial role in the regulating of autophagosome development from the ER membrane (Zhuang *et al.*, 2017). *P. patens atg5* mutant showed an impaired process of autophagy indicating that *ATG5* is essential for the autophagy process in *P. patens* (Mukae *et al.*, 2015).

Chloroplast vesiculation (CV) is another eminent pathway involved in chloroplast degradation (Wang & Blumwald, 2014). CV plays a vital role in stress-induced chloroplast disruption and mediates a different pathway to autophagy and senescence-associated vacuoles for chloroplast degradation (Wang & Blumwald, 2014).

## 1.5 Transient starch degradation

Starch is one of the primary products of photosynthesis and stores carbohydrates to support plant metabolism and growth during the dark. Starch is composed of two glucan polymers, amylopectin, and amylose. Amylopectin is a large and highly branched molecule with  $\alpha$ -1,4-linked glucose linear chains and  $\alpha$ -1,6-linked branch points, whereas amylose is smaller, leaner, and consists predominately of  $\alpha$ -1,4-D-glucose bond. Amylopectin is the major component in leaf starch and is responsible for the granular nature of starch.

In *A. thaliana* leaves, starch and sucrose are synthesized together as the products of photosynthetic carbon assimilation during the day, starch accumulates in chloroplasts, and degrades during the subsequent night to provide substrates for sucrose synthesis (Smith *et al.*, 2005). Transient starch degradation (Fig. 4) is an essential process for plant metabolism. GLUCAN WATER DIKINASE (GWD) and PHOSPHOGLUCAN WATER DIKINASE (PWD) are two essential enzymes for transient starch breakdown initiation in *A. thaliana* leaves at night (Orzechowski, 2008), which catalyze the phosphorylation of amylopectin (Kotting *et al.*, 2005; Mikkelsen *et al.*, 2005; Edner *et al.*, 2007).

In plants,  $\beta$ -AMYLASE (BAM) proteins are vital for maltose production during hydrolytic starch degradation. BAM is an exohydrolase, which acts at the non-reducing ends of  $\alpha$ -1,4-linked glucan chains to produce  $\beta$ -maltose (Fulton *et al.*, 2008). In *A. thaliana* four chloroplast BAM proteins were identified and the BAM3 protein plays a major role in the leaf starch

breakdown (Li *et al.*, 2009). Alteration in regulation of chloroplastic  $\beta$ -AMYLASES (*BAMs*), *STARCH-EXCESS 4* (*SEX4*), *MALTOSE EXCESS 1* (*MEX1*), and genes encoding starch-metabolizing enzymes such as *ISOAMYLASE 3* (*ISA3*) and *DISPROPORTIONATING ENZYME 1* (*DPE1*) may result in starch accumulation in leaves (Critchley *et al.*, 2001; Delatte *et al.*, 2006). In *A. thaliana*, any mutations that block either starch synthesis or starch breakdown might result in reduced growth (Stettler *et al.*, 2009). The maltose excess 1 mutant (*mex1*) that lacks the chloroplast envelope maltose transporter, accumulates high levels of maltose and starch in chloroplasts and develops a distinctive chlorotic phenotype as leaves mature (Stettler *et al.*, 2009). Furthermore, the *dpe1/mex1* mutants display a significant increase in the degree of the chlorotic phenotype compared to the *mex1* mutant. The increase of the chlorotic phenotype in *dpe1/mex1* mutants can be explained by the fact that mutations in *DPE1* result in the accumulation of maltotriose in addition to maltose and consequently increase chlorosis. *DPE1* encodes the D-enzyme, which is present in the chloroplast and metabolizes maltotriose. *SEX4* is a phosphoglucan phosphatase that dephosphorylates the starch granule surface and was previously shown to be required for the starch breakdown (Kotting *et al.*, 2009) and disruption of *SEX4* leads to more starch accumulation in plants. *A. thaliana sex4* mutants display more starch content in mature leaves compared to the WT (Niittyala *et al.*, 2006). Triose phosphate translocator (TPT) functions in the stromal triose-phosphates (triose-P) counter exchange. In *A. thaliana*, *tpt* mutant synthesized more starch compared to the WT. Mutants to compensate for the deficiency in their ability to export triose-phosphate from the chloroplast have adopted this strategy (Walters *et al.*, 2004).

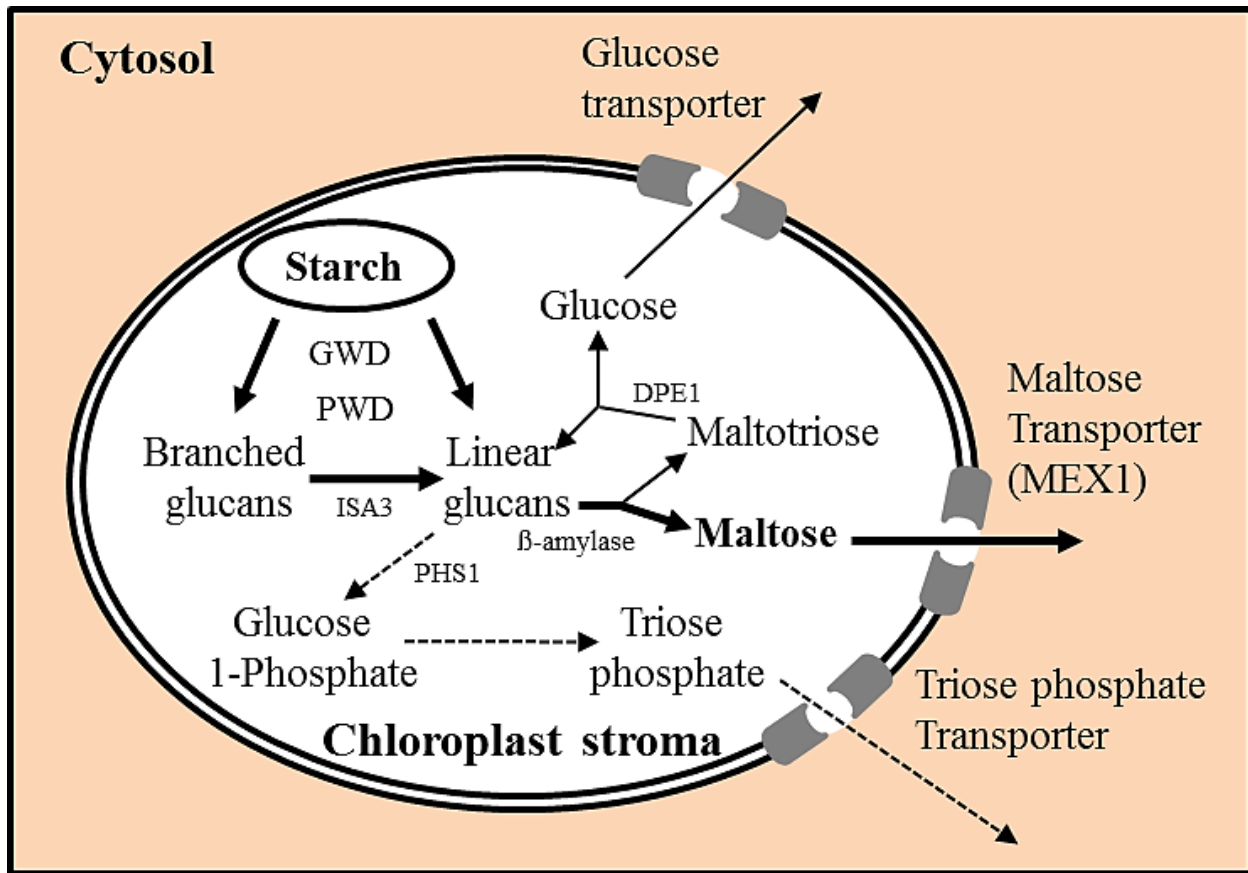


**Fig. 4. Starch degradation pathway in *A. thaliana* leaves at night.** Dashed arrows indicate steps in which uncertainty remains. GWD: GLUCAN WATER DIKINASE. PWD: PHOSPHOGLUCAN WATER DIKINASE. DPE1: DISPROPORTIONATING ENZYME 1. ISA3: ISOAMYLASE 3 (Debranching enzyme). PHS1: GLUCAN PHOSPHORYLASE 1. Modified from Smith *et al.* (2005).

## 1.6 Meristem regulation

Apical meristematic cells are a specialized group of cells that principally reside at the tips of roots and shoots. Maintenance and programming of the meristematic cells are crucial steps for the cell division, shoot, and root branching. Any misregulation of the meristematic cells may result in perturbation and disorder in cell division, shoot, and root branching. Both shoot and root meristems are generated during embryogenesis, but do not contribute to the construction of the embryo and are activated once the seedling germinates (Doerner, 2003). Following the germination, the plant experiences several developmental phases and shoot meristems change their identity in the course of these phase changes. In contrast, no identity alterations occur in root meristems during

development. In *A. thaliana* the shoot meristem identity alteration appears as leaves during the initial vegetative growth, leaves and axillary meristems during the transition to flowering, and floral meristems and bracts by the inflorescence meristem during reproductive growth (Doerner, 2003).

Shoot apical meristems (SAMs) are responsible for developing the above-ground parts of the plant, such as stems, leaves, and flowers, while the under-ground parts of plants including root systems are generated by root apical meristems (Barton & Poethig, 1993). The shoot apical meristem contains a small bank of densely cytoplasmic, undifferentiated, and dividing cells (Barton & Poethig, 1993). Based on several features such as the ability to proliferate, regenerate a new meristem if damaged and the aptitude to produce a variety of differentiated cell types, the cells in the meristem can be classified as stem cells (Sussex, 1952; Potten & Loeffler, 1990).

Several transcription factors (TFs) are involved in meristem maintenance in plants. Recessive mutations in the *WUSCHEL* (*WUS*) gene lead to an interruption in *A. thaliana* shoot meristem maintenance (Laux *et al.*, 1996). The defect is restricted to shoot and floral meristems and can be seen at all developmental stages. *WUS*, a homeodomain TF, plays a critical role in regulating meristem differentiation in plants. In *A. thaliana*, *KANADI 1* (*KAN1*), *KANADI 2* (*KAN2*), *ASYMMETRIC LEAVES 2* (*AS2*), and *YABBY 3* (*YAB3*) are known as differentiation promoting TFs. *WUS* regulates *KAN1*, *KAN2*, *AS2*, and *YAB3* genes via direct binding to their regulatory regions and represses their expression (Yadav *et al.*, 2013). The CLAVATA-*WUSCHEL* signaling pathway was first reported in *A. thaliana* and regulates stem cell maintenance via an auto-regulatory negative-feedback loop (Schoof *et al.*, 2000). *WUS* initially acts as an activator of *CLV3*, which further binds with *CLV1/2* and negatively regulates expression of *WUS* (Fig. 5).

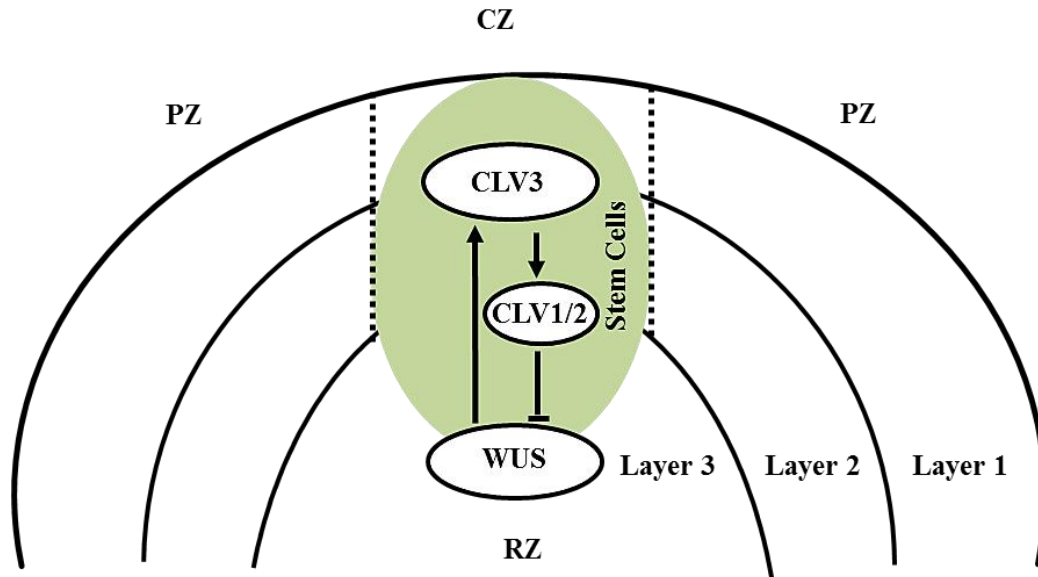


**Fig. 5. Maintenance of stem cells in shoot apical meristem.** Three functional zones of SAM are shown. CZ: central zone. PZ: peripheral zone. RZ: rib zone. WUS activates CLV3, which further binds with CLV1/2 and in turn inhibits expression of WUS. Modified from Kalve *et al.* (2014).

The *A. thaliana jabba-1D* (*jba-1D*) mutant was reported to show multiple enlarged shoot meristems (Williams *et al.*, 2005). Furthermore, *jba-1D* exhibits radicalized leaves, reduced gynoecia, and vascular defects. High *WUS* expression levels are detected in mutants since the *jba-1D* meristem phenotypes require a dramatic increase in *WUS* expression levels. Furthermore, overexpression of miR166g is essential for the development of *jba-1D* meristem phenotypes. Williams *et al.* (2005) described the indirect involvement of miRNAs in controlling meristem formation via regulation of *WUS* expression. In addition to the WUS-CLV pathway, the ERECTA pathway, as a second receptor kinase signaling pathway, represents an independent route that controls shoot apical and floral meristem size by regulating *WUS* expression (Mandel *et al.*, 2014). Mutations of the translation initiation factor *eIF3h* resulted in the formation of enlarged shoot apical meristem in *A. thaliana* (Zhou *et al.*, 2014). In *P. patens*, *WUS*-related homeobox 13-like (*PpWOX13L*) genes are homologs of stem cell regulators in flowering plants and are prerequisite for the initiation of cell growth during stem cell formation (Sakakibara *et al.*, 2014).

Eight types of stem cells were reported to be formed in *P. patens* during its life cycle (Kofuji & Hasebe, 2014). The common ancestor of land plants was haplontic and generated stem cells only

in the gametophytic generation. Other types of body fragments in moss, such as the protonema and rhizoid filaments, leafy-shoot and thalloid gametophores, and gametangia were formed during land plant evolution by the divergence of stem cells in the gametophytic generation. Stem cells follow different morphological and anatomical patterns among land plants. While stem cells in shoot and roots of angiosperms and gymnosperms are multiple cells, in *P. patens* (protonema, gametophore, leaf, rhizoid, and sporophyte), stem cells are a single-cell (Kofuji & Hasebe, 2014). According to Kofuji & Hasebe (2014), eight types of stem cells in *P. patens* are chloronema apical stem cell, caulonema apical stem cell, gametophore apical stem cell, leaf apical stem cell, rhizoid apical stem cell, antheridium apical stem cell, archegonium apical stem cell as well as a stem cell in the diploid generation of the sporophyte apical meristem. In *P. patens*, chloronema apical stem cell, which is responsible for tip growth and production of chloronema cells, has been formed from the first division of a spore (Menand *et al.*, 2007). Some chloronema apical stem cells transform into caulonema apical stem cells that give rise to caulonema cells. Caulonema cells form side branch initial cells, are programmed to become secondary chloronema apical stem cells, secondary caulonema apical stem cells, gametophore apical stem cells, and non-dividing cells (Cove & Knight, 1993). Leaf apical stem cells are produced from gametophore apical stem cells and the first cell division of a zygote forms a sporophyte apical stem cell (Kofuji & Hasebe, 2014).

## 1.7 Aim of the research

Two members of the GRAS family, PpGRAS12 (Pp1s205\_1V6.1) and PpGRAS7 (Pp1s130\_63V6.1) are validated targets of miRNA171 in *P. patens* (Axtell *et al.*, 2007).

The central questions to be addressed in this study are:

- Does miR171 regulate *PpGRAS12* expression?

The miR171 is a conserved miRNA family, exists in all major land plant groups, including bryophytes, and frequently plays a role in defining the spatiotemporal expression of their cognate target mRNAs. To tackle the question, whether miR171 regulates the spatiotemporal expression of *PpGRAS12*, the PpGRAS12::GUS protein fusion reporter lines were generated and analyzed.

- What are the functions of *PpGRAS7* and *PpGRAS12* genes?

For the functional analyses of both *GRAS* genes in *P. patens* and to address the second question, single knockout lines, as well as inducible overexpression lines for both *PpGRAS7* and *PpGRAS12* genes, were generated. To study their functions, the phenotypic analysis, as well as molecular technologies, were utilized in this study.

## **2 CHAPTER 2: MATERIAL AND METHODS**

### **2.1 Chemicals and enzymes**

Chemicals and enzymes were purchased from: AppliChem GmbH (Hessen, Germany), Bio-Rad (München, Germany), Carl-Roth GmbH (Karlsruhe, Germany), Duchefa Biochemie (Haarlem, Netherlands), Genaxxon BioScience GmbH (Biberach, Germany), Invitrogen (Karlsruhe, Germany), Fluka (Neu-Ulm, Germany), Merck (Darmstadt, Germany), Megazyme (Wicklow, Irland), New England Biolabs (Frankfurt, Germany), Promega (Mannheim, Germany), SERVA Electrophoresis GmbH (Heidelberg, Germany), Sigma-Aldrich (Deisenhofen, Germany) and Thermo Fisher scientific (München, Germany).

All buffers and solutions were prepared with deionized water or RNase free water (Invitrogen, USA). If required, the solutions were autoclaved (20 minutes (min), 121°C, 2 bar) or filter sterilized (0.22 µm; Rotilabo® Spritzenfilter, Carl-Roth GmbH, Germany).

### **2.2 Buffers and solutions**

#### **DEPC-H<sub>2</sub>O**

- 0.1% DEPC in H<sub>2</sub>O

The solution was stirred overnight at room temperature (RT) and subsequently autoclaved.

#### **CTAB buffer**

- 2% CTAB
- 1.4 M NaCl
- 20 mM EDTA
- 0.5% PVP 40
- 100 mM Tris

pH was adjusted to 8.0 and 0.2% (v/v) β-mercaptoethanol was added immediately prior to use.

### **gDNA isolation buffer**

- 200 mM Tris-HCl, pH 7.5
- 250 mM NaCl
- 25 mM EDTA
- 0.5% SDS

### **3 M sodium acetate (Autoclaved)**

- 3 M sodium acetate

pH was adjusted to 5.2 with acetic acid.

### **6x DNA loading dye**

- 10 mM Tris HCl, pH 7.6
- 60% (v/v) glycerol
- 60 mM EDTA
- 0.03% (w/v) bromophenol blue
- 0.03% (w/v) xylene cyanol

### **50x Tris acetate (TAE) buffer (Autoclaved)**

- 2 M Tris
- 1 M glacial acetic acid
- 50 mM EDTA, pH 8.0

### **TE buffer (Autoclaved)**

- 10 mM Tris-HCl
- 1 mM EDTA
- pH was adjusted to 8.0 with 1 M HCl

### **20x SSC (Autoclaved)**

- 3 M NaCl
- 0.3 M tri-sodium citrate dehydrate

pH was adjusted to 7.0 with HCl.

**20% SDS** (Filter sterilized)

- 200 g SDS
- H<sub>2</sub>O was added up to 1 L

**500 mM EDTA** (Autoclaved)

- 0.5 M EDTA

pH was adjusted to 8.0 with NaOH.

**2x RNA-denaturing buffer:**

- 500 µl formamide (deionized)
- 12 µl formaldehyde (37%)
- 200 µl 10x MOPS
- 1 µl ethidium bromide

The solution was prepared immediately prior to use.

**2x RNA loading dye**

- 10 ml formamide (deionized)
- 200 µl 0.5 M EDTA
- 10 mg xylene cyanole
- 10 mg bromophenol blue

**10x MOPS buffer** (Filter sterilized)

- 200 mM MOPS, pH 7.0 (adjusted with 2 N NaOH)
- 20 mM sodium acetate
- 10 mM EDTA

The solution was kept protected from light.

**10x FA buffer** (Filter sterilized)

- 200 mM MOPS, pH 7.0 (adjusted with 2 N NaOH)
- 50 mM sodium acetate
- 10 mM EDTA

The solution was kept protected from light.

#### **FA gel running buffer**

- 1x FA gel buffer
- 2.5 M formaldehyde

#### **RNA loading buffer**

- 0.25% bromophenol blue
- 4 mM EDTA
- 0.9 M formaldehyde
- 20% glycerol
- 30.1% formamide
- 4x FA gel buffer
- 1  $\mu$ l (10 mg/ml) ethidium bromide

#### **Hybridization buffer for Northern blot**

- 0.5 M sodium phosphate, pH 7.2
- 1 mM EDTA, pH 8.0
- 7% SDS

The components were mixed and heated to 67°C. 1 ml of the salmon sperm DNA 100  $\mu$ M/ml was denatured for 10 min at 100°C and after cooling on ice was added to the pre-warmed buffer.

#### **Washing solution I (Northern blot)**

- 1x SSC
- 0.1% SDS

#### **Washing solution II (Northern blot)**

- 0.5% SSC
- 0.1% SDS

pH was adjusted to 5.2 with acetic acid.

### **EDC cross-linking solution**

- 0.16 M EDC prepared in 0.13 M 1-methylimidazole, pH 8.0

The solution was prepared immediately prior to use.

### **1 mg/ml DAB solution**

- 50 mg DAB was dissolved in 50 ml distilled H<sub>2</sub>O

pH was adjusted to 3.8 with 0.1 N HCl. The solution was mixed using a magnetic stirrer and protected from the light. The solution was prepared immediately prior to use.

### **0.2% NBT solution**

- 0.1 g NBT (Sigma-Aldrich, USA) was dissolved in 50 mM sodium phosphate buffer (pH 7.5)

The solution was mixed using a magnetic stirrer and protected from the light. The solution was prepared immediately prior to use.

### **X-Gluc solution (Filter sterilized)**

- 0.005 g X-Gluc (5-Bromo-4-Chloro-3-Indolyl- $\beta$ -Glucoronid) (AppliChem GmbH, Germany)
- 60  $\mu$ l DMFO (N,N-Dimethylformamid)
- 1 ml of 1 M sodium phosphate buffer pH 7.0 (57.7 ml Na<sub>2</sub>HPO<sub>4</sub>, 42.3 ml NaH<sub>2</sub>PO<sub>4</sub>)
- H<sub>2</sub>O was added up to 10 ml

The solution was stored at 4°C.

### **5% Formaldehyde**

- 1 ml 37% formaldehyde dissolved in 6.4 ml water

### **5% Acetic acid**

- 0.5 ml acetic acid dissolved in 9.5 ml water

### **RNase A**

- 10 mg RNase A/10 ml Tris-HCl, pH 7.5

The solution was incubated at 100°C for 10 min and after having cooled down to room temperature 100 µl aliquots were prepared and stored at -20°C.

**3 M medium** (Filter sterilized)

- 5 mM MgCl<sub>2</sub>
- 0.1% (w/v) 2-(N-Morpholino) Ethanesulfonic acid (MES)
- 0.48 M mannitol pH 5.6, 580 mOs

**PEG solution** (Filter sterilized)

- 40% (w/v) Polyethylenglycol 4000 in 3 M medium

**0.5 M mannitol** (Filter sterilized)

- 0.5 M mannitol

The pH was adjusted to 5.6 with 1 M HCl. Osmolarity was adjusted to 560 mOsm/l with mannitol.

**10 mM β-estradiol stock solution** (Filter sterilized)

- 27.38 mg β-estradiol (Art. Nr.: E2758; Sigma-Aldrich) dissolved in 1 ml DMSO
- H<sub>2</sub>O was added up to 10 ml (10 mM)

## 2.3 Culture media

**LB medium** (Autoclaved)

- 1% (w/v) bacto agar (Carl-Roth GmbH)
- 0.5% (w/v) yeast extracts (Carl-Roth GmbH)
- 1% (w/v) NaCl

Dissolved in H<sub>2</sub>O, pH was adjusted to 7.0 with 1 N NaOH

**LB medium agar (plates)**

10 g/l bacto agar (Carl-Roth GmbH) was added for the preparation of LB solid medium.

### **LB medium with ampicillin**

Ampicillin was added to LB medium to reach the final concentration of 100 µg/ml (LB-amp).

### **Standard growth medium (Autoclaved)**

- 0.025% (w/v)  $\text{KH}_2\text{PO}_4$
- 0.025% (w/v)  $\text{MgSO}_4$
- 0.025% (w/v)  $\text{KCl}$
- 0.1% (w/v)  $\text{Ca}(\text{NO}_3)_2$
- 0.0125% (w/v)  $\text{FeSO}_4 \times 7 \text{H}_2\text{O}$

pH was adjusted to 5.8 with 1 M KOH.

### **Standard solid growth medium (Autoclaved)**

10 g/l plant agar (Duchefa Biochemie) was added for the preparation of standard solid growth medium.

### **Standard solid growth medium with glucose for sporophyte induction**

200 mg glucose dissolved in 1 L of standard liquid growth medium.

### **Standard solid growth medium with $\beta$ -estradiol**

10 mM  $\beta$ -estradiol was added to the standard solid/liquid growth medium to reach the final concentration of 2 µM.

### **Regeneration medium (Filter sterilized)**

- 5% (w/v) glucose
- 3% (w/v) mannitol

pH was adjusted to 5.6 (with 1 M HCl), 540 mOsm/ L adjusted with mannitol.

## **2.4 Plant material, cell culture, and transformation**

### **2.4.1 Plant materials and growth conditions**

All experiments were performed with *Physcomitrella patens ssp. patens* (Hedwig) ecotype ‘Gransden 2004’ cultured under standard growth conditions as described by Reski and Abel (1985). Liquid cultures were mechanically disrupted using an Ultra-Turrax device to maintain the plants in the protonema stage. The gametophore development was induced by transferring protonema tissue to the solidified standard growth medium.

### **2.4.2 Transformation of *P. patens* protoplasts**

#### **2.4.2.1 Stable transformation**

Polyethylene glycol (PEG) was used to mediate the transformation of *P. patens* protoplasts. (Schaefer *et al.*, 1991). Transformation of *P. patens* protoplasts was conducted as previously described (Strepp *et al.*, 1998). Under the sterile condition, 50 µg of linearized DNA-construct was dissolved in 100 µl of 0.1 M Ca(NO<sub>3</sub>)<sub>2</sub> and subsequently mixed with 250 µl of protoplast suspension and 350 µl of PEG solution by gently inverting the tubes to avoid damaging of the protoplasts. For the co-transformation, 25 µg of DNA construct and 25 µg of selection vector were used. The mixture was incubated for 30 min and tubes were mixed by a gentle inversion every 5 min. Afterwards the suspension was diluted stepwise by addition of 1 ml, 2 ml, 3 ml, and 4 ml of 3 M medium with time intervals of approximately 5 min to avoid the osmotic shock of the cells. After the centrifugation protoplasts were cautiously mixed with 3 ml of regeneration medium and cultivated for 24 hours (h) at 25°C in the dark and then transferred to light (16 h light and 8 h dark) for the regeneration.

#### **2.4.2.2 Transient transformation**

The transient transformation of protoplasts was performed in the same way as stable transformation (see 2.4.2.1) but with circular DNA (0.5 µg/ml) and no selection process. After

transformation, the protoplasts were resuspended in regeneration medium and cultivated for 3 days at 25°C in the dark.

### **2.4.3 Phenotypic analysis**

Liquid cultures were mechanically disrupted every 4 days to maintain the plants in the protonema stage. Phenotypic analysis regarding the growth behavior of transgenic lines as well as *P. patens* WT was performed by adjusting pure protonema cultures to an equal density of 100 mg/l dry weight and 5 µl of the adjusted cultures were spotted onto standard solid medium or solid medium supplemented with 2 µM β-estradiol (2 µM β-estradiol was used as a general inducer for all inducible overexpression (iOE) lines in all experiments; Sigma-Aldrich, USA). For the analysis of phenotypic changes at the leafy gametophore stage, the inducer was directly applied onto colonies from transgenic lines as well as WT controls. Pictures of plants were taken by Nikon stereoscopic microscope (C-DSD230, Minato, Japan).

### **2.5 Phylogenetic analysis**

Sequence alignment and phylogenetic analyses were conducted in MEGAX (Kumar *et al.*, 2018). The phylogeny was inferred using the Neighbor-Joining method (Saitou & Nei, 1987) The percentage of replicate trees in which the associated taxa clustered together in the bootstrap test (100 replicates) are shown next to the branches (Felsenstein, 1985).

### **2.6 Identification of *P. patens* homologs**

*P. patens* homologs were identified using a BLAST search of *A. thaliana* protein sequences as queries against *P. patens* database V6.1 (<http://www.cosmoss.org>) (Appendix 4 and 5). The best BLAST hits were considered as candidate homologs, which were subsequently confirmed by reciprocal BLAST against *A. thaliana* database (<https://www.arabidopsis.org/>).

## **2.7 ROS detection**

Histochemical detection of ROS ( $O_2^-$ ,  $H_2O_2$ ) using NBT and DAB were carried out as previously described by Kumar *et al.* (2014). I used 50% and 75% ethanol instead of 100% and 55°C instead of boiling.

## **2.8 Cloning and bacterial transformation**

### **2.8.1 Gateway pENTR/D-TOPO cloning**

The pENTR<sup>™</sup> Directional TOPO<sup>®</sup>Cloning Kit (Invitrogen, USA) was used to directionally clone a blunt-end PCR product into a vector for entry into the Gateway pENTR/D-TOPO cloning vector. Cloning procedures were performed according to the manufacturer's instructions.

### **2.8.2 pJET1.2 cloning**

The GeneJET<sup>™</sup> PCR Cloning Kit (Thermo Fisher Scientific, USA) was used for the cloning of PCR products into the pJET1.2/blunt Cloning Vector. Cloning procedures were performed according to the manufacturer's instructions.

### **2.8.3 Transformation of chemically competent *E. coli* cells**

For the transformation of chemically competent *E. coli* cells (strain DH5 $\alpha$ ), 1-10  $\mu$ l ligation products were gently mixed with 100  $\mu$ l competent cells (thawed on ice) and incubated on ice for 30 min. Afterwards heat shock was performed by incubation of cells at 42°C for 45 seconds (sec) and subsequent cooling on ice for 3 min. Subsequently, 250  $\mu$ l LB medium was added and the tube was incubated 1 h at 37°C, 200 rpm (INFORS HT, Switzerland). The mixture was centrifuged at 9000 rpm for 5 min, the supernatant was discarded and the pellet was suspended with 50-100  $\mu$ l of LB medium and plated onto LB-amp plates. The plates were incubated at 37°C overnight.

## 2.9 Plasmid DNA isolation

A single colony of transformed *E. coli* cells was cultured overnight in 3 ml LB medium containing the appropriate selective antibiotic at 37°C, 200 rpm (INFORS HT, Switzerland). Subsequently, small-scale plasmid DNA preparation from *E. coli* cells was carried out using the NucleoSpin® Plasmid kit (MACHEREY-NAGEL, Germany), following the manufacturer's instructions. The DNA plasmids were eluted in 30-50 µl sterile dH<sub>2</sub>O, quantified spectrophotometrically and stored at -20°C. For Large-scale plasmid DNA isolation, 300 ml LB medium containing appropriate selective antibiotics were inoculated by a single *E. coli* colony and incubated at 37°C, 200 rpm (INFORS HT, Switzerland) overnight. Subsequently, the isolation of plasmid DNA was carried out using the NucleoBond® Xtra Maxi kit (MACHEREY-NAGEL, Germany), according to the manufacturer's instructions. The purified plasmid DNA was eluted with 150-300 µl sterile dH<sub>2</sub>O, quantified and stored at -20°C.

## 2.10 Genomic DNA isolation from *P. patens*

### 2.10.1 CTAB method

The plant material (1 g of moss protonema) was homogenized under liquid nitrogen using mortar and pestle. CTAB buffer (8 ml) was added to the moss protonema and incubated at 65°C for 1 h. Samples were incubated on ice for 2 min and the homogenates were extracted twice by adding chloroform/isoamyl alcohol (24:1, v/v) and phase separation was carried out by centrifugation at 2500 xg for 10 min at 4°C. Subsequently, samples were incubated with RNase A (final concentration 100 µg/ml) at 37°C for 45 min. DNA precipitation was carried out by adding 1/10 volume of 3 M sodium acetate, pH 5.2 and 1 volume of isopropanol and incubation overnight at -20°C. The DNA was precipitated by centrifugation at 2500 xg, at 4°C for 30 min. Pellets were washed with 10 ml washing buffer (76% ethanol, 10 mM ammonium acetate) at RT for 20 min and then centrifuged for 5 min at 2500 xg. Pellets were washed with 10 ml 70% ethanol at RT for 5 min and then centrifuged for 5 min at 2500 xg. After air-drying of the pellets, pellets were resuspended in 150 µl TE buffer, pH 8.0.

### **2.10.2 gDNA isolation for PCR-screening**

The gDNA isolated was used for PCR and PCR-based screening. The plant material (approximately 4 gametophores or a similar amount of protonema tissues) was transferred into 1.5 ml Eppendorf® safe-lock tubes with a metal bead (Ø 3 mm). Subsequently, 200 µl DNA extraction buffer was added and plant material was disrupted using TissueLyser II (Qiagen, Germany). Samples were incubated for 5 min at RT and subsequently centrifuged for 5 min at 12,000 xg. The supernatant was collected in a new tube and DNA precipitation was carried out by adding 150 µl of -20°C isopropanol, 5 min incubation at RT and centrifugation at 12,000 xg, at 4°C for 10 min. Pellets were washed with 150 µl of -20°C ethanol and centrifuged for 5 min at 12,000 xg. After air-drying of the pellets, pellets were resuspended in 30 µl TE buffer supplemented with RNase A (5 mg/ml).

### **2.11 Electrophoretic separation of nucleic acids**

Separation of DNA/RNA fragments was performed by agarose gel electrophoresis in a 1x TAE buffer. For the superlative separation, agarose gels ranged from 1 to 2.5% were prepared according to the fragment expected size using 0.1x TAE buffer. For the subsequent detection of DNA/RNA, the fluorescent dye ethidium bromide was added to a final concentration of 0.4 µg/ml. Samples were mixed with a 6x DNA-loading dye prior to loading on the gel. An applicable DNA/RNA markers (New England Biolabs, USA) for the size determination and the separated nucleic acid fragments were visualized and documented using Dark hood DH-40/40 (Biostep GmbH, Germany).

### **2.12 Extraction and elution of DNA/RNA fragments from agarose gels**

The DNA/RNA fragments of interest were excised from the agarose gel using a scalpel and purified using the NucleoSpin® gel clean up kit (MACHEREY-NAGEL-Germany) according to the manufacturer's instructions.

### 2.13 DNA sequencing

The amount of DNA template after the purification was calculated due to the template length from the table below and was sent for sequencing to the Genomics Service Unit (LMU Munich, Germany).

100-200 bp	5-20 ng
200-500 bp	10-40 ng
500-1000 bp	20-50 ng
1000-2000 bp	40-100 ng
> 2000 bp	50-150 ng
Plasmids	150-300 ng

### 2.14 RNA isolation from *P. patens*

Plant tissue (100 mg fresh weight) was homogenized under liquid nitrogen and total RNA was extracted using TRIzol<sup>®</sup> Reagent (Invitrogen, USA). The frozen tissue was resuspended in 1 ml TRIzol, vortexed and incubated at room temperature for 5 min and subsequently centrifuged at 12,000 xg, at 4°C for 10 min. The supernatant was transferred to a new tube and 200 µl chloroform added followed by vortexing for 15 sec and 5 min incubation at RT. Next, the phase separation was carried out by centrifugation at 12,000 xg, at 4°C for 15 min. The upper aqueous phase was transferred to a fresh tube and the RNA was precipitated by adding 500 µl isopropanol, incubation on ice for 30 min and centrifugation at 12,000 xg, at 4°C for 10 min. The RNA pellet was washed with 1 µl of 75% ethanol by vortexing and subsequently centrifuged for at 7500 xg, at 4°C for 5 min. The supernatant was completely removed and the pellet was dried on air for 3 to 5 min. The pellet was air-dried and resuspended in 30 µl of RNase-free water.

## 2.15 Spectrophotometric nucleic acid quantification

The optical density assay was performed using NanoDrop 2000 (PeQlab, German), to determine the concentration and purity of the samples. 1  $\mu$ l of RNA or DNA sample was used and absorption (A) was measured at 260 and 280 nm. Calculation of nucleic acid concentrations was based on the assumption that  $A_{260} = 1$  corresponds to a DNA concentration of 50  $\mu$ g/ml or an RNA concentration of 40  $\mu$ g/ml, respectively. The contamination of nucleic acids with proteins was examined with the absorbance ratio of  $A_{260}/A_{230}$ .

## 2.16 PCR

### 2.16.1 Standard PCR

Polymerase chain reaction (PCR) was used for DNA amplification. Mainly, *Taq* DNA-Polymerase (Genaxxon BioScience GmbH, Germany) and Q5 (New England Biolabs, USA) were used for the amplification and reactions were carried out in 200  $\mu$ l tubes in a PeQSTAR Thermal Cycler (PeQLab, Germany).

The standard PCR reaction was carried out in a volume of 25  $\mu$ l:

x $\mu$ l	DNA (20ng)
2.5 $\mu$ l	10x <i>Taq</i> -Buffer s with 15 mM $MgCl_2$ (Genaxxon BioScience GmbH, Germany)
0.5 $\mu$ l	10 mM each dNTPs (New England Biolabs, USA)
1 $\mu$ l	10 $\mu$ M forward primer
1 $\mu$ l	10 $\mu$ M reverse primer
0.25 $\mu$ l	<i>Taq</i> DNA-Polymerase (5 U/ $\mu$ l) (Genaxxon BioScience GmbH, Germany)

RNase free  $dH_2O$  add up to 25  $\mu$ l

The standard PCR Program:

Step	Temperature	Duration	Cycles
Initial denaturation	94°C	3 min	1
Denaturation	94°C	30 s	30
Annealing	Ta	30 s	30
Elongation	72°C	1 kb/min	30
Final elongation	72°C	3 min	1
Storage	8°C	Hold	∞

Annealing temperature [Ta] has calculated according to the following formula:

$$T_a = T_m - 5^\circ\text{C}; T_m = 4 \times (\text{G+C}) + 2 \times (\text{A+T})$$

### 2.16.2 Reverse transcriptase PCR (RT-PCR)

Plant tissue was homogenized under liquid nitrogen and total RNA was extracted using TRIzol<sup>®</sup> Reagent (see 2.14). To remove genomic DNA contamination, RNA was treated for 30 min at 37°C with RNase-free DNase I (NEB, USA). The reaction was stopped by the addition of 2.5 mM EDTA and incubation for 10 min at 65°C. Total RNA (2 µg) was reversed transcribed into first-strand cDNA using M-MLV Reverse Transcriptase (200 U, NEB, USA) as previously described by Arif *et al.* (2018).

### 2.16.3 Quantitative RT-PCR (qRT-PCR)

The synthesized cDNA (ng of cDNA corresponding to 50 ng total RNA) was used as a template for quantitative PCR analysis. qRT-PCR was performed on CFX96 Real-Time System (Bio-Rad, USA) using the EvaGreen mix. The relative expression levels of genes were calculated using the  $2^{-\Delta\Delta\text{CT}}$  method (Livak & Schmittgen, 2001) with *PpEfla* as an internal control.

EvaGreen mix (2x):

1.6 µl	Glycerol (50%)
4 µl	10x <i>Taq</i> - Buffer s with 15 mM MgCl <sub>2</sub>
0.5 µl	10 mM dNTPs (New England Biolabs, USA)
0.4 µl	Fluorescein 100x (1:1000)
1.5 µl	20x Eva Green (Biotium, USA)
0.4 µl	<i>Taq</i> Polymerase (Genaxxon BioScience GmbH, Germany)
11.6 µl	RNase free dH <sub>2</sub> O

qRT-PCR mixture for one reaction (20 µl):

5 µl	cDNA (50 ng)
10 µl	2x EvaGreen mix (2x)
0.5 µl	10 µM forward primer
0.5 µl	10 µM reverse primer
4 µl	RNase free water

## 2.17 RNA gel blot

RNA gel blot analysis was performed as described (Khraiwesh *et al.*, 2008). Briefly, 20 µg of total RNA were mixed with an equal volume of RNA-denaturing buffer and incubated at 67°C for 10 min. The electrophoresis carried out in a 1x FA buffer at 100V for 4 h. The RNA was transferred overnight onto a Hybond™ Nylon membrane (GE Healthcare, Germany) using a turboblotter with 20x SSC blotting buffer. RNA was fixed on the membrane via UV cross-linking (Stratagene, USA). Prior to hybridization, pre-hybridization was performed using 40 ml of hybridization buffer at 65 for 4 h. Subsequently, hybridization was carried out overnight at 67°C using a 25 ml fresh hybridization buffer containing α<sup>32</sup>P-dCTP labeled DNA probe. Random labeling of DNA probe

was performed using Klenow Fragment (3'→5' exo-) (New England Biolabs, USA). After hybridization the membrane was washed two times with 1x SSC, 0.1% SDS and one time with 0.5x SSC, 0.1% SDS at 67°C for 10 min. Signals were detected using Typhoon Trio Variable Mode Imager System (GE Healthcare, Germany).

## **2.18 Protein isolation and immunoblot analyses**

Protein isolation and immunoblot analyses were performed as previously described (Pulido *et al.*, 2013). Specific primary antibodies were diluted to 1:5000 for, PsbD, PsbQ, PsaL, Cyt *f*, Cyt *b<sub>6</sub>*, and ACTIN and to 1:10,000 for HSP70, LHCA2, LHCB2, and RbcL. All antibodies were purchased from Agrisera (Vännäs, Sweden). Incubation with the horseradish peroxidase-conjugated secondary antibody (diluted 1:10,000) was performed for 1 h at room temperature. Detection of immune reactive bands was performed using the ECL Plus reagent (GE Healthcare, Germany). Chemiluminescent signals were visualized using a ChemiDoc MP analyzer (Bio-Rad, USA).

## **2.19 Microscopy**

### **2.19.1 Subcellular localization and confocal microscopy**

The complete *PpGRAS7* and *PpGRAS12* coding sequence were amplified by PCR from genomic DNA with the primers PpGRAS7::C\_F, PpGRAS7::C\_R primer, PpGRAS12::C\_F, and PpGRAS12::C\_R primer, respectively (Appendix 1). Both *PpGRAS7* primers harbor a *KpnI* restriction enzyme site and the PCR product was digested with *KpnI* and cloned into the *KpnI*-site of a modified pMAV4 plasmid (Martin *et al.*, 2009) where the GFP reporter gene was replaced with a citrine coding sequence. The *PpGRAS12* forward primer harbors a *SalI* restriction enzyme site, while the reverse primer harbors *BglII* restriction enzyme site and the PCR product was digested with *SalI* and *BglII*, and cloned into the *SalI*-site and *BglII*-site of pMAV4 plasmid. Individually citrine coding sequence was C-terminally fused in-frame to the *PpGRAS7* and *PpGRAS12* coding sequence. Sequence identity of the cloned PpGRAS7::citrine fusion and PpGRAS12::citrine were confirmed by sequencing. The resulting PpGRAS7::citrine and

PpGRAS12::citrine protein fusion constructs were transiently transfected into *P. patens* protoplasts. The transfected *P. patens* protoplasts were fixed by 1% formaldehyde for 10 min at room temperature (RT). Afterwards 125  $\mu$ M of glycine was added to the samples and incubated for 10 min at room temperature. Nuclei were stained by the addition of 2.5 mg/ml of 4',6-diamidino-2-phenylindole (DAPI, Sigma-Aldrich, USA) followed by gentle shaking for 30 min at RT. Fluorescence microscopy was performed using an inverted Leica TCS SP5 confocal laser scanning microscope (Carl Zeiss, Germany) equipped with a 60x glycerol-immersion objective. The excitation wavelength/emission was as follows for YFP (514 nm/520 to 620 nm), DAPI (358 nm/460 to 490 nm) and chlorophyll (633 nm/650 to 720 nm). Images were processed and assembled by ImageJ.

### **2.19.2 Transmission electron microscopy**

Fresh leaves of *P. patens* WT and mutants were fixed with 2.5% glutaraldehyde in 75 mM cacodylate buffer (pH 7.0), supplemented with 2 mM MgCl<sub>2</sub>. After fixation for one week, the samples were washed four times with 0.1 M sodium cacodylate buffer (pH 7.2) (5 min, 15 min, 80 min, and 100 min) and post-fixed for 140 min with 1% OsO<sub>4</sub> in water. After two further washing steps in the buffer, the samples were washed three times in double-distilled water (15 min, 30 min, and 120 min). Dehydration was carried out in a graded acetone series in which 1% uranyl acetate was added for 1 h within the 20% acetone step. After changing 100% acetone three times, the samples were infiltrated with Spurr's resin and polymerized at 63°C for 72 h. These samples were either semithin sectioned for light microscopy (control and overview) or ultrathin section for electron microscopy. For the latter case, we used a Zeiss EM912 with an integrated OMEGA-filter (Zeiss, Germany), operated at 80 kV in the zero-loss mode. Images were recorded using a Tröndle 2k x 2k slow-scan CCD camera (TRS Tröndle Restlichtverstärkersysteme, Germany).

### 2.19.3 Scanning electron microscopy

Gametophores from *P. patens* WT and mutants were fixed with 2.5% glutaraldehyde in 75 mM cacodylate buffer containing 2 mM MgCl<sub>2</sub>. After 4 washing steps with pure buffer, post-fixation was carried out with 1% OsO<sub>4</sub> for 90 min. Two washing steps with buffer were followed by washing three times with double-distilled water. After this, the samples were dehydrated in a graded acetone series and critical-point-dried. Finally, the samples were mounted on aluminum stubs and sputter-coated with platinum. Scanning electron microscopy was performed on a Hitachi S-4100 SEM (Hitachi, Japan) at acceleration voltages between 3 and 5 kV.

### 2.19.4 Binocular microscopy

Stereomicroscope (SMZ1500, Nikon, Japan) supported with DIGITAL SIGHT ds-FI2 camera (Nikon, Japan) was used for visualizing of mutant and capturing pictures.

## 2.20 Generation of mutants

### 2.20.1 $\Delta PpGRAS7$

The gene disruption construct was designed to partially replace the *PpGRAS7* 5'UTR (303bp) and coding sequence (142bp) with the *nptII* selection marker cassette via homologous recombination. The *PpGRAS7* knockout construct was generated by Dr. M. Asif Arif (LMU biocenter, Germany) using a Gibson Assembly cloning kit (NEB) that allows the joining of DNA fragments with overlapping DNA ends. For this, three sets of primers (Appendix 1) harboring overlapping ends were used to amplify the 5' (586 bp) and 3' (630 bp) flanking regions adjacent to the intended targeting site. The *nptII* coding sequence is controlled by the *nos* promoter and terminator derived from the vector pBSNNEV (Mueller *et al.*, 2014). All three fragments along with the pJET cloning vector were assembled together using the Gibson Assembly kit. Prior to transfection, the knockout construct was released from the pJET backbone by *EcoRI* (NEB USA) digestion and the knockout construct was transfected into *P. patens* protoplasts following standard procedures (Frank *et al.*, 2005). Protoplasts were regenerated and selected on G418-containing

medium (12.5 mg/l) and putative transgenic lines were analyzed by PCR to identify lines that had integrated the *PpGRAS7* knockout construct into the endogenous *PpGRAS7* locus. The lack of the *PpGRAS7* transcript was confirmed by RT-PCR in two independent transgenic lines. All the oligonucleotides that have been used for PCR and RT-PCR are listed in Appendix 1.

### **2.20.2 $\Delta PpGRAS\ 12$**

The gene disruption construct was designed to replace the entire *PpGRAS12* (2430 bp) with the *nptII* coding sequence selection marker cassette via homologous recombination. Designing the construct, cloning strategy and screening were performed and described by Strotbek (2015). The lack of the *PpGRAS12* transcript was confirmed by RT-PCR in two independent transgenic lines. All the oligonucleotides that have been used for PCR and RT-PCR are listed in Appendix 1.

### **2.20.3 *PpGRAS7*-iOE**

The complete *PpGRAS7* coding sequence harbors specific neutral mutations within the miRNA171 binding site that inhibits miR171-directed cleavage was amplified from the mutated version of *PpGRAS7* (Appendix 2). The cloning step was performed using the pENTR/D-TOPO cloning Kits (Invitrogen, USA). A pair of primers (Appendix 1) was designed to amplify the miR171-resistant *PpGRAS7* fragment from the plasmid harboring the mutated version of *PpGRAS7*, which was generated by Strotbek (2015) (Appendix 2). The recombinant *PpGRAS7* fragment was amplified and subsequently cloned into the Gateway pENTR/D-TOPO vector (Invitrogen, USA). The fragment orientation was checked by sequencing and the pENTR/D-TOPO vector was cloned into the PpGX8 destination vector containing a hygromycin resistance cassette (Kubo *et al.*, 2013) using the Gateway LR Reaction (Invitrogen, USA). The inducible overexpression constructs were linearized using *PmeI* (NEB, USA) and transfected into *P. patens* protoplasts.

#### **2.20.4 *PpGRAS12*-iOE**

The full *PpGRAS12* coding sequence that harbors specific silent mutations within the miRNA171 binding site that inhibits miR171-directed cleavage was amplified from the mutated version of *PpGRAS12* (Appendix 3). The cloning step was performed and described by Strotbek (2015).

#### **2.20.5 *AtRGAI*-iOE and *AtRGALI*-iOE**

The complete coding sequences of *AtRGAI* and *AtRGALI* were amplified from *A. thaliana* cDNA with gene-specific primers (Appendix 1) and cloned into the Gateway pENTR/D-TOPO vector using the pENTR/D-TOPO cloning Kits (Invitrogen, USA). Fragment orientations of both entry constructs were checked by sequencing and the pENTR/D-TOPO vector was cloned into the PpGX8 destination vector (Kubo *et al.*, 2013) using the Gateway LR Reaction (Invitrogen, USA). Both inducible overexpression constructs were linearized using *PmeI* (NEB, USA) and transfected into *P. patens* protoplasts.

#### **2.20.6 *AtSCL6-II*-iOE, *AtSCL6-III*-iOE, and *AtSCL6-IV*-iOE**

The full-length coding sequences of *AtSCL6-II*, *AtSCL6-III*, and *AtSCL6-IV* were amplified from previously constructed plasmids harboring the miR171-resistant version of *AtSCL6-II*, *AtSCL6-III*, and *AtSCL6-IV* genes (Aoyama & Chua, 1997) using gene-specific primers (Appendix 1). Subsequently, fragments were cloned into the Gateway pENTR/D-TOPO vector using the pENTR/D-TOPO cloning Kits (Invitrogen, USA). Fragment orientations of all three constructs were checked by sequencing and the pENTR/D-TOPO vector was cloned into the PpGX8 destination vector (Kubo *et al.*, 2013) using the Gateway LR Reaction (Invitrogen, USA). Afterwards all three inducible overexpression constructs were linearized using *PmeI* (NEB, USA) and transfected into *P. patens* protoplasts.

### 2.20.7 PpGRAS12::GUS protein fusion

The *PpGRAS12* coding sequence harboring a mutated or native miR171 binding site (Appendix 3) was fused to the *GUS* coding sequence and introduced to their cognate genomic locus by means of homologous recombination. Three sets of primers were used for the generation of PpGRAS12::GUS fusion constructs. The first set of primers was designed to amplify 1482 bp (5' flanking region of the construct) from the coding sequence including miR171 binding site, where the *SacI* restriction site was added to the 5' end and an *EcoRI* restriction site was added to the 3' end (Appendix 1). The second set including *EcoRI* and *SalI* restriction sites was designed to amplify the *GUS* coding region (Appendix 1). Lastly, the third set of primers was designed to amplify 1528 bp from downstream of the *PpGRAS12* coding region including the 3' UTR (3' flanking region of the construct), where the *SalI* restriction site was added to the 5' end and the *KpnI* restriction site was added to the 3' end (Appendix 1). All three fragments were digested with *EcoRI* and *SalI*, purified, ligated, and subsequently cloned into the pJET cloning vector. PpGRAS12::GUS and mPpGRAS12::GUS fusion reporter constructs were released from the pJET backbone by *SacI* and *KpnI* digestion and transfected into *P. patens* protoplasts.

### 2.21 PAM measurement

*P. patens* WT and *PpGRAS7*-iOE lines were grown on standard solid growth medium for 4 weeks. 2  $\mu$ M of  $\beta$ -estradiol was applied for 2, 4, and 8 days to induce the transcription of the transgenic genes. Chlorophyll *a* fluorescence was analyzed using an Imaging PAM chlorophyll fluorimeter equipped with the computer-operated PAM control unit IMAG-MAXI (Walz) as previously described (Zagari *et al.*, 2017). Measurements of minimal fluorescence ( $F_0$ ) were performed after acclimation for 5 min in the dark. To determine the maximum fluorescence ( $F_m$ ), a pulse (0.8 sec) of saturating white light (5000- $\mu$ mol photon  $m^{-2} s^{-1}$ ) was applied. The ratio  $(F_m - F_0)/F_m$  was calculated as  $F_v/F_m$ , the maximum quantum yield of PSII. Representative false-color images corresponding to  $F_v/F_m$  levels in the WT and inducible *PpGRAS7*-iOE lines were selected. The effective quantum yield of PSII [ $\Phi_{II} = (F_m' - F_s)/F_m'$ ] was monitored at increasing light intensities and plotted as light-responses curved.

## 2.22 Extraction of pigments

Chlorophyll isolation was performed in green light as described by Lichtenthaler and Wellburn (1983) and Arnon (1949). Pigments were extracted as previously described by Kim *et al.* (2013) and Schlicke *et al.* (2014) and annotated based on specific m/z values. Six biological replicates were used for each time point. The samples were analyzed using a combination of a Dionex Ultimate 3000 UHPLC (Thermo Fisher Scientific, USA) and an Impact II QTOF (Bruker Daltonik, Billerica, USA). The evaluation was performed by Data Analysis 4.3, Profile Analysis 2.3, and MetaboScape 1.0. (all were provided by Bruker Daltonik). All solvents were supplied in LCMS-grade by Biosolve (Valkenswaard, Netherlands).

## 2.23 Starch, maltose and sucrose quantification

Samples from *PpGRAS7*-iOE lines as well as WT control obtained from a kinetic experiment (0, 2, 4, and 8 days) after the application of 2  $\mu$ M of  $\beta$ -estradiol were harvested at two different intervals, end of the day and end of the night and frozen in liquid nitrogen. Extraction and quantification of starch were performed using a starch assay kit (Sigma-Aldrich: SA-20, St. Louis, USA). Starch was extracted using the DMSO/HCl method according to the manufacturer's protocol. Maltose and sucrose quantification was performed using maltose, sucrose and D-glucose assay kit (Megazyme: K-MASUG, Wicklow, Ireland) described according to the manufacturer's protocol.

## 2.24 Bioinformatics tools and other software

### 2.24.1 Databases

**Cosmoss:** *P. patens* database. <http://www.cosmoss.org/> (Rensing *et al.*, 2008).

**Phytozome:** The Plant Comparative Genomics portal of the Department of Energy's Joint Genome Institute. <https://phytozome.jgi.doe.gov/pz/portal.html>.

***Physcomitrella* eFP Browser:** [http://bar.utoronto.ca/efp\\_physcomitrella/cgi-bin/efpWeb.cgi](http://bar.utoronto.ca/efp_physcomitrella/cgi-bin/efpWeb.cgi)

(Ortiz-Ramirez *et al.*, 2016).

**TAIR:** The *Arabidopsis* Information Resource. <https://www.arabidopsis.org/>

**miRBase:** miRNA sequences and annotation archives. <http://microrna.Sanger.ac.uk/>

### 2.24.2 Softwares

**CLC main workbench:** DNA, RNA, and protein sequence data analysis (Qiagen, Germany).

**Quantity one 4.6.5:** image analysis and quantification (Bio-Rad, USA)

**ExPASy translate tool:** translation of nucleotide sequences into amino acid sequences.

**Pfam:** protein domains prediction. <https://pfam.xfam.org/>

**ExPASy-PROSITE:** protein domains prediction. <https://prosite.expasy.org/>

**Primer-BLAST:** primer design for qRT-PCR. <https://www.ncbi.nlm.nih.gov/tools/primer-blast/>

**Primer3 (v. 0.4.0):** primer design for PCR. <http://bioinfo.ut.ee/primer3-0.4.0/>

**Image J:** image processing (National Institutes of Health and the Laboratory for Optical and Computational Instrumentation of the University of Wisconsin, USA).

**MEGA X:** phylogenetic tree generation (Pennsylvania State University, USA).

### 3 CHAPTER 3: RESULTS

#### 3.1 Phenotypical and functional analysis of *PpGRAS7* mutants

##### 3.1.1 *PpGRAS7* is not related to the 9 recognized GRAS subfamilies in *A. thaliana*

Harboring the GRAS domain categorized *PpGRAS7* as a member of the GRAS family (Fig. 6) that are known to act as transcription factors in the nucleus (Di Laurenzio *et al.*, 1996; Heo *et al.*, 2011; Yoshida *et al.*, 2014).

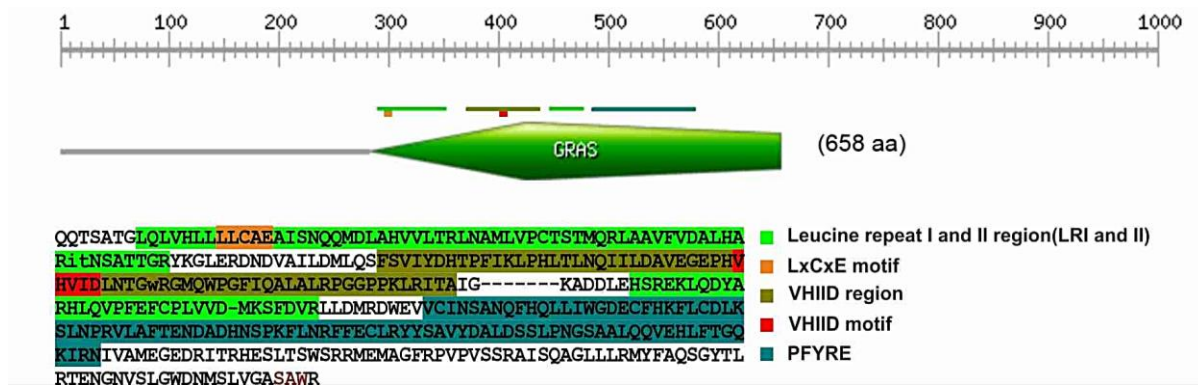


**Fig. 6.** *PpGRAS7* contains the GRAS domain. GRAS domain and GRAS domain motifs prediction were carried out using EXPASY-PROSITE (<https://prosite.expasy.org/>).

To analyze the similarity of *PpGRAS7* to other GRAS subfamily members, a phylogenetic tree including *PpGRAS7* and all 32 members of the *A. thaliana* GRAS subfamily was generated. *AtSCL26* (AB007647) has been annotated as a pseudogene and was not included in the phylogenetic analysis. The phylogenetic analysis indicates that although *PpGRAS7* contains the GRAS domain, it does not cluster with any of nine previously described GRAS subfamilies in *A. thaliana* (Fig. 7) (Zhang *et al.*, 2019).

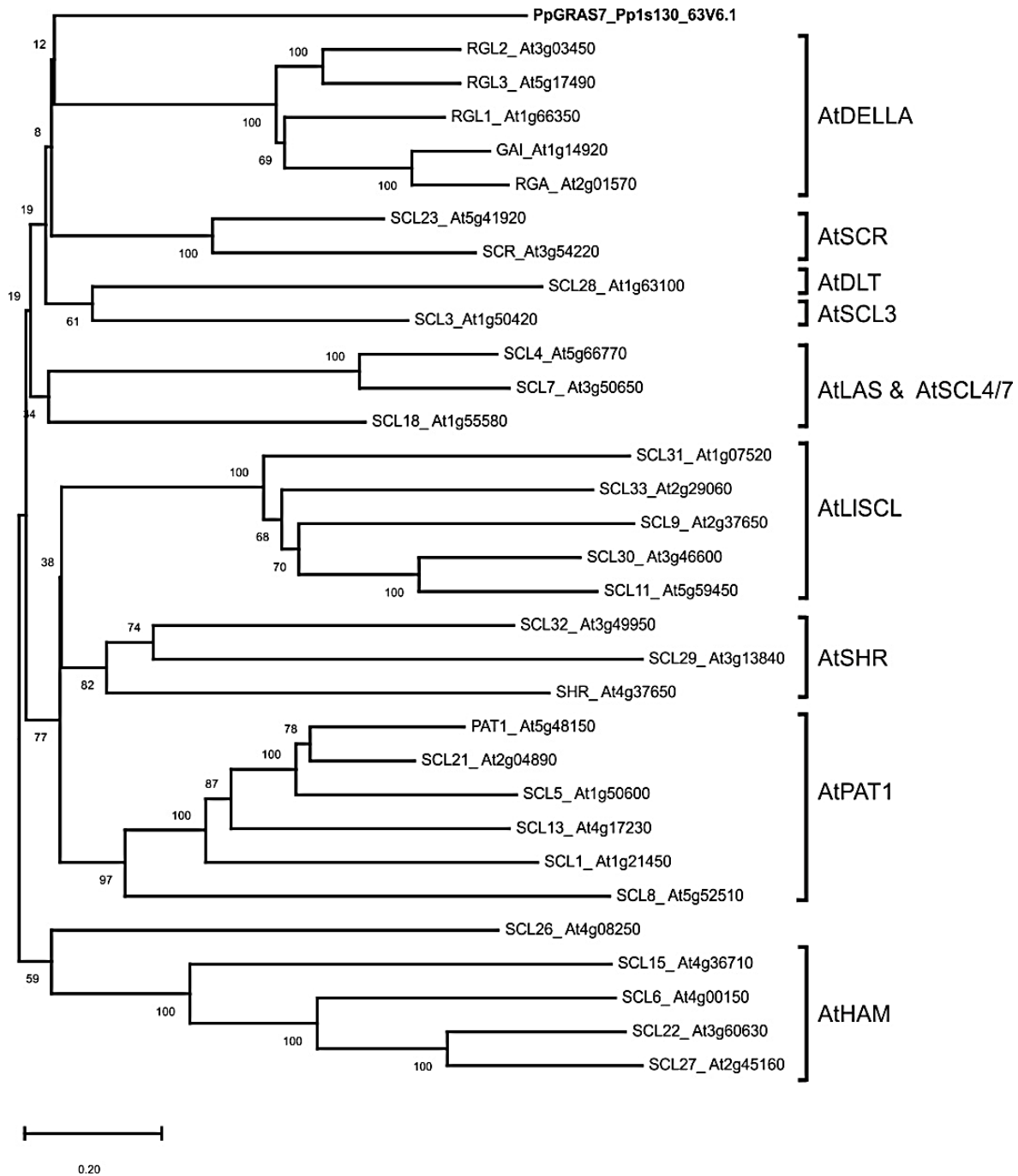


**Fig. 7. Phylogenetic analysis of PpGRAS7.** The phylogenetic tree includes PpGRAS7 and all 32 GRAS members of *A. thaliana*. Full-length protein was applied for the generation of a phylogenetic tree. Bootstrap values (based on 100 iterations) are shown for corresponding nodes. The scale bar is an indicator of the evolutionary distance in substitutions per site.

**DELLA:** Aspartic acid (D), Glutamic acid (E), Leucine (L), Leucine (L) and Alanine (A). **SCR:** SCARECROW. **DLT:** DWARF AND LOW-TILLERING. **SCL3:** SCARECROW-LIKE 3. **SCL4/7:** SCARECROW-LIKE4/7. **LAS:** LATERAL SUPPRESSOR. **LISCL:** SCL from *Lilium longiflorum* L. **SHR:** SHORT ROOT. **PAT1:** PHYTOCHROME A SIGNAL TRANSDUCTION 1. **HAM:** HAIRY MERISTEM.

### 3.1.2 Loss of the nuclear-localized PpGRAS7 protein results in a mild phenotypic deviation

The aptitude of PpGRAS7 to act as a transcription factor was tested via the subcellular localization. Using the transient expression of a C-terminal PpGRAS7::citrine protein fusion in *P. patens* protoplasts, a nuclear localization pattern for PpGRAS7 was observed by laser scanning confocal microscopy. The citrine fluorescence signals in the transformed protoplasts overlapped with nuclei stained by 4',6-diamidino-2-phenylindole (DAPI) (Fig. 8a). This finding is compatible with the previous allegation of putative transcription factor activity of GRAS family members acting in the nucleus (Di Lorenzo *et al.*, 1996; Heo *et al.*, 2011; Yoshida *et al.*, 2014).

Since functional studies on GRAS proteins in early land plants are lacking, the characterization of PpGRAS7 was initiated by the generation of targeted knockout lines via homologous recombination in *P. patens* ( $\Delta PpGRAS7$  lines were generated by Dr. M. Asif Arif, LMU biocenter, Germany). For this, a neomycin phosphotransferase II (*nptII*) selection marker cassette was inserted into a defined region of the *PpGRAS7* genomic sequence (Fig. 8b). The resulting knockout construct contained regions of 586 bp (5') and 630 bp (3') flanking the *nptII* cassette. This construct was used for the transfection of *P. patens* protoplasts in order to replace a part of the endogenous *PpGRAS7* locus via homologous recombination. After the selection of regenerating protoplasts on the geneticin-containing medium, a PCR-based screening was performed to identify transgenic lines that have integrated the DNA knockout construct within the *PpGRAS7* locus. Primers were designed to amplify a genomic region from 107 bp upstream and 175 bp downstream of the expected integration site of the knockout construct. Lines harboring the knockout construct within the *PpGRAS7* locus produced a PCR fragment with a size of 1.790 bp, while the wild type (WT) produced a shorter fragment of 282 bp due to the lack of the *nptII* cassette (1.508 bp) (Fig. 8c). The precise integration of the knockout construct into the genome was confirmed for two independent lines by 5' (black primers, Fig. 8b) and 3' (red primers, Fig. 8b) integration PCR (Fig. 8c). Furthermore, the lack of *PpGRAS7* transcript in these mutants was confirmed by RT-PCR indicating that both transgenic lines were null mutants ( $\Delta PpGRAS7$ ) (Fig. 8d). To monitor whether the deletion of  $\Delta PpGRAS7$  causes any phenotypic deviations phenotypic analysis was performed with protonema tissues of WT and the two  $\Delta PpGRAS7$  lines, which were spotted with equal densities onto standard growth medium. In the primary phase of growth including protonema and

budding stage, no distinct differences were observed in  $\Delta PpGRAS7$  lines compared to the WT. However, both  $\Delta PpGRAS7$  lines developed shorter gametophores as compared to the WT (Fig. 8e and f).

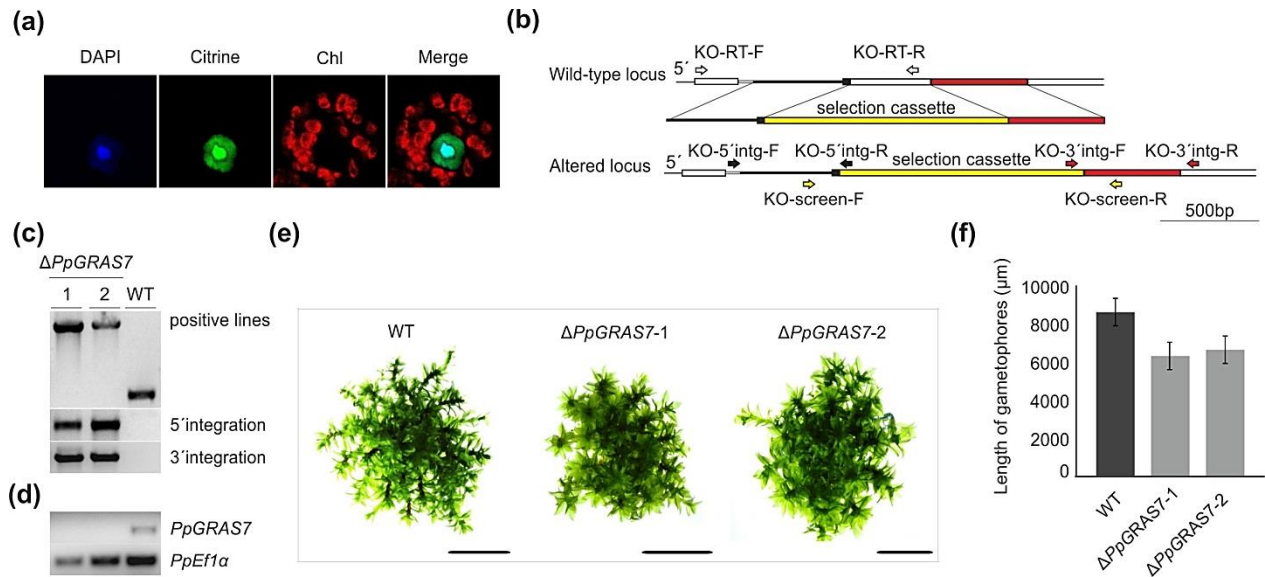


**Fig. 8. Functional characterization of the *PpGRAS7* gene.** (a) Subcellular localization of the PpGRAS7::citrine protein fusion in *P. patens* protoplast. Pictures were taken 3 days after transfection of the PpGRAS7::citrine fusion into *P. patens* protoplasts. DAPI: DAPI signal. Citrine: citrine signal. Chl: chlorophyll auto-fluorescence. Merge: merged images of citrine and chlorophyll auto-fluorescence. (b) Scheme depicting the targeted knockout approach of the *PpGRAS7* coding sequence. The yellow box indicates the *nptII* selection cassette that was used to replace a fragment within the coding sequence, whereas black (black lines indicate introns and black boxes show exons) and red boxes specify flanking regions that were used for the gene targeting. White, yellow, black, and red arrows show the primer pairs sequentially applied for PCR-based analyses of the generated knockout mutants. (c) Three panels showing amplified PCR products using genomic DNA from the indicated lines as a template. Upper panel: screening of lines using yellow (KO-screen-F and KO-screen-R) primers; note that the two knockout mutants produce a larger PCR product due to the insertion of the knockout construct. Second panel: confirmation of 5' integration of the knockout constructs using black (KO-5'intg-F and KO-5'intg-R) primers. Third panel: confirmation of 3' integration of the construct using red (KO-3'intg-F and KO-3'intg-R) primers. (d) RT-PCR from cDNA derived from the indicated lines using *PpGRAS7*-specific primers (KO-RT-F and KO-RT-R); note that the two  $\Delta PpGRAS7$  mutant lines are null mutants lacking the *PpGRAS7* transcript; RT-PCRs performed with primers for the constitutively expressed gene *PpEfl1a* served as a control to monitor successful cDNA synthesis. (e) Phenotypic analyses of knockout lines. Initially, a single gametophore of plant material from the indicated lines was transferred onto standard growth medium and pictures were taken after 45 days of growth under standard growth conditions. scale bars: 1 cm. (f) Comparison of the gametophore length in the WT and two independent  $\Delta PpGRAS7$  lines. Gametophore length was measured from colonies grown for 45 days under standard growth conditions; error bars represent standard errors (n = 30).

### 3.1.3 *PpGRAS7* overexpression leads to chlorosis

Since the  $\Delta PpGRAS7$  lines did not show considerable phenotypic deviations I aimed to gain further insights into the function of *PpGRAS7* by overexpressing a miRNA-resistant *PpGRAS7* version, which was previously generated by Strotbek (2015). For the generation of the miRNA-resistant *PpGRAS7* version, the *PpGRAS7* cDNA was amplified and six silent mutations introduced within the miR171 binding site to inhibit miR171-mediated cleavage without affecting the encoded amino acid sequence (Strotbek, 2015) (Appendix 2). The modified *PpGRAS7* coding sequence was cloned into the Gateway pENTR/D-TOPO vector. The fragment orientation was checked by sequencing and the pENTR/D-TOPO vector was cloned into the PpGX8 destination vector (Kubo *et al.*, 2013). This construct was used for the transfection of *P. patens* protoplasts. After the selection of regenerating protoplasts on hygromycin-containing medium, a PCR-based screening was performed to identify transgenic lines. The PCR-based screen (Fig. 9) led to the identification of two independent *PpGRAS7* overexpression lines (*PpGRAS7*-iOE).

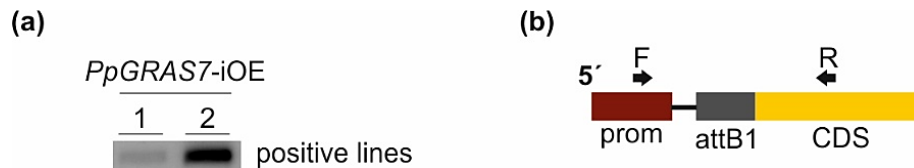


**Fig. 9. Genotyping of the *PpGRAS7*-iOE lines.** (a) Screening of the *PpGRAS7*-iOE lines using OE-screen-F and OE-screen-R primers. Positive lines show amplified PCR products using genomic DNA from the indicated lines as a template. (b) Scheme depicting the PCR screen strategy for the *PpGRAS7*-iOE lines. The OE-screen-F primer binds within the promoter region of PpGX8 vector; 70 bp upstream of the *PpGRAS7* start codon, while the OE-screen-R is located within the *PpGRAS7* coding sequence. Prom: PpGX8 promoter.

To verify the inducible expression of *PpGRAS7*, protonema tissues from both independent *PpGRAS7*-iOE lines were treated for 4 h with the inducer (2  $\mu$ M  $\beta$ -estradiol was used as a general inducer for the *PpGRAS7*-iOE lines in all experiments). Whereas the untreated *PpGRAS7*-iOE lines had similar *PpGRAS7* transcript levels as the WT control, a strong induction of the *PpGRAS7* transgene in both *PpGRAS7*-iOE lines was detected by RNA gel blot and qRT-PCR analysis (Fig. 10a and b). Next, the impact of elevated *PpGRAS7* transcript levels on the growth and development in both *PpGRAS7*-iOE lines was analyzed. I did not observe any phenotypic differences between

WT and both *PpGRAS7*-iOE lines on standard growth medium. Moreover, the growth of the WT plants on the inducer-containing medium was indistinguishable from its growth on standard growth medium. Interestingly, I observed a remarkable and distinct growth arrests of both *PpGRAS7*-iOE lines when protonema tissue was transferred to solid medium supplemented with the inducer (Fig. 10c). Within 2 weeks, I noticed not only a very strong gradual growth arrest in the *PpGRAS7*-iOE lines, but also paling and browning of usually green tissues. The growth arrests appeared to be irreversible since protonema tissue that was kept for 2 weeks under inducing conditions and was subsequently released onto standard medium without inducer remained pale and failed to recover into green protonema tissues (Fig. 10c). I also analyzed the growth behavior of both *PpGRAS7*-iOE lines upon growth in the liquid medium. For this, protonema tissues from the WT and both *PpGRAS7*-iOE lines were transferred into the liquid medium supplemented with the inducer and growth of the cultures was monitored by the determination of the dry weight every 2 days. Already 2 days after  $\beta$ -estradiol induction, I observed a strong decrease in the growth rate of both *PpGRAS7*-iOE lines reaching finally a brown color and growth arrest after 8 days of the induction (Fig. 10d). WT lines did not show any alterations of the phenotype under inducible conditions. Further, I also examined the effect of *PpGRAS7* induction at later growth stages with colonies that were grown on solid medium and developed leafy gametophores. For this, 2  $\mu$ M  $\beta$ -estradiol was directly applied onto the colonies of both *PpGRAS7*-iOE lines and the WT control. To monitor *PpGRAS7* induction during the experiment, gametophores from both lines were harvested immediately before the inducer treatment and 2, 4, and 8 days after the induction. *PpGRAS7* expression analysis by qRT-PCR revealed an approximately 650-fold induction of the transcript after 2 days of induction. *PpGRAS7* transcript levels were still about 150-fold upregulated compared to the WT control after 4 and 8 days (Fig. 11). The elevated levels of the *PpGRAS7* transcripts in the gametophores have led to severe chlorosis, browning of the tissue and finally the loss of chlorophyll and entire degradation of chloroplasts (Fig. 10e). Furthermore, the time-course analysis was performed to monitor the effect of permanent growth on the inducer-containing medium, which supported the initial observation that elevated *PpGRAS7* levels cause chloroplast degradation (Fig. 10f). While prolonged treatment with the inducer did not have any visible effect in the WT, strong chlorosis appeared already 4 days after induction in both *PpGRAS7*-iOE lines followed by shrinking of the

plastids and further loss of chlorophyll. Chloroplasts disappeared completely in the phylloid cells after 45 days (Fig. 10f).

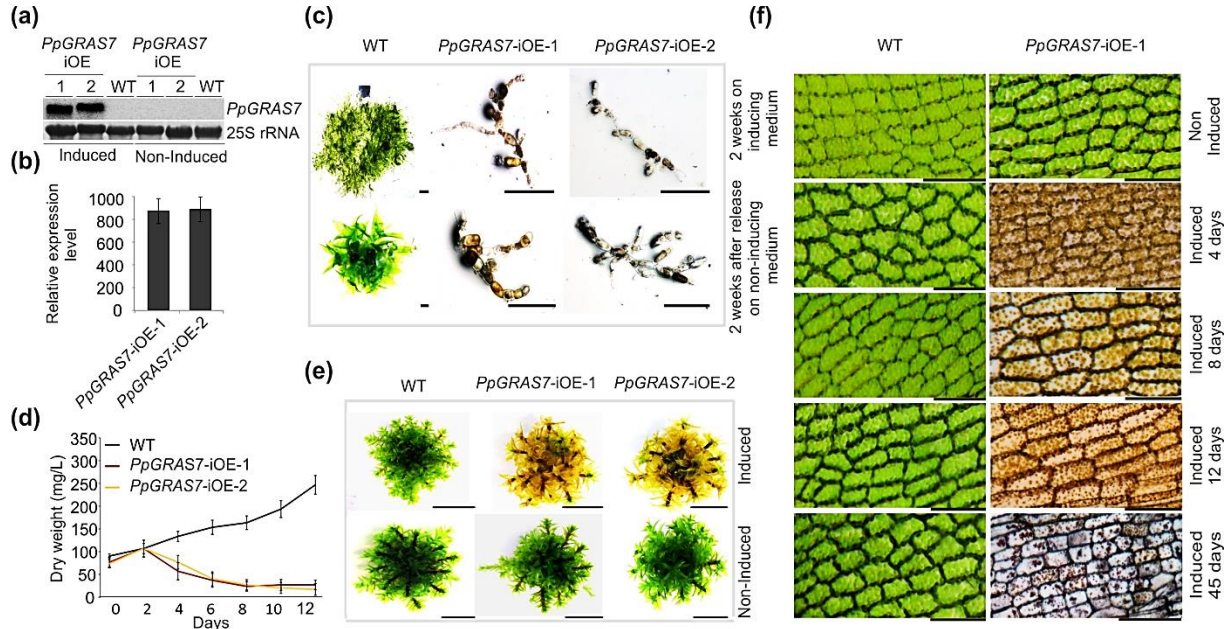


**Fig. 10. Generation and phenotypic analysis of inducible *PpGRAS7* overexpression lines.** (a) RNA gel blots from the WT and two independent *PpGRAS7*-iOE lines grown for 4 h in the standard liquid medium (non-induced) or liquid medium supplemented with the inducer (induced). The blot was hybridized with a *PpGRAS7*-specific probe and 25S rRNA (from the EtBR stained gel) was used to monitor equal loading. (b) The relative expression level of *PpGRAS7*. WT and *PpGRAS7*-iOE lines were induced with 2  $\mu$ M  $\beta$ -estradiol and expression levels of *PpGRAS7* in the induced lines and induced WT were monitored after 4 h of induction via RT-PCR using *PpGRAS7*-specific primers. WT levels were set to 1. Error bars indicate mean values  $\pm$  SE (n = 3). (c) Equal amounts of protonema tissues from the WT and both *PpGRAS7*-iOE lines were spotted on standard growth medium supplemented with the inducer. Upper panel: protonema tissues after growth for 14 days on inducing medium. Lower panel: 14 days after growth on inducing medium protonema tissue was transferred onto standard growth medium without inducer for 2 weeks. Scale bars: 1 mm. (d) Equal amounts of *PpGRAS7*-iOE and WT lines were grown in standard liquid medium without inducer. Protonema tissues were induced and the dry weight of samples was measured every 2 days for a period of 12 days. Error bars indicate mean values  $\pm$  SE (n = 3). (e) Upper panel: chlorosis in the *PpGRAS7*-iOE lines treated for a period of 7 days with the inducer. Lower panel: the non-induced WT and *PpGRAS7*-iOE lines. Scale bars: 1 cm. (f) Defects and the degradation of chloroplasts in the phylloid of induced *PpGRAS7*-iOE lines. Phylloid tissues derived from the untreated WT and *PpGRAS7*-iOE-1 line as well as treated with the inducer. Pictures were taken 4, 8, 12, and 45 days after the induction with the inducer. Scale bars: 1 mm. Based on the phenotype similarity in both independently generated *PpGRAS7*-iOE lines, *PpGRAS7*-iOE-1 line was used as a representative.

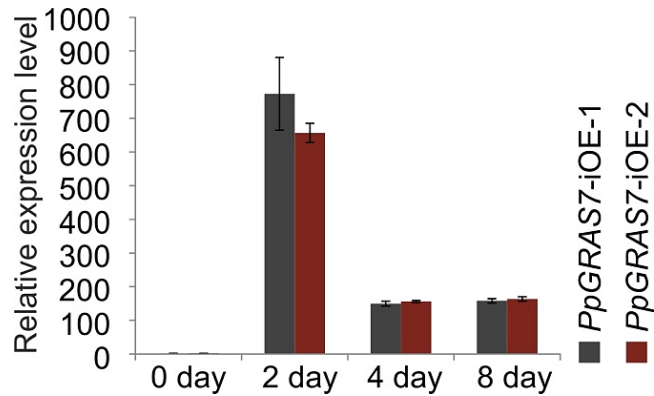


**Fig. 11. Expression analysis of *PpGRAS7*.** The relative expression level of *PpGRAS7*. Lines were induced with 2  $\mu$ M  $\beta$ -estradiol and the expression levels of *PpGRAS7* in the induced lines and induced WT were monitored after 2, 4, and 8 days of induction via qRT-PCR using *PpGRAS7*-specific primers. 0 days indicates non-induced *PpGRAS7*-iOE lines. WT levels were set to 1. Error bars indicate mean values  $\pm$  SE (n = 3).

### 3.1.4 *PpGRAS7* overexpression induces metabolic misbalances

Based on the observed chlorotic phenotype upon elevated *PpGRAS7* transcript levels in *PpGRAS*-iOE lines, I expected changes in the chloroplast ultrastructure. To obtain insights into putative ultrastructural changes of the chloroplast, in cooperation with Dr. Andreas Klingl (LMU biocenter, Germany), we performed transmission electron microscopy (TEM) of phylloid tissues derived from the WT and *PpGRAS7*-iOE-1 line that were treated for 8 days with the inducer and untreated samples. Strikingly, in response to elevated *PpGRAS7* transcript levels, a noticeable starch accumulation was observed in the *PpGRAS7*-iOE-1 line when compared to the WT (Fig. 12a). The accumulation of starch was confirmed by starch measurement in the *PpGRAS7*-iOE-1 line after 2, 4, and 8 days of induction with the inducer. Compared to the WT and non-induced *PpGRAS7*-iOE-1 controls I detected an up to 5.5-fold starch accumulation at 8 days of induction in transformants (Fig. 12b). While in the WT and the non-induced *PpGRAS7*-iOE-1 line starch levels decreased during the night period, there were no marked differences in the amount of starch at the end of the day and end of the night in the induced *PpGRAS7*-iOE-1 line at the analyzed time points (2, 4, and 8 days). This indicates that induction of *PpGRAS7*-iOE-1 line leads to an inhibition of starch degradation, rather than a stimulation of starch synthesis.

Transient starch breakdown is dependent on glucan phosphorylation mediated by the enzymes GLUCAN WATER DIKINASE (GWD) and PHOSPHOGLUCAN WATER DIKINASE (PWD), while STARCH EXCESS 4 (SEX4), a glucan phosphatase dephosphorylates starch-bound phosphate (Streb *et al.*, 2012). The further steps involved in starch degradation involve plastidic  $\beta$ -AMYLASES (BAMs), ISOAMYLASE 3 (ISA3), and disproportionating enzyme 1, D-enzyme (DPE1), while the maltose transporter MALTOSE EXCESS 1 (MEX1) is responsible for the export of maltose from the chloroplast into the cytosol (Critchley *et al.*, 2001; Delatte *et al.*, 2006). To investigate whether miss-regulation of these steps is involved in the inhibition of starch degradation I studied the impact of elevated *PpGRAS7* transcript levels on the expression of *P. patens* homologs encoding these proteins in the *PpGRAS7*-iOE lines. *P. patens* homologs of *GWD*, *PWD*, *BAM*, *SEX4*, *MEX1*, *DPE1*, and *ISA* genes were identified using a BLAST search of AtGWD, AtPWD, AtBAM, AtSEX4, AtMEX1, AtDPE1, and AtISA protein sequences against the *P. patens* database (<http://www.cosmoss.org>) (Appendix 4). The best BLAST hits were considered as candidate homologs, which were subsequently confirmed by reciprocal BLAST against the *A. thaliana* database (<https://www.arabidopsis.org/>). Based on the protein sequence homology in *P. patens* I found four genes similar to *AtBAM3* (named *PpBAM3a*, *PpBAM3b*, *PpBAM3c* and, *PpBAM3d*) and two genes similar to *AtGWD*, *AtPWD*, *AtSEX4*, *AtMEX1*, and *AtDPE1* (named *PpGWD1a*, *PpGWD1b*, *PpPWD1a*, *PpPWD1b*, *PpSEX4a*, *PpSEX4b*, *PpMEX1a*, *PpMEX1b*, *PpDPE1a*, and *PpDPE1b*), which were selected for expression analysis (Appendix 4). A 2.5-fold increase in *PpGWDa* transcript levels was observed in both *PpGRAS7*-iOE lines, whereas *PpGWDb*, *PpPWDa*, and *PpPWDb* remained unchanged compared to the WT (Fig. 12c). Analysis of the expression of *PpBAM3a* and *PpBAM3d* showed 2-fold downregulation compared to the WT (Fig. 12c). A decreased expression of *PpBAM3* may explain the accumulation of starch in the *PpGRAS7*-iOE lines, while the upregulation of *PpGWDa* could indicate a compensatory effort of the plant to lower the excess of starch. *PpDPE1a* and *PpDPE1b* transcript levels were about two and four-fold upregulated compared to the WT, respectively (Fig. 12c). Besides, the expression of *PpMEX1a*, *PpISA3*, and *PpSEX4b* was increased in the induced *PpGRAS7*-iOE lines compared to the WT (Fig. 12c).

The triose phosphate translocator (TPT) is responsible for the stromal triose-phosphates (triose-P) counter exchange. Based on the protein sequence homology I found two triose phosphate translocator (TPT) genes in *P. patens* homologs to *A. thaliana* TPT gene, namely *TPTa* and *TPTb*. To monitor the expression of TPT in the *PpGRAS7*-iOE lines, pure protonema from the *PpGRAS7*-iOE-1 line as well as WT was induced with the inducer for 2, 4, and 8 days. No significant differences compared to the WT were observed for *PpTPTb*, while a drastic downregulation was detected for the *PpTPTa* in the *PpGRAS7*-iOE-1 line especially at the end of the day after 2, 4, and 8 days (Fig. 12d). Besides, no significant differences compared to the WT were observed for *TPTa* at the end of the night after 2 and 4 days, while the downregulation of the *TPTa* was noticed at the end of the night after 8 days. As the TPT is light-triggered, the downregulation of the *TPTa* at the end of the day in the *PpGRAS7*-iOE-1 line may explain the starch accumulation in the *PpGRAS7*-iOE lines. The analysis of maltose content revealed an increase of maltose in the *PpGRAS7*-iOE-1 line after 8 days of induction (Fig. 12e). I also detected elevated levels of sucrose in the *PpGRAS7*-iOE-1 line after 8 days of induction (Fig. 12f). Increasing the amount of maltose, sucrose, and starch, in response to an elevated level of *PpGRAS7* indicates an unbalanced sugar and starch metabolism in induced transformants.

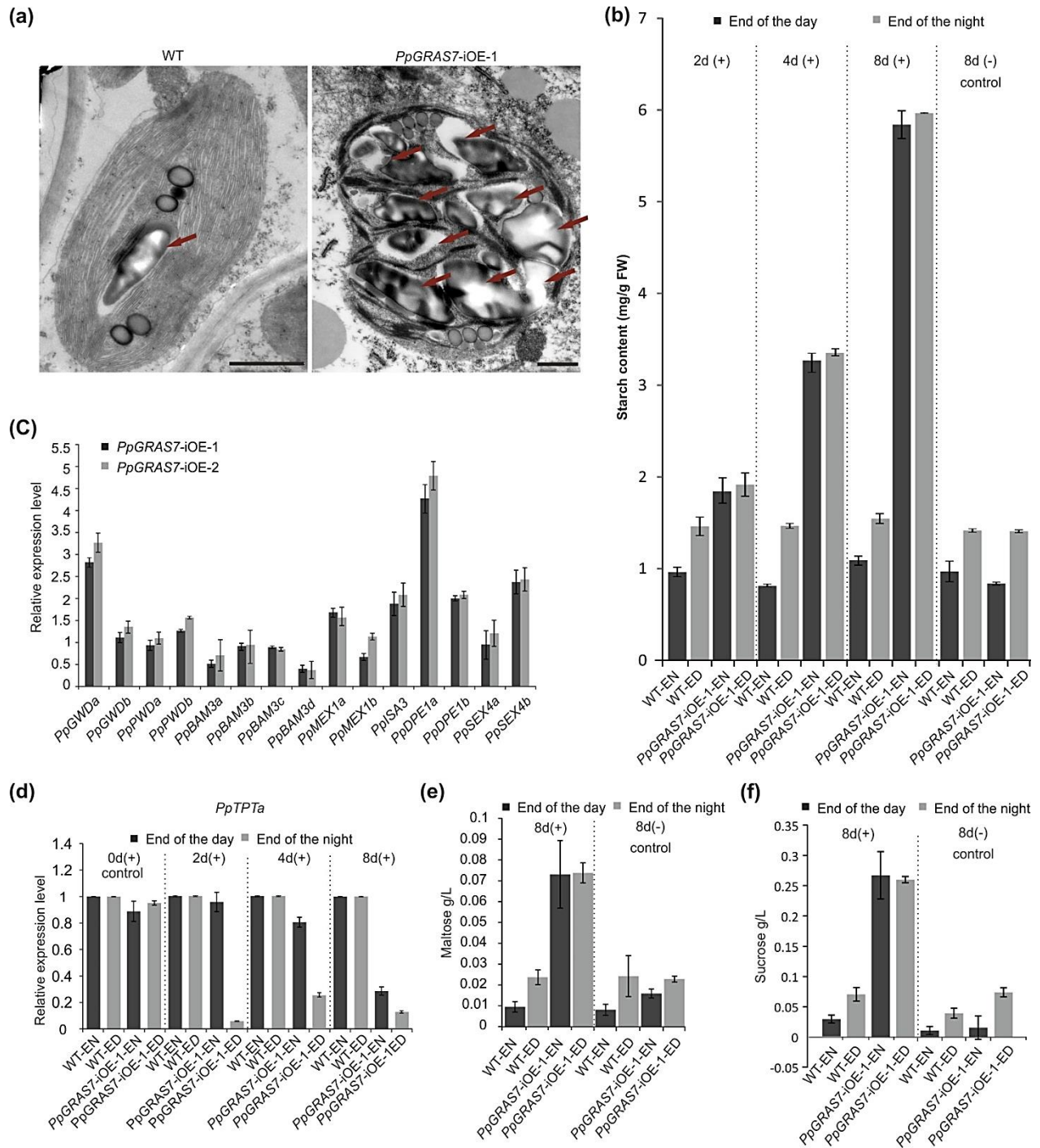


**Fig. 12. Metabolic analysis of the *PpGRAS7*-iOE lines.** (a) TEM analysis of *PpGRAS7*-iOE-1 (*PpGRAS7*-iOE line #1). Phylloid tissues that were treated for 8 days with the inducer. Arrows point to starch granules. Scale bars correspond to 1  $\mu$ m and 500 nm for the WT and *PpGRAS7*-iOE-1 line, respectively. Based on the phenotype similarity in both independently generated *PpGRAS7*-iOE lines, *PpGRAS7*-iOE-1 line was used as a representative. (b) Quantification of the starch content in the WT and *PpGRAS7*-iOE-1 line as mg per gram fresh weight. *PpGRAS7*-iOE-1 line and the WT were grown in standard liquid medium for 2 weeks. Protonema tissues were induced and the starch content was measured after 2, 4, and 8 days. (+) indicates induced and (-) non-

induced. Error bars indicate mean values  $\pm$  SE (n = 3). (c) The relative expression level of genes for starch biosynthetic or catabolic enzymes (*PpGWD*, *PpPWD*, *PpBAM*, *PpSEX4*, *PpMEX1*, and *PpDPE1*) in the WT and *PpGRAS7*-iOE lines after 4 h of induction. Relative expression levels were normalized to *PpEfla* and transcript levels in the WT were set to 1. Error bars indicate mean values  $\pm$  SE (n = 3). (d) The relative expression level of the *PpTpTa* gene in the WT and *PpGRAS7*-iOE-1 line after 2, 4, and 8 days of induction. Relative expression levels were normalized to *PpEfla* and transcription levels in the WT were set to 1. (e) Quantification of maltose content. The pure protonema from the *PpGRAS7*-iOE-1 line and WT were induced with 2  $\mu$ M  $\beta$ -estradiol and the maltose content was measured after 8 days. Error bars indicate mean values  $\pm$  SE (n = 3). (f) Quantification of sucrose content. The pure protonema from *PpGRAS7*-iOE-1 line and the WT were induced with 2  $\mu$ M  $\beta$ -estradiol and the sucrose content was measured after 8 days. Error bars indicate mean values  $\pm$  SE (n = 3).

### 3.1.5 Light triggers cell chlorosis in the *PpGRAS7*-iOE lines.

Based on the observed chlorotic phenotypes in the induced *PpGRAS7*-iOE lines, I investigated the effect of different light regimes on the *PpGRAS7*-iOE lines phenotype. Protonema tissue from the WT and *PpGRAS7*-iOE-1 line was grown on standard medium with 2  $\mu$ M  $\beta$ -estradiol and exposed for 2 weeks to continuous light (80  $\mu$ E) and different day length regimes (16 h light with 80  $\mu$ E /8 h dark and 8 h light with 40  $\mu$ E /16 h dark). Continuous light noticeably increased the severity of the phenotype in the *PpGRAS7*-iOE-1 line (Fig.13a). I further observed a milder phenotypic deviation in the plants, which were exposed to the long night period (16 h dark) and the reduced light intensity (Fig. 13a). Generally, under stress-induced conditions levels of reactive oxygen species (ROS) are elevated and a light-induced accumulation of ROS could account for the observed phenotype. To monitor elevated ROS levels, I used the nitrotetrazolium blue chloride (NBT) and 3,3'-diaminobenzidine (DAB) in the *PpGRAS7*-iOE-1 line as well as the WT to detect  $O_2^-$  and  $H_2O_2$  oxidative species, respectively, after 8 h of induction with the inducer. DAB is oxidized by  $H_2O$  in the presence of peroxidases and forms reddish brown precipitates, while NBT reacts with  $O_2^-$  and produces a dark blue compound. I did not detect any brown staining in the *PpGRAS7*-iOE-1 line indicating an elevated level of *PpGRAS7* does not affect the  $H_2O_2$  level. While I did not detect blue staining in the WT and the non-induced *PpGRAS7*-iOE-1 line, I observed dark-blue staining in the tissue of the induced *PpGRAS7*-iOE-1 line indicating elevated  $O_2^-$  levels (Fig. 13b).

Previous studies in *A. thaliana* showed that autophagy and senescence are two established cellular pathways that are involved in the degradation of chloroplast proteins (Martinez *et al.*, 2008; Liu & Bassham, 2012). To address whether the activation of these pathways may underlie the observed changes in the chloroplast morphology and subsequent chloroplast degradation, I analyzed the expression of previously identified senescence-associated marker genes, *PpSAG12*, *PpSAG13*, *PpSAG18*, and *PpSINI* (Mukae *et al.*, 2015) in the *PpGRAS7*-iOE lines after the inducer treatment (Mukae *et al.*, 2015). Protonema tissues of the *PpGRAS7*-iOE lines were induced with the inducer for a period of 4 h and the expression of selected senescence-associated marker genes were analyzed by qRT-PCR. Transcript levels of *PpSAG13*, *PpSAG18*, and *PpSINI* were significantly increased in both *PpGRAS7*-iOE lines (Fig. 13c), whereas transcript levels of *PpSAG12* remained unaffected. Degradation and partial disruption of the plastid membrane of the induced *PpGRAS7*-iOE-1 line (Fig. 12a) may indicate the involvement of an autophagy-related process. Expression analysis of the reported *P. patens* autophagy marker genes *PpATG5* and *PpATG7* (Mukae *et al.*, 2015) during induction indicated significant upregulation of *PpATG5* in both *PpGRAS7*-iOE lines compared to the WT (Fig. 13d). The upregulation of the *PpATG5* gene might explain the degradation and partial disruption of plastids in the *PpGRAS7*-iOE lines upon the induction.

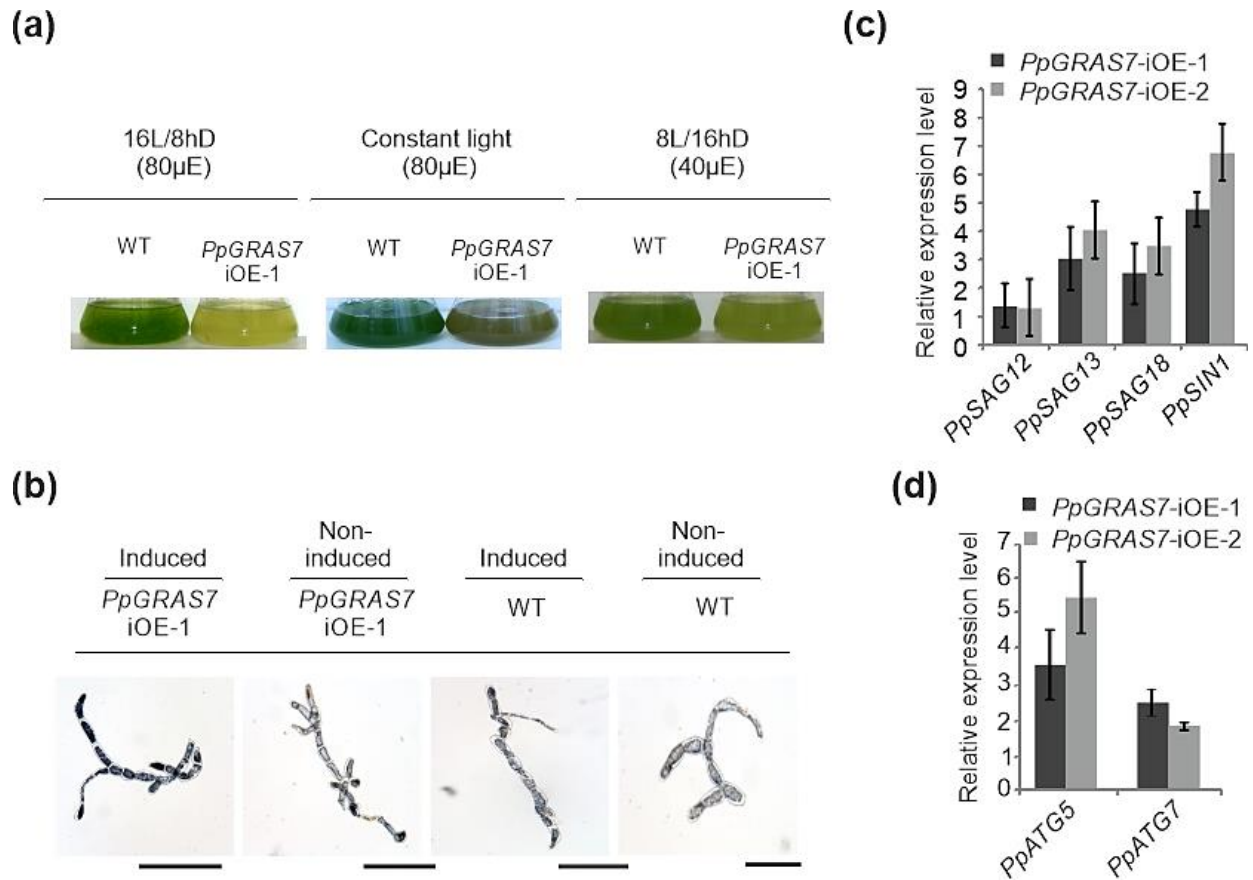


**Fig. 13. Light increases the severity of phenotype.** (a) Intensity and duration of light enhance the chlorotic phenotype severity. Protonema cultures from the WT and *PpGRAS7*-iOE-1 line were grown in the inducing liquid medium and exposed for 2 weeks to continuous light (80  $\mu$ E) or different day length regimes (16 h light (80  $\mu$ E) /8 h dark and 8 h light (40  $\mu$ E) /16 h dark). (b) ROS detection by NBT staining in protonema tissue from the WT and *PpGRAS7*-iOE-1 line after 8 h growth in normal (non-induced) or inducing medium (induced). Scale bar: 1 mm. (c) The relative expression level of senescence-related genes in the WT and *PpGRAS7*-iOE lines after 4 h of induction. Relative expressions were normalized to *PpEfla* and transcription rates in the WT levels were set to 1. Error bars indicate mean values  $\pm$  SE (n = 3). (d) The relative expression level of autophagy-related genes in the WT and *PpGRAS7*-iOE lines after 4 h of induction with the inducer. Relative expressions were normalized to *PpEfla* and transcription rates in the WT were set to 1. Error bars indicate mean values  $\pm$  SE (n = 3).

### 3.1.6 *PpGRAS7* overexpression lines display impaired photosynthesis

The inducer-dependent growth arrest and chlorosis led us to investigate the expression of a subset of genes involved in photosynthesis, cell growth, cell division, and stress response (Appendix 5). *P. patens* homologs of genes were identified using a BLAST search of *A. thaliana* proteins that have been associated with these processes as queries (Appendix 5) against the *P. patens* database (<http://www.cosmoss.org>). The best BLAST hits were considered as candidate homologs, which were subsequently confirmed by reciprocal BLAST against the *A. thaliana* database (<https://www.arabidopsis.org/>). Four-week-old *PpGRAS7*-iOE lines and WT were grown on solid medium with 2  $\mu$ M  $\beta$ -estradiol for 24 h and the expression of a set of candidate genes was analyzed by qRT-PCR. Sixty genes (Appendix 6: genes with a red plus) were analyzed and nineteen genes were found to be differentially regulated as compared to the WT (Fig. 14a). The chlorotic phenotype of the induced *PpGRAS7*-iOE lines might be linked to a stress response since three transcripts encoding a heat shock 70 protein (*PpHsp70*), a heat shock factor 3 (*PpHsf3*) and a 9-cis-epoxycarotenoid dioxygenase (*PpNCED*) were upregulated. A group of genes encoding protochlorophyllide oxidoreductase (*PpPORAa*, *PpPORA**b*), subunits of photosystem I (PSI) (*PpPsaA*, *PpPsaB*, *PpPsaC*) and II (PSII) (*PpPsbA*, *PpPsbD*, *PpPsbM*) and the light-harvesting chlorophyll *a/b* binding proteins (*PpLHCB2*) showed at least two-fold downregulation in response to an elevated *PpGRAS7* gene expression presumably contributing to the chlorosis and chloroplast damage. Furthermore, I found a reduction in the expression of a group of genes involved in cell growth and development including *CLAVATA1* (*PpCLV1*), *PpTIP2;2*, AGAMOUS protein like-1 (*PpAGL1*) and *CYCLIN-D1* (*PpCYCD1*). *CYCD1* is involved in the control of the cell cycle and cell division and its strong downregulation may extensively affect cell growth and growth arrest during induction (Fig. 10c, upper panel).

Based on the chlorotic phenotype and the altered gene expression of photosynthesis-related genes, I presumed that photosynthesis could be affected. In cooperation with Dr. Pablo Pulido (LMU biocentre, Germany), the accumulation of several proteins, which are involved in photosynthesis was analyzed in the  $\Delta$ *PpGRAS7*-1 line, *PpGRAS7*-iOE-1 line, and WT in a kinetic experiment (0 (non-induced), 2, 4, and 8 days) after the application of 2  $\mu$ M of  $\beta$ -estradiol (Fig. 14b). Thylakoid membrane proteins and soluble plastid proteins including LHCA, LHCB, PsaL, PsbQ, PsbD, Cytb<sub>6</sub>, and Cytf showed significantly reduced levels in *PpGRAS7*-iOE-1 line in

response to *PpGRAS7* overexpression, while expression levels of LHCA, LHCB, PsaL, PsbQ, PsbD, *Cytb<sub>6</sub>*, and *Cytf* were indistinguishable from the WT. Furthermore, a decrease of RbcL in response to the upregulation of *PpGRAS7* was detected in *PpGRAS7*-iOE-1 line. The detected changes in the abundance of proteins that represent crucial components of the main photosynthetic complexes prompted us to measure photosynthetic parameters in the *PpGRAS7*-iOE lines together with WT control. Pulse amplitude modulation (PAM) chlorophyll fluorescence parameters of the WT and *PpGRAS7*-iOE lines were analyzed (in cooperation with Dr. Pablo Pulido and Dr. Jörg Meurer, LMU biocenter, Germany) in a kinetic experiment (0 (non-induced), 2, 4, and 8 days) in the presence of 2  $\mu$ M of  $\beta$ -estradiol as well as the non-induced WT and *PpGRAS7*-iOE-1 line. The maximum quantum yield of PSII ( $F_v/F_m$ ) was comparable in the *PpGRAS7*-iOE-1 line and WT in the absence of the inducer. However,  $F_v/F_m$  gradually decreased in the *PpGRAS7*-iOE-1 line as compared to the WT within 8 days of induction (Fig. 14c and d). An even more pronounced kinetic reduction was detected for the effective quantum yield of PSII in the *PpGRAS7*-iOE-1 line (Fig. 14e). In addition, PSI parameters of the *PpGRAS7*-iOE-1 line revealed that the donor side of PSI is limited but not the acceptor side, which indicates that the electron transport towards the PSI is rate-limiting due to the deficiency of PSII and/or the intersystemic electron transport chain (Fig. 14f).

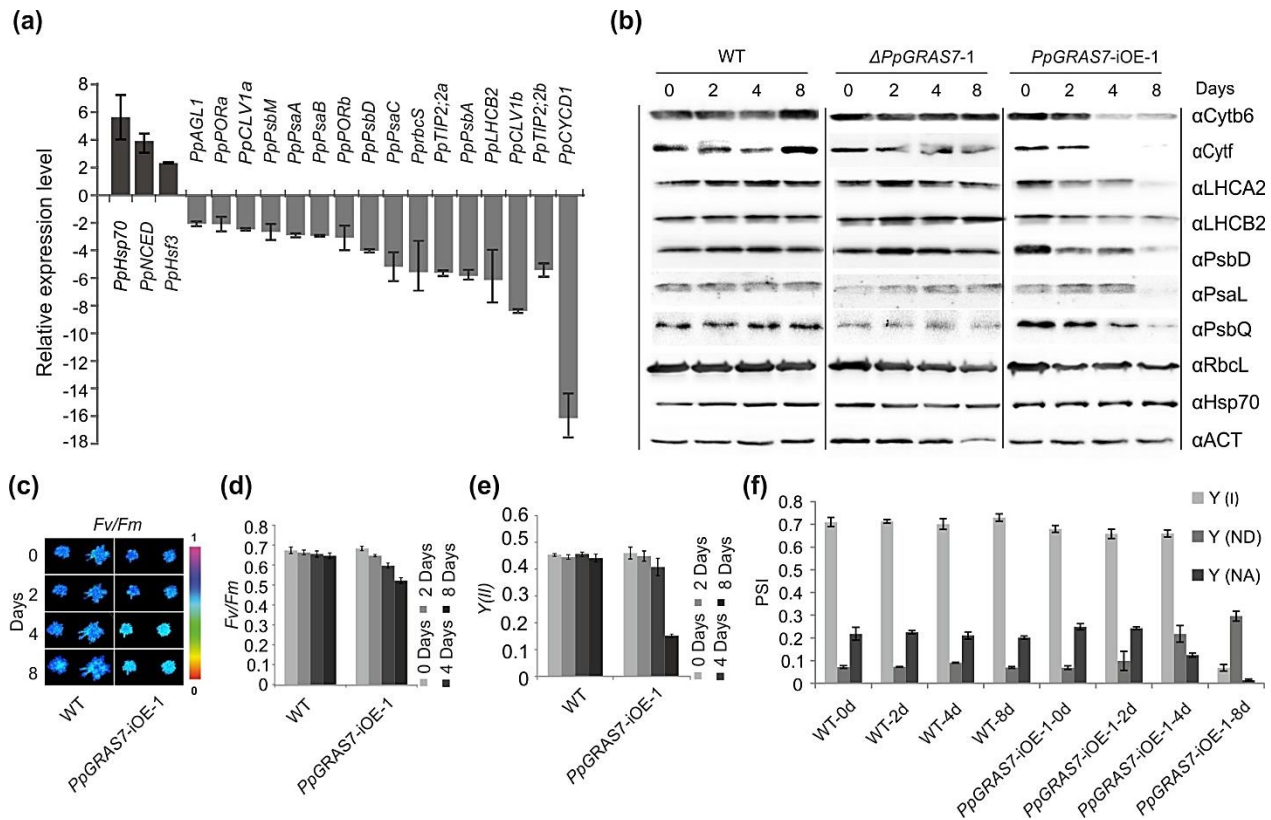


**Fig. 14. Expression analysis of plastid proteins and photosynthetic measurements in the  $\Delta PpGRAS7$  and *PpGRAS7-iOE* lines.** (a) Expression of genes in response to *PpGRAS7* upregulation. Plants were grown on standard solid growth medium for 4 weeks, induced for 24 h and RNA from gametophore tissue was used for qRT-PCR. Error bars indicate mean values  $\pm$  SE ( $n = 2$ ). (b) Plastid proteins were analyzed from samples harvested at the indicated time points (0 (untreated), and 2, 4, and 8 days after induction with 2  $\mu$ M of  $\beta$ -estradiol). Representative images of immunoblots with the indicated antibodies are shown. Equal amounts of total proteins from the WT, *PpGRAS7* mutant ( $\Delta PpGRAS7$ ), and *PpGRAS7-iOE-1* lines were examined.  $\alpha$ ATC was used as a control. (c) Chlorophyll fluorescence images of the *PpGRAS7-iOE* lines examined at the indicated time points after the application of 2  $\mu$ M of  $\beta$ -estradiol. The color scale indicates the photosynthetic parameter *Fv/Fm* signal intensities. (d) Quantification of *Fv/Fm* values from panel c. Error bars indicate mean values  $\pm$  SE ( $n = 3$ ). (e) The effective quantum yield of PSII ( $Y(II)$ ) at the indicated time points after the application of 2  $\mu$ M of  $\beta$ -estradiol (f). PSI absorbance measurements. Error bars indicate mean values  $\pm$  SE ( $n = 3$ ).

### 3.1.7 *PpGRAS7* overexpression affects pigment accumulation

Based on the observed chlorotic phenotype in the *PpGRAS7-iOE* lines, I assumed an alteration in pigments. To quantify chlorosis, pigment analysis was carried out in cooperation with Dr. Martin Lehmann (LMU biocenter, Germany). Chlorophyll extraction was carried out 8 days after the induction of gametophores from the *PpGRAS7-iOE* lines and WT with 2  $\mu$ M  $\beta$ -estradiol. Total

chlorophyll analyses revealed a lower chlorophyll *a* to chlorophyll *b* ratio upon *PpGRAS7* overexpression (Fig. 15a). The reduction of photosystem II efficiency is associated with a reduced content of chlorophylls, carotenoids and a lower chlorophyll *a* to chlorophyll *b* ratio. *PpGRAS7*-iOE-1 line as well as WT were grown in the standard liquid medium and 2  $\mu$ M of  $\beta$ -estradiol was applied for 2, 4, and 8 days. Several pigment compounds showed a differential pattern in the induced transgenic lines when compared to the induced WT controls. The compounds can be divided into three distinct subclasses: pigments, which are precursors of carotenoid biosynthesis, compounds produced upon the chlorophyll degradation, and compounds, which are involved in porphyrin and chlorophyll metabolism. A gradual reduction of carotenoid derivative 1 (4-Ketomyxol), carotenoid derivative 2 (adonixanthin), carotenoid derivative 3 (capsanthin), and carotenoid derivative 4 (zeinoxanthin) that reached the maximum 8 days after  $\beta$ -estradiol-mediated transgene induction was observed in the *PpGRAS7*-iOE-1 line (Fig. 15b). The chlorophyll degradation product dioxobilin-type non-fluorescent chlorophyll catabolite-618 (DNCC-618) showed an up to the 9-fold increase in the *PpGRAS7*-iOE-1 line 8 days after induction (Fig. 15c). In contrast, the pheophytin *a* level gradually decreased and was hardly detectable in the *PpGRAS7*-iOE-1 line after 8 days of induction (Fig. 15c). Compounds of the chlorophyll biosynthetic pathway including protoporphyrin IX, protochlorophyllide *a* and hydroxychlorophyll *a* also showed a marked reduction in the *PpGRAS7*-iOE-1 line at all time points that might explain the reduction of total chlorophyll (Fig. 15d).

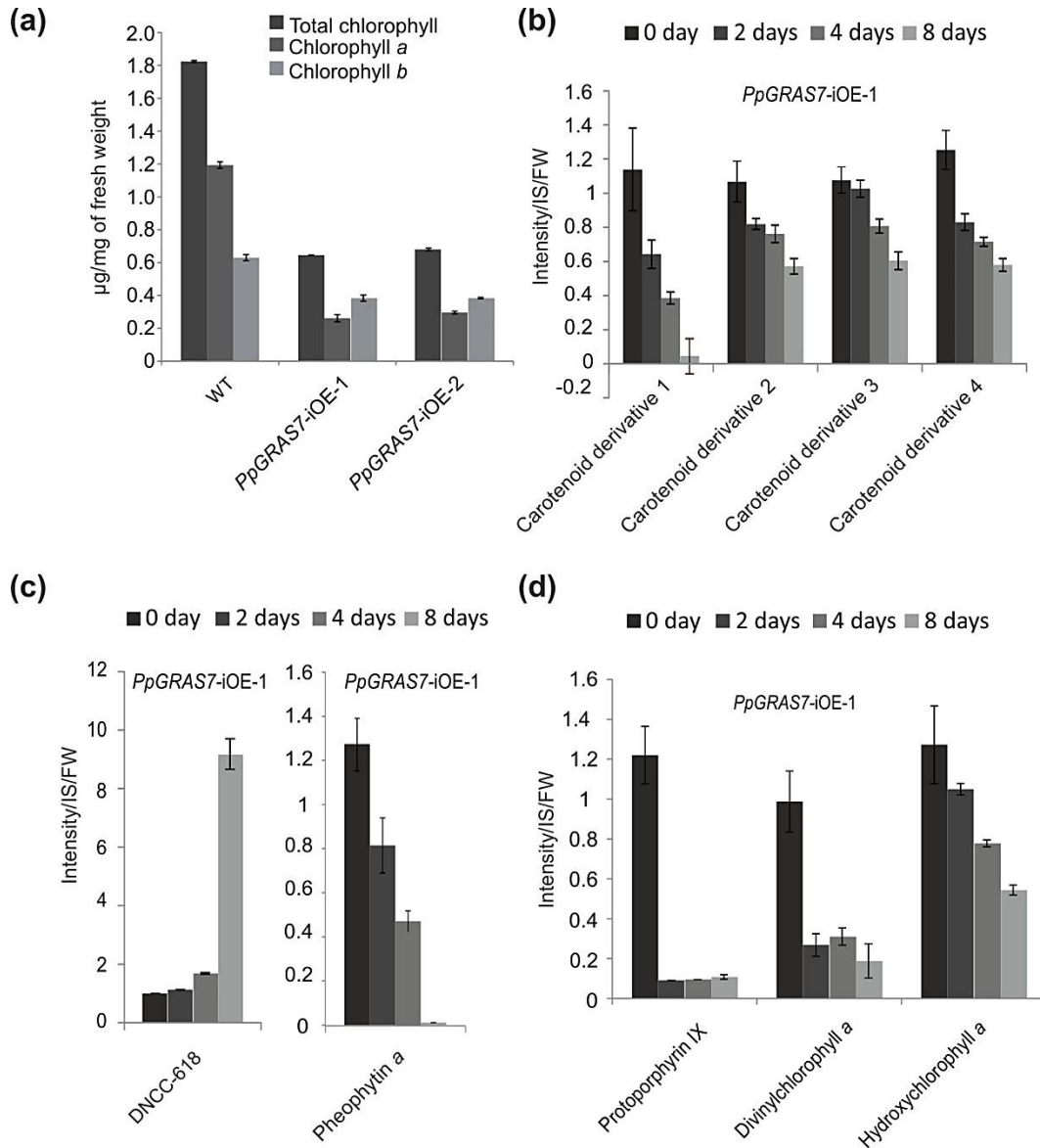


**Fig. 15. Pigment analysis in response to transgene induction in the *PpGRAS7-iOE-1* line.** (a) The chlorophyll content was analyzed from protonema tissues grown in the standard liquid medium after 8 days of induction. Error bars indicate mean values  $\pm$  SE (n = 3). (b) Pigments and intermediate products of carotenoid biosynthesis. Pigments were extracted from 6 biological replicates and analyzed. Carotenoid derivative 1: 4-Ketomyxol. Carotenoid derivative 2: Adonixanthin. Carotenoid derivative 3: Capsanthin. Carotenoid derivative 4: Zeinoxanthin. Error bars indicate mean values  $\pm$  SE (n = 6). (c) Pigments produced during chlorophyll degradation. Pigments were extracted from 6 biological replicates and analyzed. Error bars indicate mean values  $\pm$  SE (n = 6). (d) Specific products and intermediates of the porphyrin metabolism. Pigments produced during chlorophyll degradation. Pigments were extracted from 6 biological replicates and analyzed. Error bars indicate mean values  $\pm$  SE (n = 6). Intensity/IS/FW: The intensity of detected signals/ intensity of the internal control/fresh weight. Note: Pigments were extracted from protonema tissues grown in the standard liquid medium 0, 2, 4, and 8 days after the induction. All-time points were compared with non-induced (time 0) and the WT. WT levels were set to 1.

## 3.2 Phenotypical and functional analysis of *PpGRAS12* mutants

### 3.2.1 The knockout of nuclear-localized *PpGRAS12* causes defects in sporophyte production

The plant-specific *GRAS* genes are a family of transcription factors with a key role in plant growth and development. Harboring the *GRAS* domain categorized *PpGRAS12* as a member of the *GRAS* family (Fig. 16).

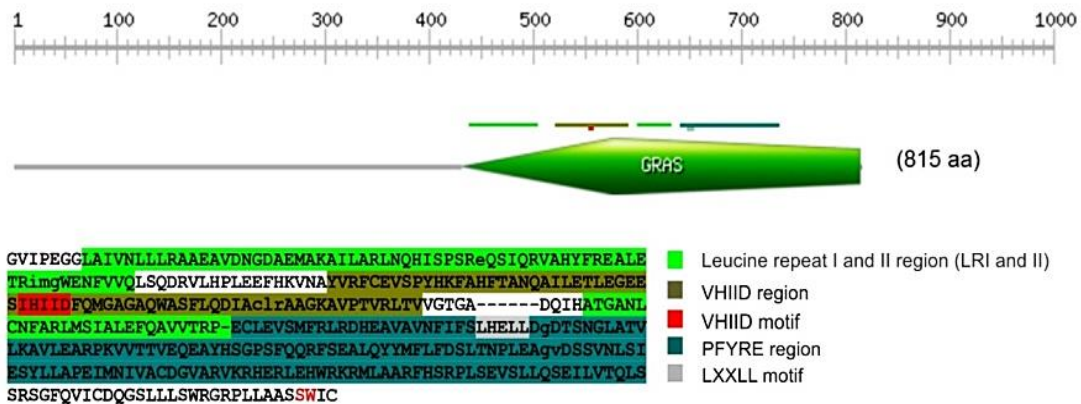


**Fig. 16. GRAS domain structure in *PpGRAS12*.** GRAS domain prediction and GRAS domain motifs prediction using EXPASY-PROSITE (<https://prosite.expasy.org/>).

The subcellular localization assay was performed to study the capability of *PpGRAS12* to act as a transcription factor. Using the transient expression of *PpGRAS12::citrine* protein fusion in *P. patens* protoplasts, a nuclear localization pattern as well as a cytoplasmic accumulation for *PpGRAS12*, was observed by laser scanning confocal microscopy. The citrine fluorescence signals in the transformed protoplasts overlapped with nuclei stained by 4',6-diamidino-2-phenylindole (DAPI) (Fig. 17). This observation (nuclear localization) was in agreement with the proposed function of *GRAS* proteins as transcription factors (Di Laurenzio *et al.*, 1996; Gallagher & Benfey, 2009; Heo *et al.*, 2011; Yoshida *et al.*, 2014). In addition, there are two possible explanations for the cytoplasmic accumulation of the *PpGRAS12*. First, it might be due to the ectopic expression

of the PpGRAS12 and the second possibility is that the localization of PpGRAS12 requires a dimer partner and possibly because of a limited amount of the dimer partner PpGRAS12 is detectable in the cytoplasm.

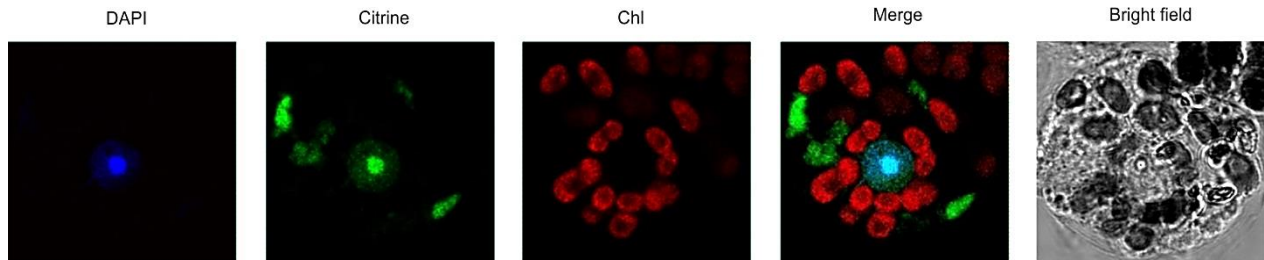


**Fig. 17. Subcellular localization of the PpGRAS12::citrine protein fusion in *P. patens* protoplast.** Pictures were taken 3 days after transfection of the PpGRAS12::citrine fusion into *P. patens* protoplasts. DAPI: DAPI signal. Citrine: citrine signal. Chl: chlorophyll auto-fluorescence. Merge: merged images of citrine and chlorophyll auto-fluorescence.

To analyze the function of *PpGRAS12*,  $\Delta PpGRAS12$  targeted knockout lines were previously generated by Strotbek (2015). The  $\Delta PpGRAS12$  lines were generated by the targeted disruption via the insertion of the *nptII* cassette at the *PpGRAS12* locus (Fig. 18a). Using homologous recombination, gene targeting was performed and two independent knockout lines were selected by 5' and 3' integration PCR (Strotbek, 2015) and loss of the *PpGRAS12* transcript confirmed by reverse transcriptase PCR (RT-PCR) (Fig. 18b). In the primary phase of growth including protonema and budding stage, no distinct differences were observed in the  $\Delta PpGRAS12$  lines compared to the WT. Mild phenotypic deviations (formation of shorter gametophores compared to the WT) were observed in the  $\Delta PpGRAS12$  lines at the gametophytic growth stage (Fig. 18c) and confirmed by the statistical comparison of the length of gametophore in the WT and two independent  $\Delta PpGRAS12$  lines (Fig. 18d). Further phenotypic analysis revealed that the absence of the *PpGRAS12* gene significantly influences the sporophytic stage and consequently fewer sporophytes were produced in the knockout lines compared to the WT (Fig. 18e).

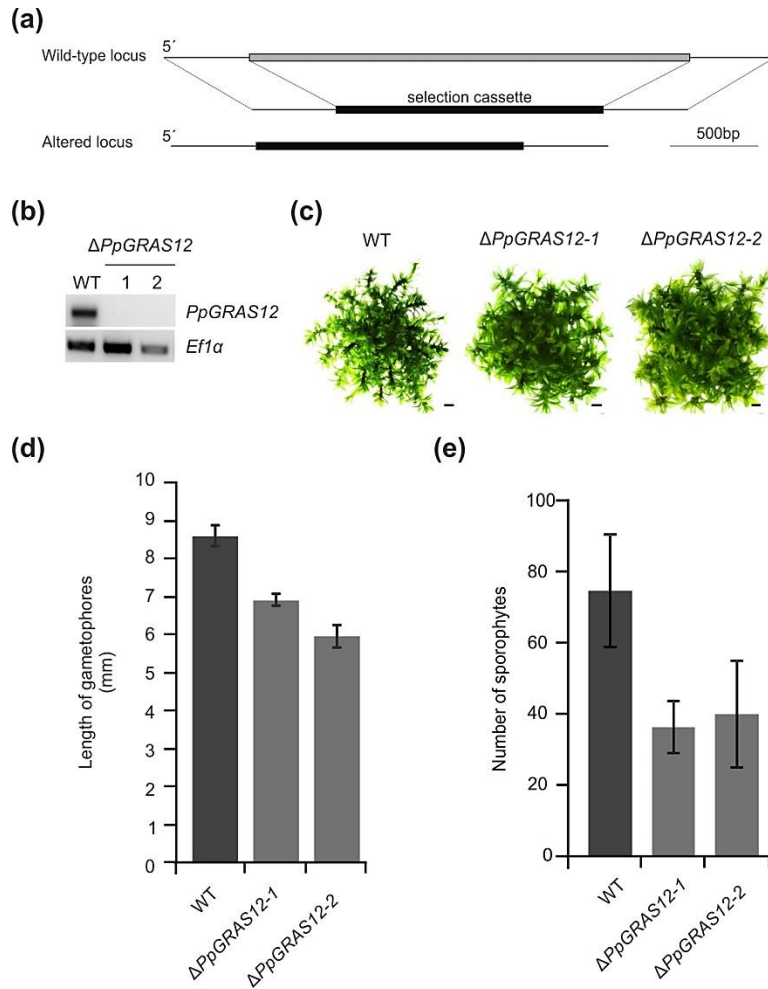


**Fig. 18. Generation and phenotypic analysis of the  $\Delta PpGRAS12$  lines.** (a) Scheme depicting the targeted knockout approach of the *PpGRAS12* coding sequence. (b) RT-PCR from cDNA derived from the indicated lines using *PpGRAS12*-specific primers; note that the two  $\Delta PpGRAS12$  mutant lines are null mutants lacking the *PpGRAS12* transcript; RT-PCRs performed with primers for the constitutively expressed gene *PpEflα* served as a control to monitor successful cDNA synthesis. (c) Phenotypic analyses of the knockout lines. Initially, a single gametophore from the indicated lines was cultured on standard growth medium and pictures were taken after 45 days of growth under standard growth conditions. Scale bars: 1 mm. (d) Comparison of the gametophore length in the WT and two independent  $\Delta PpGRAS12$  lines. Gametophore length was measured from colonies grown for 45 days under standard growth conditions; error bars represent standard errors (n = 30). (e) Comparison of the sporophyte numbers in the WT and two independent  $\Delta PpGRAS12$  lines; error bars represent standard errors (n = 27).

### 3.2.2 *PpGRAS12* overexpression leads to the formation of multiple apical meristems

I observed a mild phenotypic deviation in the  $\Delta PpGRAS12$  lines at the gametophytic growth stage (Fig. 18c and d) and prominent phenotypic aberrations at the sporophytic generation (Fig.

18e). To analyze the impact on *P. patens* growth and development upon *PpGRAS12* overexpression, *PpGRAS12* inducible overexpression lines (*PpGRAS12*-iOE lines) were previously generated by Strotbek (2015).

Phenotypic analysis of the *PpGRAS12*-iOE lines as well as WT was performed by adjusting pure protonema cultures to an equal density of 100 mg/l dry weight and 5  $\mu$ l of the adjusted cultures were spotted onto standard solid growth medium supplemented with 2  $\mu$ M of  $\beta$ -estradiol or without inducer. I did not observe any phenotypic differences between WT and both *PpGRAS12*-iOE lines on standard growth medium without inducer. Highly specific and distinct growth arrests were observed in the *PpGRAS12*-iOE lines upon the induction (Fig. 19a, upper panel). Interestingly, I observed that the *PpGRAS12*-iOE lines were able to recover after release to non-inducing conditions (Fig. 19a, lower panel). For the growth behavior analysis of the *PpGRAS12*-iOE lines in the liquid medium, protonema tissues from the WT and both *PpGRAS12*-iOE lines were transferred into the liquid medium supplemented with 2  $\mu$ M of  $\beta$ -estradiol and growth of the cultures was monitored by the determination of the dry weight every 2 days. I observed a decrease in the growth rate of both *PpGRAS12*-iOE lines compared to the WT 2 days after the induction (Fig. 19b). The decrease in the growth rate of both *PpGRAS12*-iOE lines was followed a downward trend until 8 days of growth in the induced medium and then a slight recovery was observed in both *PpGRAS12*-iOE lines (Fig. 19b). However, the growth rate in both *PpGRAS12*-iOE lines was less than the WT after 12 days of growth in the induced medium. The slight increase after 8 days might be related to the gradual degradation of the inducer. Additionally, the influence of *PpGRAS12* induction at later growth stages with colonies that were grown on solid medium and developed leafy gametophores was investigated. For this, 2  $\mu$ M of  $\beta$ -estradiol was directly applied onto the colonies of both *PpGRAS12*-iOE lines as well as WT. Strikingly, atypical enlargement of the stem-like structures in the vicinity of the gametophore tip cell was observed in both *PpGRAS12*-iOE lines 7 days after the induction (Fig. 19c). Furthermore, I noticed an abnormal enlarged structure at the tip cell of both *PpGRAS12*-iOE lines (Fig. 19c). Further investigation using scanning electron microscopy revealed that the abnormal structure, which was formed in response to an elevated level of *PpGRAS12* at the tip cell zone, is indeed multiple apical meristems (Fig. 19d).

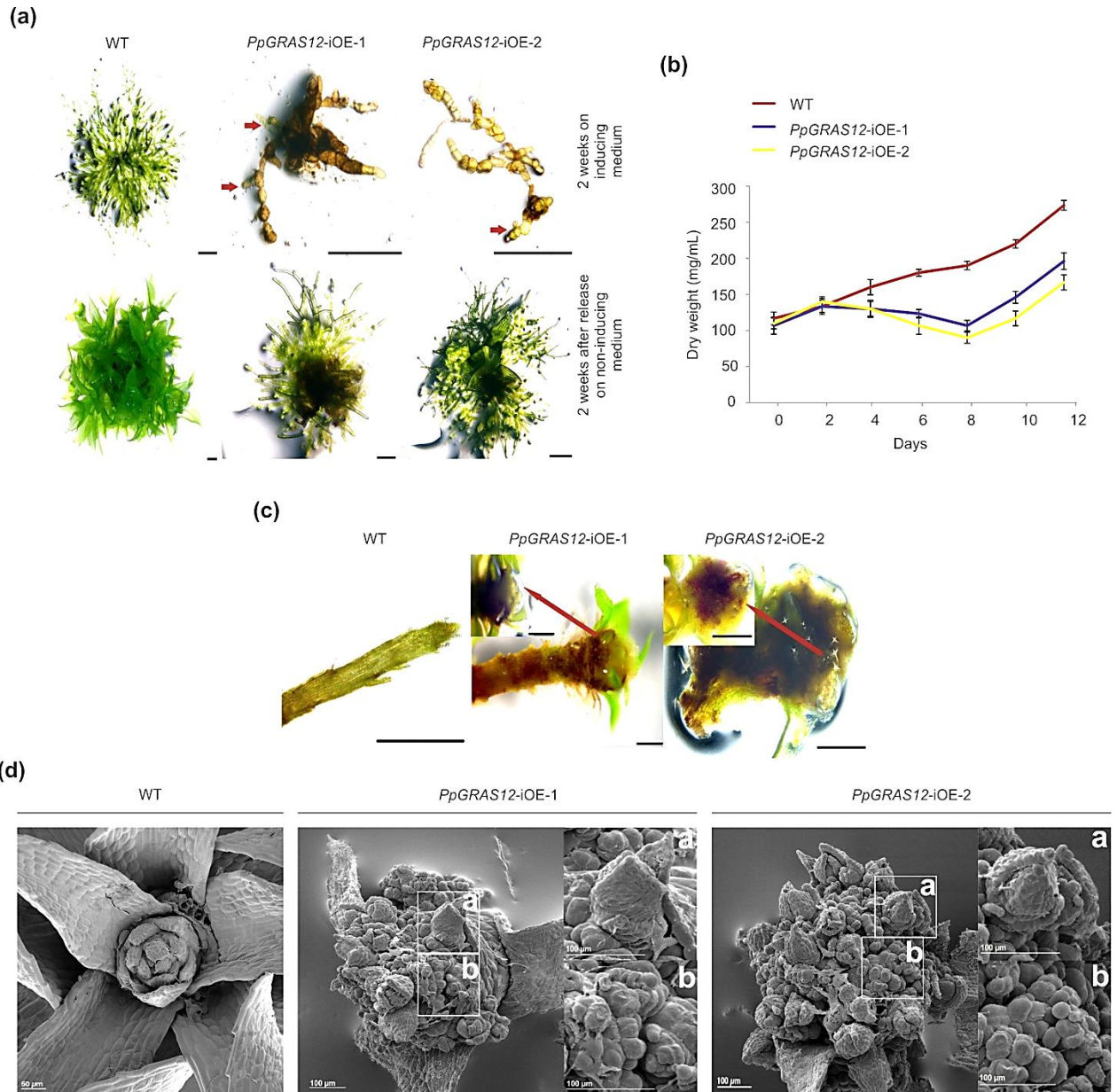


**Fig. 19. Phenotypic analysis of the *PpGRAS12*-iOE lines.** (a) Equal amounts of protonema tissues from the WT and both *PpGRAS12*-iOE lines were spotted on standard solid growth medium supplemented with 2  $\mu$ M  $\beta$ -estradiol. Upper panel: protonema tissue after growth for 14 days on the medium supplemented with 2  $\mu$ M  $\beta$ -estradiol. Lower panel: 14 days after growth on inducing medium protonema tissue was transferred onto standard growth medium without inducer for 2 weeks. Red arrows: green cells. Scale bars: 1 mm. (b) *PpGRAS12*-iOE lines and WT were grown in the standard liquid medium. The pure protonema from the *PpGRAS12*-iOE lines and WT were induced with 2  $\mu$ M of  $\beta$ -estradiol and dry weight of samples was measured every 2 days for a period of 12 days. Error bars indicate mean values  $\pm$  SE ( $n = 3$ ). (c) Formation of abnormal structures at the tip cell of both *PpGRAS12*-iOE lines. Scale bar: 1 mm for the WT and 0.5 mm for the mutants. (d) SEM analysis of *PpGRAS12*-iOE lines. Multiple apical meristem formation in the *PpGRAS12*-iOE lines upon the induction with 2  $\mu$ M of  $\beta$ -estradiol. Box a: a leafy gametophore that was formed from an individual apical meristem. Box b: multiple apical meristems.

Moreover, individual apical cells were able to form a leafy gametophore (Fig. 19d and 20a). If a new gametophore, which has previously emerged from an individual apical meristem, once more was exposed to the inducer, multiple apical meristems were formed over again from the tip cell (Fig. 20b).

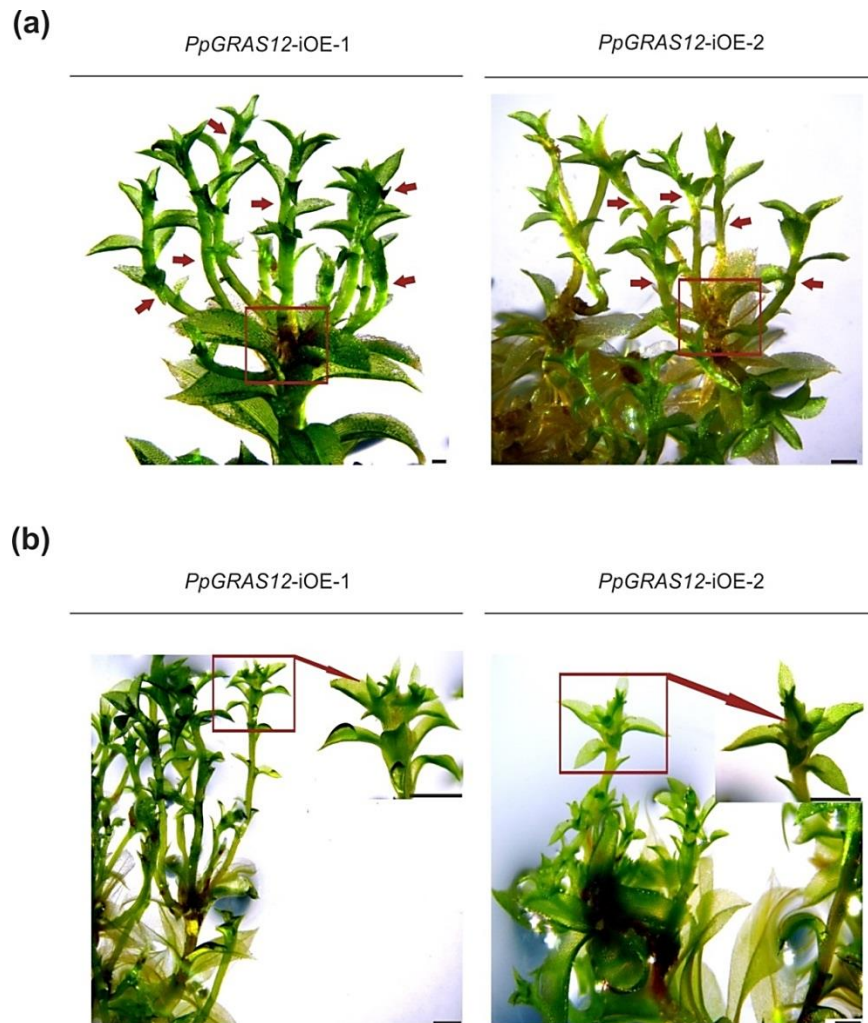


**Fig. 20. Multiple gametophore formation from multiple apical meristems in the induced *PpGRAS12*-iOE lines.** (a) Multiple gametophores were formed from multiple apical meristems in the *PpGRAS12*-iOE lines upon the induction. The red box shows the development of multiple gametophores from apical meristems in the *PpGRAS12*-iOE lines. Red arrows indicate a single gametophore. Pictures were taken 75 days after the induction; scale bar: 1 mm. (b) Renewal of induction resulted in the formation of multiple apical meristems and consequently the formation of multiple gametophores on the top of previous gametophores. The red arrow shows multiple gametophores. Pictures were taken, 12 days after the renewal of induction; scale bar: 1 mm.

It was assumed that the continuous induction of *PpGRAS12* with the inducer results in the maintenance of multiple apical meristems, whereas degradation of the inducer leads to the formation of new gametophores from multiple meristems. To monitor *PpGRAS12* induction during the experiment, *PpGRAS12*-iOE lines were induced with the inducer and gametophores were harvested after 4 hours, 3 weeks, and 8 weeks. *PpGRAS12* expression analysis by qRT-PCR revealed 150-fold induction of the transcript after 4 h of induction (Fig. 21a). Compatible with my hypothesis, I observed a decrease of the *PpGRAS12* transcript level to WT level after 3 and 8 weeks of induction. This finding supports the idea that the continuous induction of *PpGRAS12* leads to the formation and maintenance of multiple apical meristems in *P. patens*. In contrast, the gradual degradation of  $\beta$ -estradiol results in reduced level of *PpGRAS12* and consequently the development of gametophores from multiple apical meristems. *A. thaliana CLV1* was previously reported to play an important role in maintaining meristem identity and controlling meristem size (Clark *et al.*, 1993). *PpCLV1* (Whitewoods *et al.*, 2018) expression analysis by qRT-PCR showed downregulation of both *PpCLV1a* and *PpCLV1b* in response to the upregulation of *PpGRAS12* (Fig. 21b).

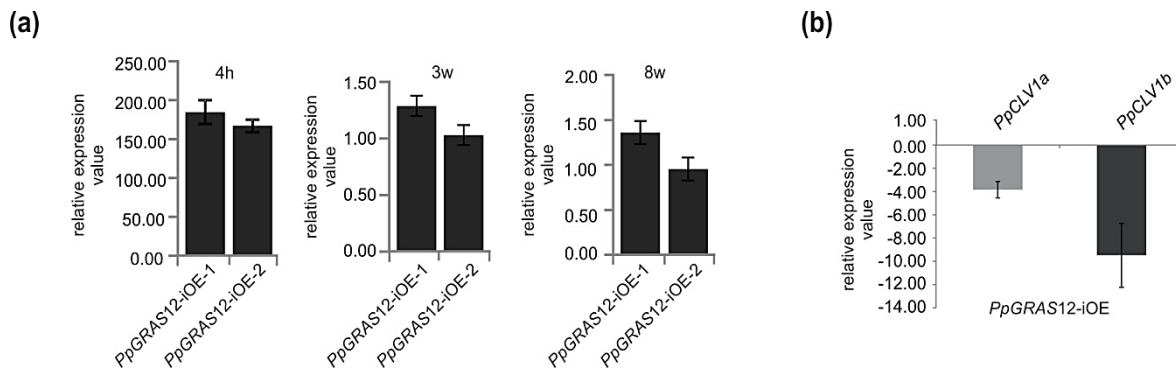


**Fig. 21. Expression analysis of *PpGRAS12*.** (a) The relative expression level of *PpGRAS12*. Lines were induced with 2  $\mu$ M  $\beta$ -estradiol and expression levels of *PpGRAS12* in the induced lines and the induced WT, were monitored after 4 h (hours), 3 w (weeks), and 8 w (weeks) of induction via qRT-PCR using the *PpGRAS12*-specific primers (Appendix 6). Relative expressions were normalized to *PpEfl1a* and transcript levels in the WT were set to 1. Error bars indicate mean values  $\pm$  SE (n = 3). (b) The relative expression levels of *PpCLV1* genes in the WT and *PpGRAS12*-iOE lines. Plants were grown on standard solid growth medium for 4 weeks, induced for 24 h and RNA from gametophore tissue was used for qRT-PCR. Relative expressions were normalized to *PpEfl1a* and transcript rates in the WT were set to 1. Error bars indicate mean values  $\pm$  SE (n = 2).

### 3.2.3 MiR171 regulates *PpGRAS12*

Plant miRNAs frequently play a role in defining the spatiotemporal expression of their cognate target mRNAs. To study whether miR171 regulates the spatiotemporal expression of *PpGRAS12*, the *PpGRAS12::GUS* protein fusion reporter lines were generated. To generate the *PpGRAS12::GUS* protein fusion reporter lines, the *PpGRAS12* coding sequence harboring a mutated miR171 binding site or the native coding sequence (miR171-sensitive) (Appendix 3) was fused to the *GUS* coding sequence and introduced to their cognate genomic locus by means of homologous recombination (Fig. 22a). Constructs were detected via PCR screening (purple primers) (Fig. 22b). The precise integration of the *PpGRAS12::GUS* fusion construct into the genome was confirmed for two independent lines by 5' (black primers, Fig. 22b) and 3' (red primers, Fig. 22b) integration PCR (Fig. 22c). Validation of the m*PpGRAS12::GUS* (miR171-resistant) was performed for two positive lines by subsequent digestion of RT-PCR products with *PauI* (GCGCGC) that was introduced within the miR171 binding site of the m*PpGRAS12::GUS* fusion construct as silent mutations (Fig. 22d and Appendix 3).

The natural expression of the *PpGRAS12* gene is low and below the histochemical GUS staining detection limit. Histochemical GUS staining was performed for both miR171-resistant and miR171-sensitive lines. The correspondent blue color, which shows the activity of the GUS and consequently the expression of *PpGRAS12* gene, was not observed in *PpGRAS12::GUS* protein fusion reporter lines at protenema and gametophore stages. However, the blue color was only detected in the archegonia and egg cells of m*PpGRAS12::GUS* protein fusion reporter lines (Fig. 23). Expression of GUS in archegonia and egg cell of the miR171-resistant lines indicates that miR171 significantly regulates expression of *PpGRAS12* in archegonia and egg cells.

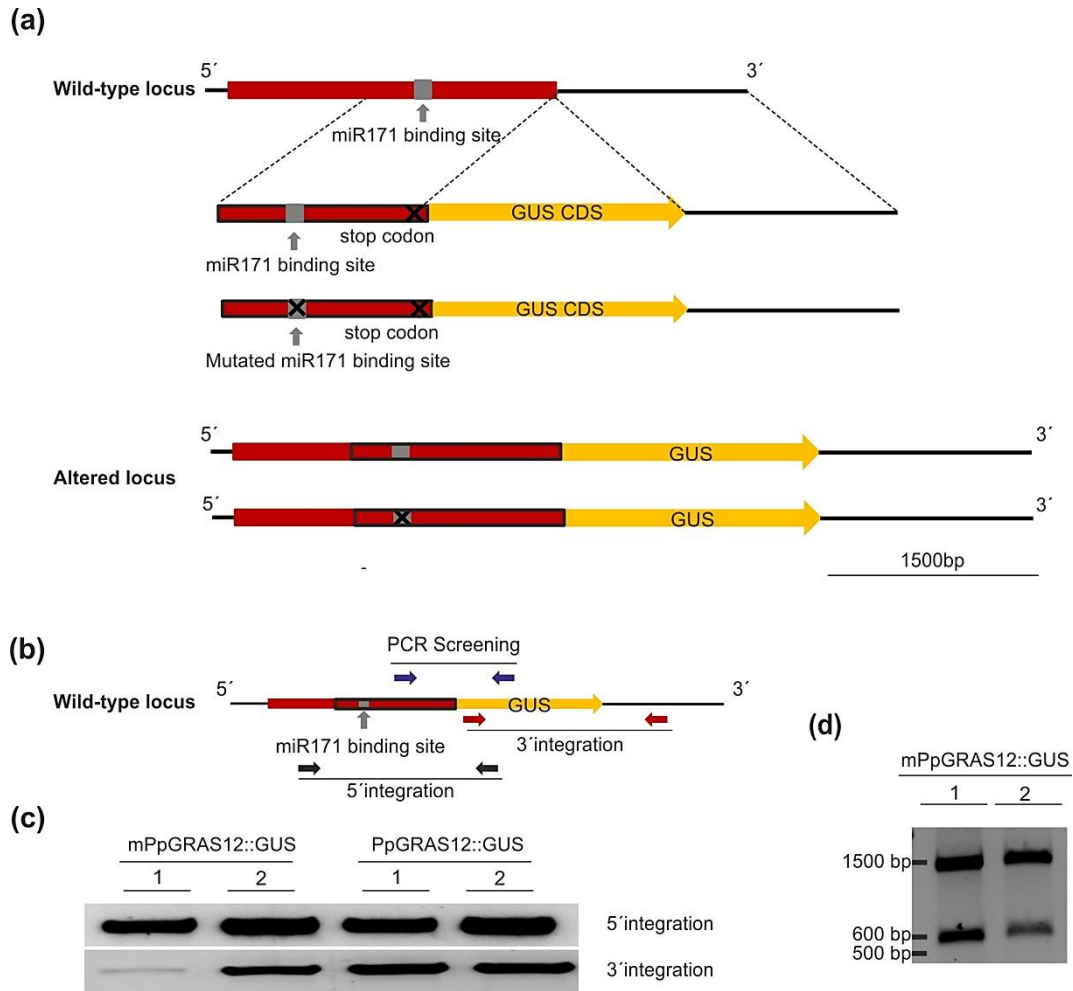


**Fig. 22. Generation of the PpGRAS12::GUS protein fusion reporter lines.** (a) Scheme representing the generation of the PpGRAS12::GUS and mPpGRAS12::GUS fusion reporter constructs. Two variants of GUS fusion reporter constructs (PpGRAS12::GUS fusion reporter constructs with the native miR171 binding site and mPpGRAS12::GUS fusion reporter construct with the mutated miR171 binding site) were generated and introduced to their cognate genomic locus by means of homologous recombination. The red box indicates the *PpGRAS12* coding region. The red box with the black border lines indicates 1482 bp from the coding sequence including the miR171 binding site (native/mutated), which was fused to *GUS* coding sequence (yellow box). The *PpGRAS12* stop codon was removed and the coding sequence fused to the *GUS* coding sequence. (b) Purple, red, and black arrows show the primer pairs sequentially applied for PCR-based analyses of the PpGRAS12::GUS protein fusion reporter lines. (c) Upper panel: confirmation of 5' integration of the constructs using black (Appendix 1) primers. Lower panel: confirmation of 3' integration of the construct using red (Appendix 1) primers. (d) Validation of mPpGRAS12::GUS protein fusion reporter lines by digestion of RT-PCR products with *PauI* (GCGCGC) that was introduced within the miR171 binding site of the mPpGRAS12::GUS fusion construct as silent mutations.



**Fig. 23. Histochemical GUS staining of the PpGRAS12::GUS and mPpGRAS12::GUS protein fusion reporter lines.** Correspondent blue colors were detected only in the archegonia and egg cells of mPpGRAS12::GUS protein fusion reporter lines. Red arrows: egg cells. Scale bars 1 mm.

### **3.3 Overexpression of *AtRGA1*, *AtRGL1*, *AtSCL6-II*, *AtSCL6-III*, and *AtSCL6-IV* in *P. patens***

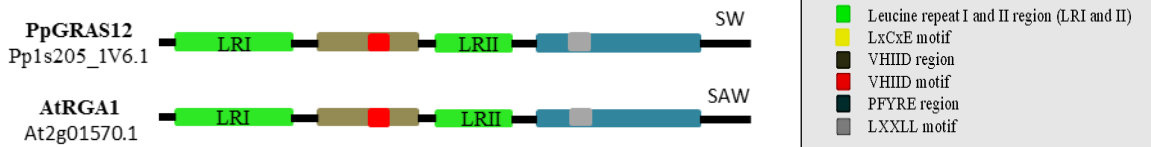
#### **3.3.1 *AtRGA1* and *AtRGL1* share the highest protein sequence similarities with *PpGRAS12* and *PpGRAS7***

GRAS protein subfamilies are known to be involved in various processes of plant growth and development. As it was shown in chapter 3 (3.1 and 3.2), *PpGRAS7* and *PpGRAS12* are members of the GRAS family; *PpGRAS7* is involved in plastid degradation and starch over-accumulation, whereas *PpGRAS12* plays roles in meristem maintenance. To investigate *PpGRAS7* and *PpGRAS12* homologs in *A. thaliana*, protein sequence analysis was performed. For this, the full-length *PpGRAS12* and *PpGRAS7* protein sequences were achieved from the *P. patens* database (<http://www.cosmoss.org>), and a BLAST search against the *A. thaliana* database (<https://www.arabidopsis.org/>) was carried out. Based on the protein sequence similarities, it was observed that *AtRGA1* shares the highest protein sequence similarity (37%) with *PpGRAS12* and *AtRGL1* shares the highest protein sequence similarity (37%) with *PpGRAS7* (Fig. 24a and b). *AtRGA1* (At2g01570.1) and *AtRGL1* (At1g66350.1) are members of the GRAS family (DELLA subfamily) and play a critical role in gibberellic acid signal transduction (Rich *et al.*, 2017). To gain insights into the function of *AtRGA1* and *AtRGL1* in *P. patens* I aimed to perform inducible overexpression of these genes in *P. patens*. To generate *AtRGA1* and *AtRGL1* inducible overexpression lines, a  $\beta$ -estradiol inducible gene expression system was used (Kubo *et al.*, 2013). Cloning, transformation, and selection were performed in the same way as described for the generation of the *PpGRAS7*-iOE lines (see 3.1.3). Using PCR-based screening, two independent *AtRGA1* overexpression (*AtRGA1*-iOE) and two independent *AtRGL1* overexpression (*AtRGL1*-iOE) lines were identified (Fig. 25a and b) (Appendix 1). *AtRGA1*-iOE lines were identified using the OE-screen<sup>2</sup>-F primer (forward primer) (Appendix 1), which binds within the promoter region of the *PpGX8* vector (70 bp upstream of the *AtRGA1* start codon) and the OE-screen<sup>2</sup>-R primer (reverse primer) (Appendix 1) that is located within the coding sequence of *AtRGA1*. The same strategy, but using OE-screen<sup>3</sup>-F primer (Appendix 1) and OE-screen<sup>3</sup>-R primer (Appendix 1) was applied to identify *AtRGL1*-iOE lines.

(a)

Score = 236 bits (602), Expect = 7e-68, Method: Compositional matrix adjust.  
Identities = 143/385 (37%), Positives = 215/385 (56%), Gaps = 27/385 (7%)

PpGRAS12	436	EGGLAIYVNLRLRAAEAVDNGDAEMAKAILARLNQHSRQSIQRVAHYFREALETRIM	495
AtRGA1	216	ENGVRLVHALMACAEAIQQNNLTAEALVKQIGC-LAVSQAGAMRKVATYFAEALARRI-	273
PpGRAS12	496	GWENFVVQLSQDRVLHPLEEFHKVNAYVRFCEVSPYHKFAHFTANQAILETLEGEESIHI	555
AtRGA1	274	----YRLSFPQNDHCLSDTLQMHFY----ETCPYLKFAHFTANQAILEAFEGKRRVHV	325
PpGRAS12	556	IDFQMGAGACWASFLQDIACLRRAAGKAVPTVRLTVVGTGA----DQIHATGANLGNFARL	611
AtRGA1	326	IDFSMNQGLQWPAALMQALA-LREGGP--PTFRLTGIGPPAPDNSDHLHEVGCCKLAQALAE	382
PpGRAS12	612	MSIALEFQAVVTRPEC-LEVSMFRLR--DHEAVAVNFIISLHELLEDGDTNGLATVLRKAV	668
AtRGA1	383	IHVFEYRGEFVANSIADLDASMLELRPSDTEAVAVNSVFELHRLKLL--GRPGGIEKVLGVV	440
PpGRAS12	669	LEARKVVTVTVEQAYHSGSPFQQRFSEALQYMFLEDSLTFLEAGVDSVNLISIESYL	728
AtRGA1	441	KQIKFVIITVVEQESNHNGPVFLDRFTESLHYSTLFDLSLE----GVFNSQDKVMSEVY	495
PpGRAS12	729	LAPEIMNIVACDGVARVRRHERLEHWRKRMLAARFHSRPLSEVSLQSEILVTLQLSRRSG	788
AtRGA1	496	LGIKQICNLVACEGPDVERHETLSQWGNRFSGSSGLAPAHLSNAFKAQSMLLSVFNSSGQG	555
PpGRAS12	789	FQVICDQSSLLSWRGRBLLAASW	813
AtRGA1	556	YRVEESNGCLMLGWHTREPLITTSAW	580



(b)

Score = 243 bits (621), Expect = 1e-72, Method: Compositional matrix adjust.  
Identities = 139/374 (37%), Positives = 202/374 (54%), Gaps = 19/374 (5%)

PpGRAS7	288	TGLQLVHLLLCAEAIISNQMDLAHVLTSLNMLVPCSTMTQRLAAVFDALHARITNS	347
AtRGL1	148	TG++LVH LL CAEA+ + LA ++ + + M+++A F + L RI	204
PpGRAS7	348	ATTGRYKGLERDNDVAIDLMLQSFV-IYDHTPFKLPHLTLNQTILDAVEGEPHVHVID	406
AtRGL1	205	----YRIYPRD-DVALSSFSDTLQIHFYESCPLYKFAHFTANQAILEVFAEAERKVVHVID	258
PpGRAS7	407	LNTGWRGMQWFGFIQALALRPGGPFKLRITAIKGA-DDLEHSREKLQDYARHLQVFFFC	465
AtRGL1	259	LGLN-HGLQWPAIQLALALRPNPFDRLTGIGYSLTDIQEVGWKLGQLASTIGVNFVFFK	317
PpGRAS7	466	PLVVD-MKSFVDRLLDMR-DWEVVCINSANQFHQLLIWGEDCFHKFLCDLKSINPRVLA	523
AtRGL1	318	STALNNLSDLKPEMLDIRPGLSEVAVNSVFELHRLLAHPG-SIDKFLSTIKSIRPDIMTV	376
PpGRAS7	524	TENDADHNSPKFLNRFPECLRYSAVYDALDSSLPNQSAALQVHFTGQKIRINIVAME	583
AtRGL1	377	VEQEANHNGTVFLDRFTESLHYSSLFDSLEGP-PSQDRVMSE---LFLGRQIINLVACE	432
PpGRAS7	584	GEDRITRHSLSWSRRMEMAGFRFPVSSRAISQAGLLLRMYFAQSGYTLRTENGNVSL	643
AtRGL1	433	GEDR+ RHE+L W R + GF+PV + S A QA +LL +Y GY + G + L	492
PpGRAS7	644	GWDNMSLVGASAWR	657
AtRGL1	493	GWQTRPLIATSAWR	506



**Fig. 24. Protein sequence and GRAS domain similarities between PpGRAS and AtDELLA subfamilies.** (a) AtRGA1 showed the highest protein sequence similarity to PpGRAS12. (b) AtRGL1 showed the highest protein sequence similarity to PpGRAS7. GRAS domain and GRAS domain motifs prediction were carried out using EXPASY-PROSITE (<https://prosite.expasy.org/>).

To validate the inducible expression of *AtRGAI* and *AtRGLI*, protonema tissues from two independent *AtRGAI*-iOE lines and two independent *AtRGLI*-iOE lines were treated for 4 h with the inducer and the induction of *AtRGAI* and *AtRGLI* was detected by RNA gel blots (Fig. 25c and d).

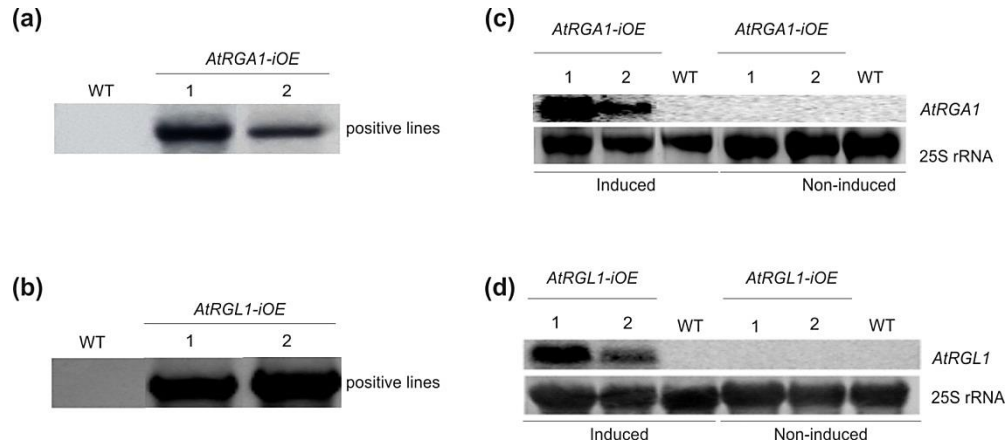


**Fig. 25. Screening and confirmation of the *AtRGAI*-iOE and *AtRGLI*-iOE lines.** (a) Screening of the *AtRGAI*-iOE lines using PGX8-specific (forward primer (OE-screen<sup>2</sup>-F), Appendix 1) and *AtRGAI*-specific (reverse primer (OE-screen<sup>2</sup>-R), Appendix 1) primers. Positive lines show amplified PCR products using genomic DNA from the indicated lines as a template. (b) Screening of the *AtRGLI*-iOE lines using PGX8-specific (forward primer (OE-screen<sup>3</sup>-F), Appendix 1) and *AtRGLI*-specific (reverse primer (OE-screen<sup>3</sup>-R), Appendix 1) primers. Positive lines show amplified PCR products using genomic DNA from the indicated lines as a template. (c) RNA gel blots from the WT and two independent *AtRGAI*-iOE lines. WT and two independent *AtRGAI*-iOE lines were grown for 4 h in the standard liquid medium (non-induced) or liquid medium supplemented with the inducer (induced). Subsequently, RNAs were harvested and used for the gel blot analysis. *AtRGAI*-specific probes were used for hybridizations. 25S rRNA (from the EtBR stained gel) was used to monitor equal loading. (d) RNA gel blots from the WT and two independent *AtRGLI*-iOE lines. WT and two independent *AtRGLI*-iOE lines were grown for 4 h in the standard liquid medium (non-induced) or liquid medium supplemented with the inducer (induced). Subsequently, RNAs were harvested and used for the gel blot analysis. *AtRGLI*-specific probes were used for hybridizations. 25S rRNA (from the EtBR stained gel) was used to monitor equal loading.

Next, a phenotypic analysis of the *AtRGAI*-iOE and *AtRGLI*-iOE lines was performed. For this, pure protonema cultures of the *AtRGAI*-iOE and *AtRGLI*-iOE lines as well as WT were adjusted to an equal density of 100 mg/l dry weight and 5  $\mu$ l of the adjusted cultures were spotted onto standard solid medium supplemented with 2  $\mu$ M  $\beta$ -estradiol or without inducer. No phenotypic differences were detected between WT and the mutants (two independent *AtRGAI*-iOE lines and two independent *AtRGLI*-iOE lines) on standard growth medium without inducer. I

observed a strict and distinct growth arrest in the *AtRGAI*-iOE lines at the protonema growth stage upon the induction (Fig. 26a). Besides, a strict and highly specific growth arrest was also observed in the *AtRGLI*-iOE lines at the protonema growth stage upon the induction (Fig. 26b). Additionally, I studied the influence of *AtRGAI* and *AtRGLI* induction at the later growth stage. For this, 2  $\mu$ M of  $\beta$ -estradiol was directly applied onto the colonies of *AtRGAI*-iOE and *AtRGLI*-iOE lines as well as WT that were grown on solid medium and developed leafy gametophores. The formation of multiple apical meristems and consequently the formation of multiple gametophores from multiple apical meristems was observed in the induced *AtRGAI*-iOE lines (Fig. 26c), which was partially comparable to the phenotype of the induced *PpGRAS12*-iOE lines. The slight phenotypic difference between the induced *AtRGAI*-iOE and *PpGRAS12*-iOE lines is referred to the size and number of formed gametophores from multiple apical meristems. It was noticed that less and smaller gametophores were formed from multiple apical meristems in the *AtRGAI*-iOE lines compared to the *PpGRAS12*-iOE lines upon the induction (Fig. 27). Formation of a reduced number of gametophores from multiple apical meristems in the *AtRGAI*-iOE lines compared to the *PpGRAS12*-iOE lines indicates that an elevated level of *AtRGAI* leads to the formation of less apical meristems in *P. patens*. Furthermore, chlorosis and browning of the tissues were observed in the *AtRGLI*-iOE lines upon the induction. The chlorotic phenotype in the *AtRGLI*-iOE lines was remarkably identical to the chlorotic phenotype of the *PpGRAS7*-iOE lines (Fig. 26d and 10e).

Based on the similarity of the observed chlorotic phenotype in the *AtRGLI*-iOE and *PpGRAS7*-iOE lines, the molecular analyses of *AtRGLI*-iOE lines were carried out. As it was shown in Fig. 12a, an elevated level of *PpGRAS7* led to a remarkable starch accumulation in *P. patens*. To investigate whether overexpression of *AtRGLI* results in over-accumulation of starch in *P. patens*, we performed transmission electron microscopy of phylloid tissues derived from WT and *AtRGLI*-iOE-1 line, which were treated for 8 days with the inducer. TEM results revealed no starch over-accumulation in the induced *AtRGLI*-iOE-1 line and the WT as compared to the induced *PpGRAS7*-iOE-1 line (Fig. 28a). This finding indicates, unlike *PpGRAS7* overexpression, an elevated level of *AtRGLI* does not lead to the starch over-accumulation in *P. patens*.

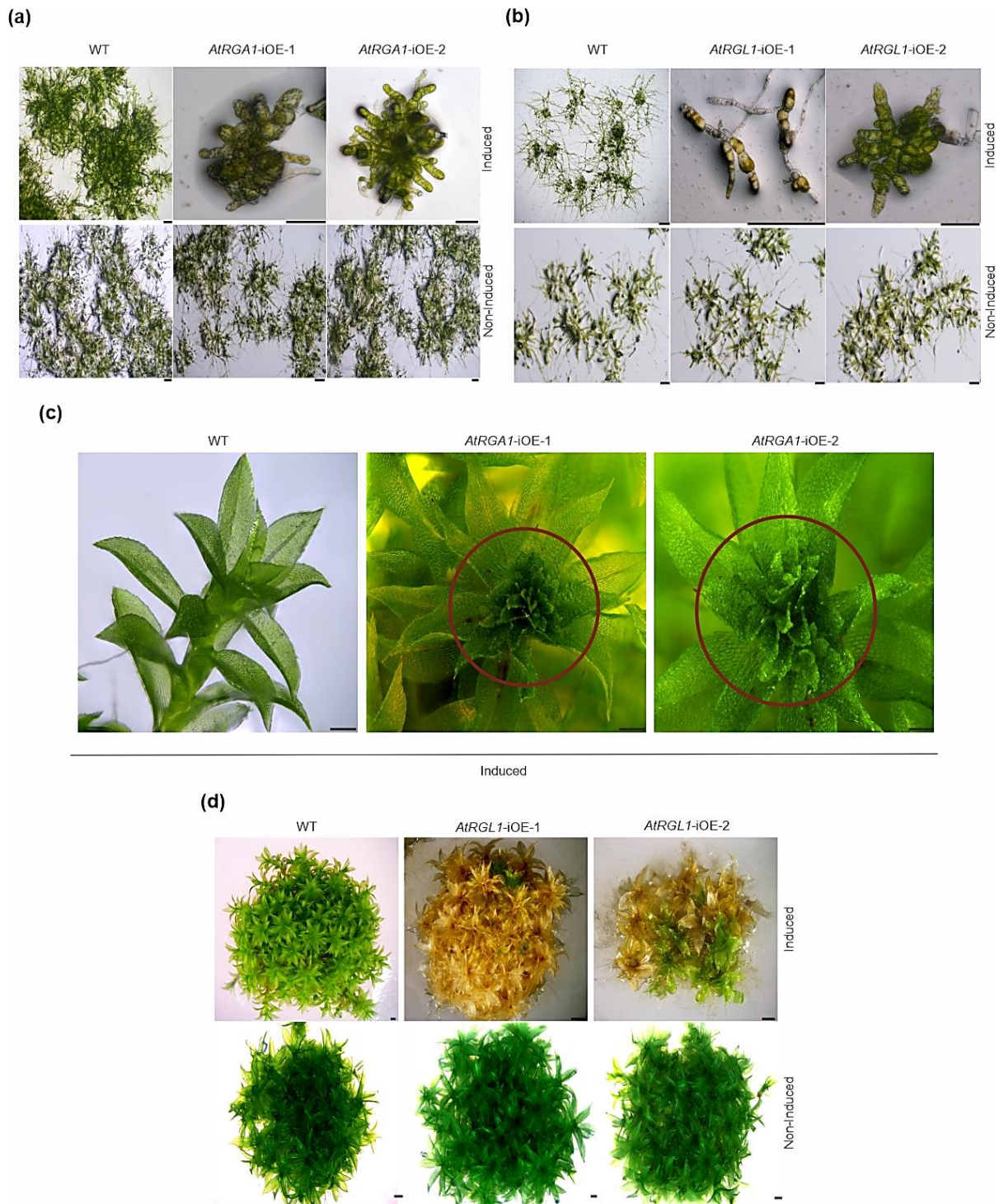


**Fig. 26. Phenotypic analysis of the *AtRGA*-iOE and *AtRGL1*-iOE lines.** (a) and (b) Equal amounts of protonema tissues from WT, *AtRGA1*-iOE lines (two independent lines) (a) and *AtRGL1*-iOE lines (two independent lines) (b) were spotted on standard growth medium supplemented with 2  $\mu$ M  $\beta$ -estradiol. Pictures were taken 14 days after the induction. Scale bars: 1 mm. (c) Multiple gametophore formation in the *AtRGL1*-iOE lines treated for a period of 4 weeks with 2  $\mu$ M  $\beta$ -estradiol. Scale bars: 1 mm. (d) Chlorosis in the *AtRGL1*-iOE lines treated for 4 weeks with 2  $\mu$ M  $\beta$ -estradiol. Scale bars: 1 mm.

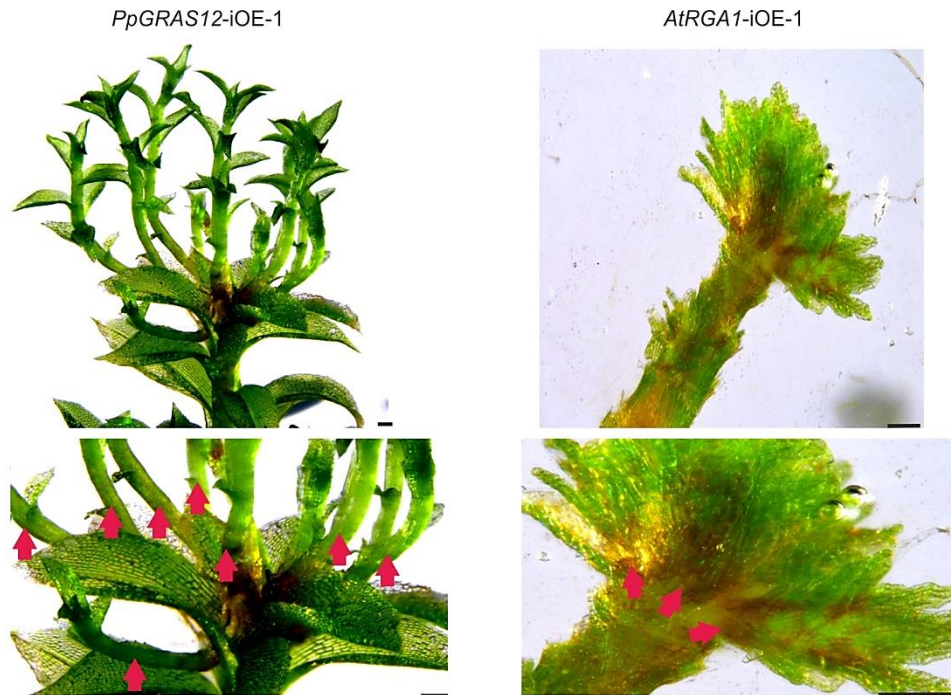
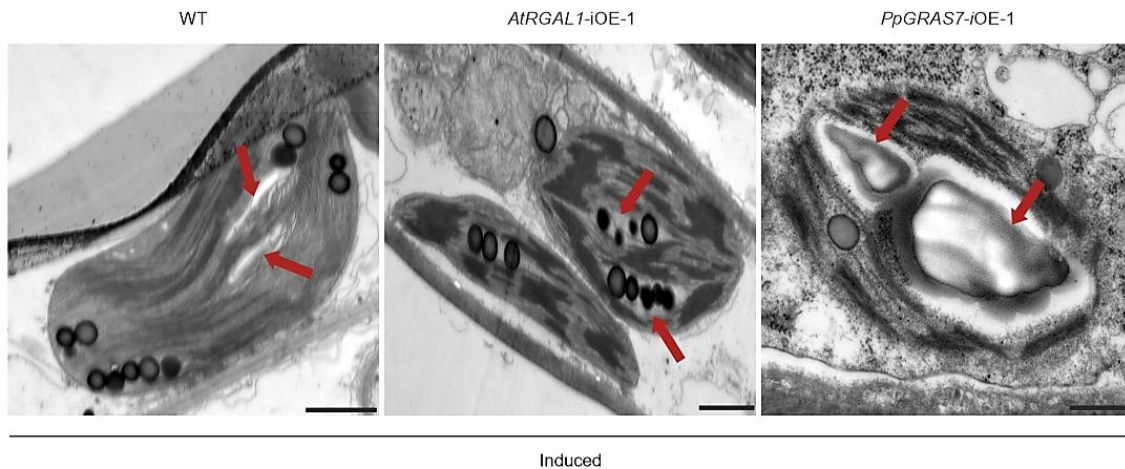


**Fig. 27.** Phenotypic analysis of the *PpGRAS12*-iOE (pictures have been taken from Fig. 20a) and *AtRGA1*-iOE lines. Formation of multiple gametophores in the *PpGRAS12*-iOE-1 and *AtRGA1*-iOE-1 lines upon the induction. Pink arrows point to gametophores. Scale bars: 1 mm.

As I showed in Fig. 14b, the chlorotic phenotype in the *PpGRAS7*-iOE lines was accompanied by a significant reduction of thylakoid membrane proteins including LHCA, LHCB, PsaL, PsbQ, PsbD, *Cytb<sub>6</sub>*, and *Cytf*. Based on the chlorotic phenotype in the *AtRGL1*-iOE lines, which was comparable to *PpGRAS7*-iOE lines, it was presumed that photosynthesis in the *AtRGL1*-iOE lines could also be affected. To investigate the impact of *AtRGL1* overexpression in *P. patens*, the abundance of several proteins that are involved in photosynthesis was investigated in the *AtRGL1*-iOE-1 line as well as WT in a kinetic experiment (0 (untreated), 2, 4, and 8 days) after the application of 2  $\mu$ M of  $\beta$ -estradiol (Fig. 28b). A significant reduction in thylakoid membrane proteins and soluble plastid proteins including LHCA, LHCB, PsaL, PsbQ, PsbD, *Cytb<sub>6</sub>*, and *Cytf* were observed in the *AtRGL1*-iOE-1 line in response to the upregulation of *AtRGL1*. This finding is compatible with the previous reduction of thylakoid membrane proteins in the *PpGRAS7*-iOE-1 line in response to the upregulation of *PpGRAS7*.

(a)



(b)

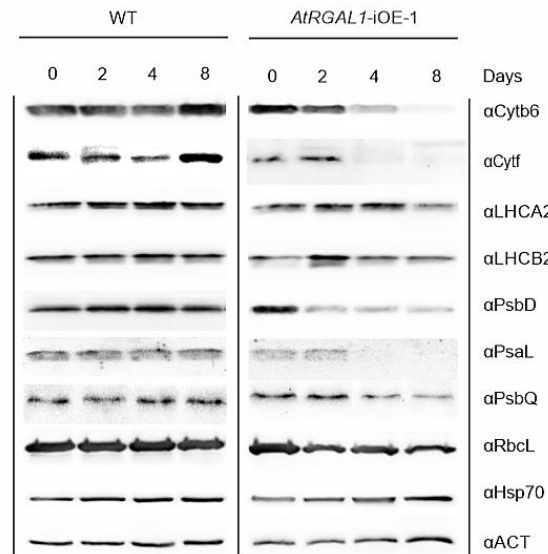


**Fig. 28. Molecular analysis of *AtRGL1* overexpression in *P. patens*.** (a) TEM analysis of the *AtRGL1*-iOE-1 line. Phylloid tissues derived from the WT and *AtRGL1*-iOE-1 line that were treated for 8 days with the inducer. WT and the *AtRGL1*-iOE-1 line showed similar starch content, whereas the *PpGRAS7*-iOE-1 line displayed large amounts of starch. Red arrows: starch. Scale bar corresponds to 1  $\mu$ m, 1  $\mu$ m and 500 nm for the WT, *AtRGL1*-iOE-1 line, and *PpGRAS7*-iOE-1 line, respectively. (b) The accumulation of chloroplast proteins was analyzed from samples harvested at the indicated time points (0 (untreated), 2, 4, and 8 days) after the treatment with 2  $\mu$ M of  $\beta$ -estradiol. Representative images of immunoblots with the indicated antibodies are shown. Equal amounts of total protein extracts from the WT and *AtRGL1*-iOE-1 line were inspected.  $\alpha$ ATC was used as a control.

### 3.3.2 Overexpression of the *ASCL6-II* in *P. patens* leads to chlorosis and the formation of multiple apical meristems

*PpGRAS7* and *PpGRAS12* were previously identified as miR171 targets in *P. patens* (Axtell *et al.*, 2007). As I showed in chapter 3 (see 3.2 and 3.1), an elevated level of *PpGRAS12* led to the formation of multiple apical meristems and overexpression of *PpGRAS7* resulted in plastid degradation and starch over-accumulation. *A. thaliana SCL6-II* (*At2g45160*), *SCL6-III* (*At3g60630*), and *SCL6-IV* (*At4g00150*) are reported as targets of miRNA171 (Llave *et al.*, 2002). *AtSCL6-II*, *AtSCL6-III*, and *AtSCL6-IV* play a critical role in the regulation of shoot branch production in *A. thaliana* (Wang *et al.*, 2010). To study the impact of *AtSCL6-II*, *AtSCL6-III*, and *AtSCL6-IV* overexpression in *P. patens*, *AtSCL6-II-iOE*, *AtSCL6-III-iOE*, and *AtSCL6-IV-iOE* lines were generated using a  $\beta$ -estradiol inducible gene expression system (Kubo *et al.*, 2013). For this, the full-length coding sequence of the *AtSCL6-II*, *AtSCL6-III*, and *AtSCL6-IV* were amplified from previously generated plasmids harboring the miR171-resistant version of *AtSCL6-II*, *AtSCL6-III*, and *AtSCL6-IV* genes (Aoyama & Chua, 1997). Cloning, transformation, and selection were performed in the same way as described for the generation of the *PpGRAS7-iOE* lines (see 3.1.3). Using PCR-based screening, I identified two independent overexpression lines for each *AtSCL6-II*, *AtSCL6-III*, and *AtSCL6-IV* (Fig. 29a, b, and c). The same strategy as used for the screening of the *AtRGAI-iOE* lines was applied for screening of the *AtSCL6-II-iOE*, *AtSCL6-III-iOE*, and *AtSCL6-IV-iOE* lines. For each gene, a forward primer that binds within the promoter region of the PpGX8 vector (70 bp upstream of the ATG (start codon) of the gene), and a reverse primer, which binds within the coding sequence of the gene were used. OE-screen<sup>4</sup>-F, OE-screen<sup>5</sup>-F, and OE-screen<sup>6</sup>-F (Appendix 1) were applied as forward screening primers for *AtSCL6-II*, *AtSCL6-III*, and *AtSCL6-IV*, while OE-screen<sup>4</sup>-R, OE-screen<sup>5</sup>-R, and OE-screen<sup>6</sup>-R (Appendix 1) were used as reverse screening primers for *AtSCL6-II*, *AtSCL6-III*, and *AtSCL6-IV*, respectively. To validate the inducible expression of *AtSCL6-II*, *AtSCL6-III*, and *AtSCL6-IV*, protonema tissues from the *AtSCL6-II-iOE*, *AtSCL6-III-iOE*, and *AtSCL6-IV-iOE* lines were induced 4 h with 2 $\mu$ M of  $\beta$ -estradiol and the induction of *AtSCL6-II*, *AtSCL6-III*, and *AtSCL6-IV* genes were confirmed by RNA gel blots (Fig. 29d, e, and f).

Phenotypic analysis of the *AtSCL6-II*-iOE, *AtSCL6-III*-iOE, and *AtSCL6-IV*-iOE lines was carried out by adjusting pure protonema cultures of the inducible overexpression lines as well as WT to an equal density of 100 mg/l dry weight and 5  $\mu$ l of the adjusted cultures were spotted onto solid medium supplemented with 2  $\mu$ M  $\beta$ -estradiol or without inducer. A distinct and strict growth arrest was observed in both *AtSCL6-II*-iOE, *AtSCL6-III*-iOE lines at the protonema stage, whereas the growth of protonema tissues in the induced *AtSCL6-IV*-iOE lines was indistinguishable from the WT (Fig. 30a). To investigate the effect of *AtSCL6-II*, *AtSCL6-III*, and *AtSCL6-IV* induction at later growth stages, 2  $\mu$ M of  $\beta$ -estradiol was directly applied onto the colonies of the inducible overexpression lines and WT control that were grown on solid medium and developed leafy gametophores. I observed the formation of multiple apical meristems as well as chlorosis in the *AtSCL6II*-iOE lines in response to an elevated level of *AtSCL6-II* at the gametophytic vegetative growth stage in *P. patens* (Fig. 30b and c). A mild chlorosis was observed in the *AtSCL6-III*-iOE lines at the gametophytic vegetative growth stage, whereas the growth of the *AtSCL6-IV*-iOE lines was indistinguishable from the WT (Fig. 30c).

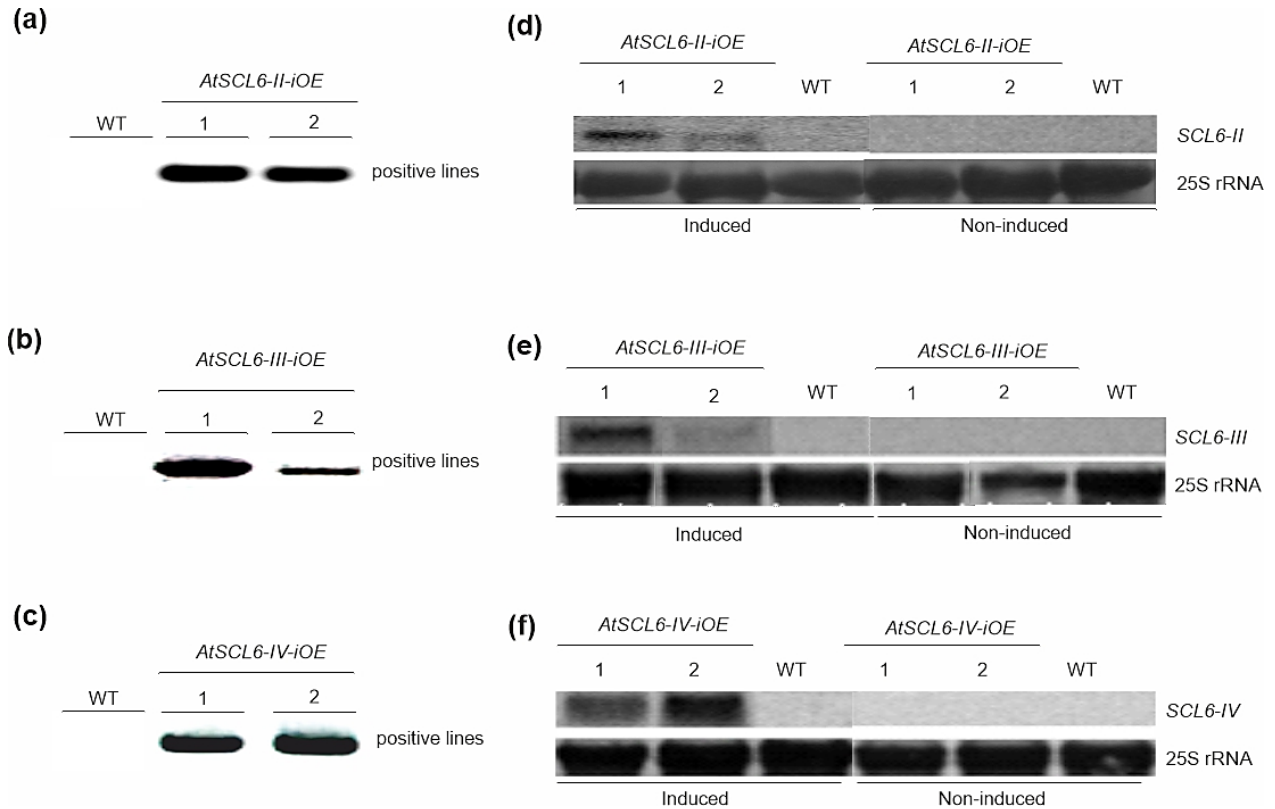


**Fig. 29. Screening and confirmation of the *AtSCL6-II-iOE*, *AtSCL6-III-iOE*, and *AtSCL6-IV-iOE* lines.** (a) Screening of the *AtSCL6-II-iOE* lines using PGX8-specific (forward primer (OE-screen<sup>4</sup>-F), Appendix 1) and *AtSCL6-II*-specific (Reverse primer, (OE-screen<sup>4</sup>-R, Appendix 1) primers. Positive lines show amplified PCR products using genomic DNA from the indicated lines as a template. (b) Screening of the *AtSCL6-III-iOE* lines using PGX8-specific (forward primer (OE-screen<sup>5</sup>-R), Appendix 1) and *AtSCL6-III*-specific (Reverse primer (OE-screen<sup>5</sup>-R), Appendix 1) primers. Positive lines show amplified PCR products using genomic DNA from the indicated lines as a template. (c) Screening of the *AtSCL6-IV-iOE* lines using PGX8-specific (forward primer (OE-screen<sup>6</sup>-F), Appendix 1) and *AtSCL6-IV*-specific (Reverse primer (OE-screen<sup>6</sup>-F), Appendix 1) primers. Positive lines show amplified PCR products using genomic DNA from the indicated lines as a template. (d) RNA gel blots from the WT and two independent *AtSCL6-II-iOE* lines. (e) RNA gel blots from the WT and two independent *AtSCL6-III-iOE* lines. (f) RNA gel blots from the WT and two independent *AtSCL6-IV-iOE* lines. All *AtSCL6-II-iOE*, *AtSCL6-III-iOE*, and *AtSCL6-IV-iOE* lines as well as WT were grown for 4 h in the standard liquid medium (non-induced) or liquid medium supplemented with the inducer (induced). Subsequently, RNAs were harvested and used for the gel blot analysis. *AtSCL6-II*, *AtSCL6-III*, and *AtSCL6-IV*-specific probes were used for hybridization. 25S rRNA (from the EtBR stained gel) was used to monitor equal loading.

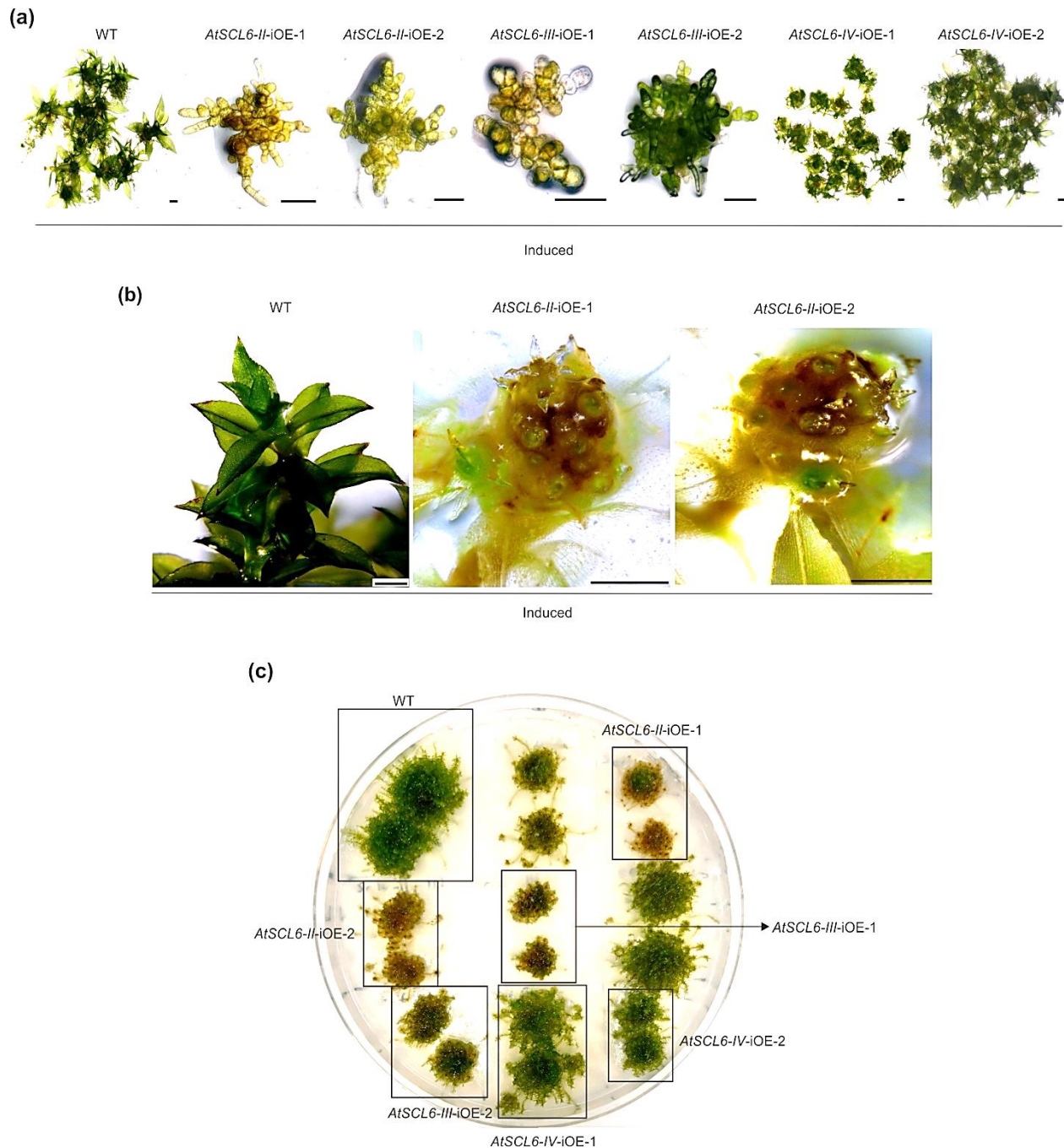


**Fig. 30. Phenotypic analysis of the *AtSCL6-II-iOE*, *AtSCL6-III-iOE*, and *AtSCL6-IV-iOE* lines.** (a) Equal amounts of protonema tissues from the WT, *AtSCL6-II-iOE* lines (two independent lines), *AtSCL6-III-iOE* lines (two independent lines), and *AtSCL6-III-iOE* lines (two independent lines) were spotted on standard growth medium supplemented with 2  $\mu$ M of  $\beta$ -estradiol. Pictures were taken 2 weeks after the induction. Scale bars: 1 mm. (b) Multiple apical meristem formation in the *AtSCL6-II-iOE* lines. 2  $\mu$ M of  $\beta$ -estradiol was directly applied onto colonies from *AtSCL6-II-iOE* lines as well as WT control. Pictures were taken 4 weeks after the induction. Scale bars: 1 mm. (c) Chlorosis in the *AtSCL6-II-iOE* and *AtSCL6-III-iOE* lines. 2  $\mu$ M of  $\beta$ -estradiol was directly applied onto colonies from transgenic lines as well as WT control. Pictures were taken 4 weeks after the induction.

## 4 DISCUSSION

### 4.1 *PpGRAS7* is involved in chloroplast degradation and starch over-accumulation

GRAS proteins are an important family of plant-specific proteins that regulate plant growth and development via transcriptional regulation and signal transduction processes (Hofmann, 2016; Li *et al.*, 2016). The conserved GRAS domain consists of several distinct motifs including LHRI, VHIID, LHRII, PFYRE and the SAW motif (Pysh *et al.*, 1999). Compatible with a GRAS domain structure (Pysh *et al.*, 1999; Tian *et al.*, 2004; Hirsch & Oldroyd, 2009), *PpGRAS7* contains the same order of the conserved GRAS motifs (Fig. 6). Here I showed that *PpGRAS7* displays a nuclear localization pattern, which is in agreement with previous reports demonstrating that most of the GRAS proteins are localized in the nucleus and act as transcription factors (Di Lorenzo *et al.*, 1996; Gallagher & Benfey, 2009; Heo *et al.*, 2011). Based on the subcellular nuclear localization of the analyzed *PpGRAS7::citrine* fusion protein I hypothesize that *PpGRAS7* possibly acts as a transcription factor in *P. patens*.

In the moss *P. patens*, two *GRAS* mRNAs were previously identified as miR171 targets (Axtell *et al.*, 2007). The phylogenetic analysis shows despite containing the GRAS domain, *PpGRAS7* does not belong to any of the previously described GRAS subfamilies. Interestingly, *PpGRAS7* showed a closer relation to the AtDELLA clade compared with the AtHAM family, and AtRGL1 shares the highest similarity (37%) with *PpGRAS7*. However, the functional analysis of the *PpGRAS7*-iOE lines suggests a different molecular function for *PpGRAS7* compared with other members of the GRAS family. In *A. thaliana*, the DELLA subfamily is known to contain negative regulators of gibberellic acid (GA) responses. Overexpression of *AtRGL1* in *A. thaliana* resulted in significantly increased leaf longevity in age-triggered senescence (Chen *et al.*, 2017), while *PpGRAS7* overexpression resulted in elevated expression of senescence marker genes (*PpSAG13*, *PpSAG18*, and *PpSINI*) and promoting chlorosis in *P. patens*. Although *PpGRAS7* showed a partial sequence similarity to AtRGL1, my results suggest a different function for *PpGRAS7*.

In this study, I showed the involvement of *PpGRAS7* in plastid degradation and starch over-accumulation. Furthermore, I observed that *PpGRAS7* overexpression led to an increase of maltose content in the *PpGRAS7*-iOE lines. In *A. thaliana*, the accumulation of maltose leads to imbalances in chloroplast homeostasis and causes a chlorotic phenotype (Stettler *et al.*, 2009). The observed phenotype and molecular characteristics in the lines overexpressing *PpGRAS7* have not been observed for DELLA and HAM family members or any other member of the large GRAS family such as PAT1, LISCL, SCL3, SCR, SHR, or LAS. In *A. thaliana* PAT1, SCL5, and SCL21 (PAT1 subfamily) are known to act as positive regulators in phytochrome A signal transduction (Bolle *et al.*, 2000; Torres-Galea *et al.*, 2013), while SCL13 (PAT1 subfamily) is mainly involved in phytochrome B signal transduction (Torres-Galea *et al.*, 2006). SCR and SHR play a crucial role in root radial patterning in *A. thaliana* (Cui *et al.*, 2007). SCL3 mediates cell elongation during root development (Heo *et al.*, 2011) and LAS subfamilies (MOC1, LS, and LAS) function in axillary meristem initiation in *A. thaliana* (Schumacher *et al.*, 1999; Greb *et al.*, 2003; Li *et al.*, 2003). In lily (*Lilium longiflorum* L.), LISCL was reported to participate in the microsporogenesis of anthers (Morohashi *et al.*, 2003). Based on the observed phenotype and the role of *PpGRAS7* in plastid degradation and starch over-accumulation, I suggest a novel function for this GRAS family member.

A decrease in the concentrations of photosynthetic pigments such as chlorophylls and carotenoids is one of the major causes of chlorosis. Chlorophyll fluorescence analysis showed a general reduction of PSII efficiency in the induced *PpGRAS7*-iOE lines (Fig. 14c and d). The reduction of PSII efficiency is associated with a reduced content of chlorophylls, carotenoids and a lower chlorophyll *a/b* ratio (Mariotti *et al.*, 2018). Strong chlorosis and degradation of plastids were observed in the *PpGRAS7*-iOE lines upon the induction. These results were accompanied by a reduction of the chlorophyll content and reduced accumulation of a group of pigments related to carotenoid biosynthesis (Fig. 15a and b). Reduction of the chlorophyll content was accompanied by a strong decrease of thylakoid membrane proteins including PpLHCA, PpLHCB, PpPsaL, PpPsbQ, PpPsbD, PpCyt<sub>b6</sub>, and PpCyt<sub>f</sub> in response to the *PpGRAS7* overexpression. In accordance with the observed reduction of the photosynthetic machinery, I showed the downregulation of a group of photosynthetic genes encoding proteins of specific photosynthetic complexes in the *PpGRAS7*-iOE lines including *PpPsaA*, *PpPsaB*, *PpPsaC*, *PpPsbD*, *PpPsbM*, *PpLHCB2*, in

response to the induction of the *PpGRAS7* gene. I also observed the downregulation of *PpPORAa*, and *PpPORA b* in response to the upregulation of the *PpGRAS7* gene. This suggests that the observed deficiencies in photosynthesis are partially caused by the misregulation of nuclear genes encoding photosynthesis-associated proteins. Taken together, the observed phenotype, including chlorosis and paling of tissues, is most likely caused by a combinatory effect of these molecular changes. Based on the observed phenotype and differentially regulated genes in the induced *PpGRAS7*-iOE lines, I hypothesize a group of genes as putative targets of *PpGRAS7*. Downregulation of *PpCYCD1* and *PpCLV1* in response to *PpGRAS7* upregulation can explain the remarkable and distinct growth arrest in the *PpGRAS7*-iOE lines, whereas the downregulation of *PpPsaA*, *PpPsaB*, *PpPsaC*, *PpPsbA*, *PpPsbD*, *PpPsbM*, and *PpLHCB2* in response to an elevated level of *PpGRAS* might explain the paling phenotype in the *PpGRAS7*-iOE lines. Besides, the downregulation of *PpTPT* in response to the upregulation of *PpGRAS7*, possibly induce over-accumulation of starch in the *PpGRAS7*-iOE lines. Therefore, I speculate that *PpGRAS7*, directly or indirectly, might act in the repression of *PpCYCD1*, *PpCLV1*, *PpPsaA*, *PpPsaB*, *PpPsaC*, *PpPsbA*, *PpPsbD*, *PpPsbM*, *PpLHCB2*, and *PpTPT*.

Moreover, upon *PpGRAS7* overexpression elevated light intensities and extended light periods increased the severity of the phenotype indicating that the phenotypic changes are most likely triggered by light conditions. I also cannot exclude that some secondary effects, such as oxidative stress, have a crucial impact on the phenotype. The ROS accumulation in the *PpGRAS7*-iOE lines is most likely the result of decreased levels of carotenoids, which fulfill a protective function based on quenching of chlorophyll triplet states to prevent the generation of highly reactive singlet oxygen species (Ritz *et al.*, 2000; Fraser *et al.*, 2001). The pigments analyses revealed lower levels of zeinoxanthin, which is a precursor of lutein that is the predominant carotenoid in plant photosynthetic tissues and plays a critical role in light-harvesting complex assembly and function (Pogson *et al.*, 1996). Light absorption through chlorophylls is accompanied by light absorption through carotenoids. LHCB proteins, constituting the antenna system of PSII, bind lutein, violaxanthin and neoxanthin at four distinct binding sites (Liu *et al.*, 2004). Based on my results, I hypothesize that decreased pigment levels, in particular carotenoids, increase ROS accumulation in the *PpGRAS7*-iOE lines. Any reduced functionality of *LHCB* interrupts light energy transfer to the reaction centers of PSII and reduces the PSII efficiency. Another possibility for elevated ROS

levels is the observed decreased *LHCB* mRNA and protein levels, since *A. thaliana lhcb* mutants are characterized by increased ROS levels (Xu *et al.*, 2012). This is compatible with my finding that shows the downregulation of *LHCB2* in the *PpGRAS7*-iOE lines at both, transcript and protein levels. Therefore, I hypothesize that the reduced *LHCB* levels may contribute to the elevated ROS levels in the *PpGRAS7*-iOE lines upon the induction.

In *P. patens*, *atg5* mutants are deficient in the process of autophagy (Mukae *et al.*, 2015). Interestingly, the expression of *PpATG5* is upregulated in the *PpGRAS7*-iOE lines upon the induction. I also noticed an increase in the expression of senescence-associated genes, *PpSAG13*, *PpSAG18*, and *PpSENI* in response to *PpGRAS7* overexpression. Autophagy and senescence are considered to be responsible for chlorophyll and chloroplast degradation. Thus, it is likely that *PpGRAS7* functions in the expression of autophagy- and senescence-related nuclear genes. Senescence in plants is a process characterized by interruption of photosynthesis, the disintegration of organelle structure, degradation of chlorophyll and chloroplast proteins and upregulation of senescence-associated genes (BuchananWollaston, 1997). Senescence underlies the expression of certain genes including some *SAGs* (Mukae *et al.*, 2015). At the transcription level, the onset of senescence and leaf yellowing is demonstrated by an increase in the expression of senescence-associated genes (*SAGs*) encoding enzymes involved in the degradation of chlorophyll (Gan & Amasino, 1997). Based on the observed phenotype and upregulation of *PpATG5*, *PpSAG13*, *PpSAG18*, and *PpSENI* upon *PpGRAS7* overexpression I speculate that autophagy- and senescence-related processes are responsible for the plastid degradation in the *PpGRAS7*-iOE lines.

*PpGRAS7* overexpression also caused a marked downregulation of *PpBAM3a* and *PpBAM3d* transcripts and concomitantly increased starch content (Fig. 12c) suggesting a potential impact of *PpGRAS7* in regulating *PpBAM3a* and *PpBAM3d* transcription. In plants, BAM proteins are vital for maltose production during hydrolytic starch degradation and a lowered *PpBAM3* level likely contributes to starch accumulation in the *PpGRAS7*-iOE lines. In contrast, the upregulation of *PpGWDa* could indicate a compensatory effort of the plant to lower the excess of starch. Since maltose and fructose levels are increased in the *PpGRAS7*-iOE lines most likely sugar metabolism in general was inhibited.

Moreover, reduced starch hydrolysis via the  $\beta$ -amylase pathway in the *PpGRAS7*-iOE lines most likely causes a lack of energy supply for the entire plant cell metabolism that can explain the

failure of recovery of the *PpGRAS7*-iOE lines after the transfer to non-inducing conditions. Additionally, *PpGRAS7* overexpression led to similar starch levels at the end of the day and the end of the night, indicating a perturbed starch metabolism and a failure of starch degradation during the night. In *A. thaliana* four chloroplast BAM proteins were identified and the chloroplast BAM3 protein plays a major role in the leaf starch breakdown (Li *et al.*, 2009). The total  $\beta$ -amylase activity is reduced in leaves of *A. thaliana bam3* mutants, which induced elevated starch levels (Fulton *et al.*, 2008). This is consistent with my results, suggesting that the reduced activities of  $\beta$ -amylase may lead to the accumulation of starch (Walters *et al.*, 2004). During photosynthesis, the TPT of the chloroplast inner envelope membrane mediates the counter exchange of stromal triose-P derived from CO<sub>2</sub> fixation with cytosolic orthophosphate (P<sub>i</sub>) and consequently providing the cytosol with the precursors for sucrose synthesis. Optimum rates of photosynthesis require the regulated exchange of metabolites through TPT. I found a drastic downregulation of TPT at the transcript level in response to *PpGRAS7* overexpression. In accordance with the *PpGRAS7*-iOE phenotype, the *A. thaliana* mutant lacking TPT displays increased starch synthesis compared to the WT, thereby likely compensating for its deficient export of triose-P out of the chloroplast. The decreased export of triose phosphates leads to an accumulation of phosphorylated intermediates in the chloroplast, resulting in a reduction of stromal P<sub>i</sub>, which in turn has the potential to restrict ATP synthesis and consequently CO<sub>2</sub> fixation (Edwards & Walker, 1983). Under normal growth conditions, the potential inhibition of photosynthesis due to P<sub>i</sub> limitation is ameliorated by activation of ADP-Glc pyrophosphorylase (AGPase) (Sowokinos, 1981; Sowokinos & Preiss, 1982), leading to an increase in the rate of starch synthesis and consequently release of P<sub>i</sub>. Moreover, if sucrose biosynthesis diminishes during the day, the limitation of P<sub>i</sub> import redirects photosynthetic carbon flow into starch biosynthesis (Schneider *et al.*, 2002). These data suggest a metabolic compensation strategy for the reduced levels of TPT by diverting assimilate into starch, releasing the P<sub>i</sub> required for the photosynthetic light reaction. Using an alternative pathway is an escape strategy for plants to cope with new conditions. ISA3, an isoform of isoamylase, was shown to be an important starch-degrading enzyme in plants (Ferreira *et al.*, 2017). *A. thaliana isa3* mutants show reduced starch degradation and a strong starch-excess phenotype (Wattebled *et al.*, 2005). In contrast to the downregulation of *PpBAM3*, I found an increase in *PpDPE1* and *PpISA3* in the *PpGRAS7*-iOE lines. An upregulation of isoamylase when the  $\beta$ -amylases is downregulated

might indicate that plants engaged all alternative options to unload and consume extra starch. The upregulation of *PpDPE1* in the *PpGRAS7*-iOE lines reflects another strategy of the plant to utilize starch in order to provide sufficient energy. In summary, my data suggest an important role of the nuclear-localized *PpGRAS7* protein in chloroplast metabolism by regulation expression of genes involved in chloroplast starch and sugar metabolism, photosynthesis, chlorosis, and senescence.

## **4.2 *PpGRAS12* plays an important role in meristem regulation and maintenance**

Compatible with GRAS family members (Pysh *et al.*, 1999; Tian *et al.*, 2004; Hirsch & Oldroyd, 2009), *PpGRAS12* contains the same order of the conserved GRAS motifs (Fig. 16). Here, I also showed that *PpGRAS12* is nuclear-localized, which is in agreement with the proposed function of GRAS proteins as transcription factors (Di Laurenzio *et al.*, 1996; Gallagher & Benfey, 2009; Heo *et al.*, 2011).

The presence of the miR170/171 binding site is a characteristic of most members of HAM families. *A. thaliana* orthologs of *Petunia HAM* were shown to be targets of miR170/171 (Llave *et al.*, 2002). The *A. thaliana* HAM proteins are involved in meristem regulation and the CLV3-WUS pathway (Zhou *et al.*, 2018). WUS is a homeodomain transcription factor, which is expressed in the rib meristem of the *A. thaliana* shoot apical meristem. The CLAVATA-WUSCHEL signaling pathway regulates stem cell maintenance via an auto-regulatory negative-feedback loop (Schoof *et al.*, 2000). HAM and WUS share collective targets *in vivo* and their physical interaction are vital in driving downstream transcriptional programs and promoting shoot stem cell proliferation (Zhou *et al.*, 2015). *AtGPR23*, *AtTPT2;2*, and *AtTPL* are reported as collective targets of HAM and WUS and they are noticeably affected when WUS and HAM interact (Zhou *et al.*, 2015). WUS is an activator of CLV3, which further binds to CLV1/2 and negatively regulates the expression of WUS. Tomato (*Solanum lycopersicum*) encodes three HAM homologs that are guided for cleavage by miR171 (Hendelman *et al.*, 2016) and their silencing led to over-proliferation of cells in the periphery of the meristems. *HAM* genes not only function in the meristem maintenance, but also play minor roles in the morphogenesis of a simple leaf in tomato (Hendelman *et al.*, 2016). *PpGRAS12* is one of the validated targets of the miR171 in *P. patens* (Axtell *et al.*, 2007). The

miR171-GRAS module was elucidated as a key player in meristem maintenance (Huang *et al.*, 2017). Analysis of the PpGRAS12::GUS protein fusion reporter lines showed a regulatory function of miR171 in *PpGRAS12* expression. I observed a noticeable expression of the *PpGRAS12* gene in the archegonia and egg cells of the mPpGRAS12::GUS protein fusion reporter lines compared with the PpGRAS12::GUS lines and WT. This suggests that miR171 controls the expression of *PpGRAS12* in *P. patens* archegonia and egg cells. Loss of function  $\Delta PpGRAS12$  lines displayed a fewer number of sporophytes compared to the WT. Egg cells give rise to sporophytes. Based on the elevated expression of *PpGRAS12* in the egg cells of the mPpGRAS12::GUS protein fusion reporter lines and reduced sporophyte production in the  $\Delta PpGRAS12$  lines, I suggest that PpGRAS12 plays a role in egg cell regulation and sporophyte production.

An extreme growth arrest was observed in the *PpGRAS12*-iOE lines at the protonema stage upon the induction. Furthermore, I observed the formation of multiple apical meristems at the gametophytic vegetative stage in the *PpGRAS12*-iOE lines upon the induction. The shoot apical meristem (SAM) is responsible for the post-embryonic growth and generates plant aerial structures. An appropriate continuous growth in plants depends on the SAM ability to maintain the balance between self-renewal of stem cells and cell recruitment for lateral organ formation (Lee *et al.*, 2019). The WUS and CLV signaling pathway are key factors of meristematic activity in the SAM (Clark *et al.*, 1993; Laux *et al.*, 1996). In *A. thaliana clv1* mutant develops enlarged and indeterminate floral meristems (Clark *et al.*, 1995). Furthermore, mutation of the *CLV1* gene has resulted in an increased number of all floral organ types (Leyser & Furner, 1992). Compatible with the previous studies (Clark *et al.*, 1993; Clark *et al.*, 1995), I observed the downregulation of *CLV1* genes along with the formation of multiple and enlarged apical meristems in the *PpGRAS12*-iOE lines. This might indicate that an elevated level of *PpGRAS12* represses the expression of *CLV1* genes, which might induce the formation of multiple and enlarged apical meristems in the *PpGRAS12*-iOE lines. This result indicates the involvement of *PpGRAS12* in meristem identity control. Multiple apical cells have remained while the plant was constantly induced with the inducer. When the inducer degraded, new gametophores have developed from multiple apical meristems. This shows that a continuous upregulation of the *PpGRAS12* is essential for the formation and maintenance of multiple apical meristems in *P. patens*. In summary, my results

indicate the involvement and key role of *PpGRAS12* in meristem regulation, maintenance and identity control.

### **4.3 *AtRGL1* overexpression induces chlorosis in *P. patens***

As it was shown in chapter 3 (3.1), *PpGRAS7* a member of the GRAS family and the validated target of miR171 (Axtell *et al.*, 2007), was localized in the nucleus and elevated levels of *PpGRAS7* resulted in plastid degradation and starch over-accumulation. In chapter 3 (3.2), I showed that *PpGRAS12*, another member of the GRAS family and the validated target of miR171 (Axtell *et al.*, 2007), is also localized in the nucleus. Furthermore, I showed that overexpression of *PpGRAS12* led to the formation of multiple apical meristems. Based on the protein sequence similarities, I showed that *AtRGA1* shares the highest similarity (37%) with *PpGRAS7* and *AtRGL1* shares the highest similarity (37%) with *PpGRAS12*. I observed a growth arrest in the *AtRGA1*-iOE lines in the primary phase of growth. Although the detected growth arrest in the *AtRGA1*-iOE lines was not as strict as the growth arrest in the *PpGRAS12*-iOE lines, cell growth was notably affected. Furthermore, overexpression of *AtRGA1* resulted in the initiation of multiple apical meristems and consequently the formation of multiple gametophores at the gametophytic vegetative growth stage in *P. patens*. I further noticed that multiple gametophores, which were formed in response to an elevated level of *AtRGA1* shared partial similarities with the observed phenotype in the induced *PpGRAS12*-iOE lines. Based on the observed phenotype in the *AtRGA1*-iOE lines, I suggest a partial functional homology between *PpGRAS12* and *AtRGA1* in *P. patens*. In addition, similar to the induced *PpGRAS7*-iOE lines, a severe growth arrest was observed in the induced *AtRGL1*-iOE lines at the protonema stage. The overexpression of *AtRGL1* appeared to impose a strict growth arrest at the protonema growth stage, but unlike *PpGRAS7* overexpression was not lethal to the plant. Furthermore, chlorosis and paling of tissues were observed in the *AtRGL1*-iOE lines at the gametophytic vegetative growth stage in response to the elevated level of the *AtRGL1*. This phenotype was similar to the chlorosis and paling of tissues in the induced *PpGRAS7*-iOE lines. The immunoblot analyses showed a significant reduction in thylakoid membrane proteins including LHCA, LHCB, PSAL, PSBQ, PSBD, *CYTb<sub>6</sub>*, and *CYTf* in the *AtRGL1*-iOE-1 line in response to the upregulation of *AtRGL1*. This finding was in agreement with

the previous reduction of thylakoid membrane proteins in the *PpGRAS7*-iOE-1 line in response to the upregulation of *PpGRAS7*. Elevated levels of both *AtRGL1* and *PpGRAS7* led to a growth arrest and chlorosis in *P. patens*. Furthermore, overexpression of the *PpGRAS7* led to the starch over-accumulation in *P. patens*. The SEM analysis of *P. patens* phylloid tissues revealed that an elevated level of *AtRGL1* has no impact on the starch content in *P. patens*. Despite the difference in starch contents, based on the partial phenotype similarities and comparable reduction of thylakoid membrane proteins in both *PpGRAS7*-iOE and *AtRGL1*-iOE lines upon the induction, I suggest a partial functional homology between *PpGRAS7* and *AtRGL1* in *P. patens*.

#### **4.4 Overexpression of miRNA171-targeted *AtSCL6-II* leads to the formation of multiple apical meristems and chlorosis in *P. patens***

*A. thaliana SCL6-II*, *SCL6-III*, and *SCL6-IV* are validated targets of miRNA171 (Llave *et al.*, 2002). I observed a growth arrest in the *AtSCL6-II*-iOE and *AtSCL6-III*-iOE lines at the protonema stage upon the induction, whereas the growth of the *AtSCL6-IV*-iOE lines was indistinguishable from the WT. The growth arrest, which was detected in the induced *AtSCL6-II*-iOE and *AtSCL6-III*-iOE lines displayed similarities with the growth arrests in both *PpGRAS7*-iOE and *PpGRAS12*-iOE lines upon the induction. Only the *AtSCL6-II*-iOE lines have formed multiple apical meristems in response to an elevated level of *AtSCL6-II* gene. The observed multiple apical meristems in the *AtSCL6-II*-iOE lines at the gametophytic vegetative growth stage in response to an elevated level of *AtSCL6-II* gene in *P. patens* was comparable to the phenotype in the induced *PpGRAS12*-iOE lines. Furthermore, the *AtSCL6-II*-iOE lines displayed chlorosis and paling of tissues upon the induction in *P. patens*. *A. thaliana SCL6-II* is one of three validated targets of miR171 (Llave *et al.*, 2002) and previously was shown to be involved in the regulation of shoot branch production (Wang *et al.*, 2010) and chlorophyll biosynthesis (Ma *et al.*, 2014). *AtSCL6-II* inhibits the expression of the key gene encoding PROTOCHLOROPHYLLIDE OXIDOREDUCTASE (POR) (Ma *et al.*, 2014). Since the formation of multiple apical meristems and chlorosis in the induced *AtSCL6-II*-iOE lines were detected in the *PpGRAS12*-iOE and *PpGRAS7*-iOE lines, respectively, I speculate that *AtSCL6-II* might be the functional homolog of both *PpGRAS12* and *PpGRAS7*.

## 5 REFERENCES

- Allen E, Xie Z, Gustafson AM, Carrington JC. 2005.** microRNA-directed phasing during *trans*-acting siRNA biogenesis in plants. *Cell* **121**(2): 207-221.
- Aoyama T, Chua NH. 1997.** A glucocorticoid-mediated transcriptional induction system in transgenic plants. *Plant J* **11**(3): 605-612.
- Arif MA, Alseekh S, Harb J, Fernie A, Frank W. 2018.** Abscisic acid, cold and salt stimulate conserved metabolic regulation in the moss *Physcomitrella patens*. *Plant Biol (Stuttg)* **20**(6): 1014-1022.
- Arnon DI. 1949.** Copper enzymes in isolated chloroplasts. Polyphenoloxidase in *Beta vulgaris*. *Plant Physiol* **24**(1): 1-15.
- Aukerman MJ, Sakai H. 2003.** Regulation of flowering time and floral organ identity by a MicroRNA and its *APETALA2*-like target genes. *Plant Cell* **15**(11): 2730-2741.
- Axtell MJ, Bowman JL. 2008.** Evolution of plant microRNAs and their targets. *Trends Plant Sci* **13**(7): 343-349.
- Axtell MJ, Snyder JA, Bartel DP. 2007.** Common functions for diverse small RNAs of land plants. *Plant Cell* **19**(6): 1750-1769.
- Baena-Gonzalez E, Rolland F, Thevelein JM, Sheen J. 2007.** A central integrator of transcription networks in plant stress and energy signalling. *Nature* **448**(7156): 938-U910.
- Baldwin A, Wardle A, Patel R, Dudley P, Park SK, Twell D, Inoue K, Jarvis P. 2005.** A molecular-genetic study of the *Arabidopsis Toc75* gene family. *Plant Physiol* **138**(2): 715-733.
- Bartel DP. 2004.** MicroRNAs: genomics, biogenesis, mechanism, and function. *Cell* **116**(2): 281-297.
- Barton MK, Poethig RS. 1993.** Formation of the shoot apical meristem in *Arabidopsis thaliana* an analysis of development in the wild-type and in the shoot meristemless mutant. *Development* **119**(3): 823-831.
- Bolle C. 2004.** The role of GRAS proteins in plant signal transduction and development. *Planta* **218**(5): 683-692.
- Bolle C, Koncz C, Chua NH. 2000.** PAT1, a new member of the GRAS family, is involved in phytochrome A signal transduction. *Genes Dev* **14**(10): 1269-1278.
- Boutet S, Vazquez F, Liu J, Beclin C, Fagard M, Gratias A, Morel JB, Crete P, Chen XM, Vaucheret H. 2003.** *Arabidopsis* HEN1: a genetic link between endogenous miRNA controlling development and siRNA controlling transgene silencing and virus resistance. *Curr Biol* **13**(10): 843-848.

- Bouvier-Nave P, Berna A, Noiriél A, Compagnon V, Carlsson AS, Banas A, Stymne S, Schaller H. 2010.** Involvement of the *PHOSPHOLIPID STEROL ACYLTRANSFERASE1* in plant sterol homeostasis and leaf senescence. *Plant Physiol* **152**(1): 107-119.
- Buchanan-Wollaston V. 1997.** The molecular biology of leaf senescence. *J Exp Bot* **48**(307): 181-199.
- Busch W, Miotk A, Ariel FD, Zhao Z, Forner J, Daum G, Suzaki T, Schuster C, Schultheiss SJ, Leibfried A, et al. 2010.** Transcriptional control of a plant stem cell niche. *Dev Cell* **18**(5): 849-861.
- Chen L, Xiang S, Chen Y, Li D, Yu D. 2017.** *Arabidopsis* WRKY45 interacts with the DELLA protein RGL1 to positively regulate age-triggered leaf senescence. *Mol Plant* **10**(9): 1174-1189.
- Cho WK, Geimer S, Meurer J. 2009.** Cluster analysis and comparison of various chloroplast transcriptomes and genes in *Arabidopsis thaliana*. *DNA Res* **16**(1): 31-44.
- Chung T, Suttangkakul A, Vierstra RD. 2009.** The ATG autophagic conjugation system in maize: ATG transcripts and abundance of the ATG8-lipid adduct are regulated by development and nutrient availability. *Plant Physiol* **149**(1): 220-234.
- Clark SE, Running MP, Meyerowitz EM. 1993.** CLAVATA1, a regulator of meristem and flower development in *Arabidopsis*. *Development* **119**(2): 397-418.
- Cove DJ, Knight CD. 1993.** The moss *Physcomitrella patens*, a model system with potential for the study of plant reproduction. *Plant Cell* **5**(10): 1483-1488.
- Cove DJ, Perroud PF, Charron AJ, McDaniel SF, Khandelwal A, Quatrano RS. 2009.** The moss *Physcomitrella patens*: a novel model system for plant development and genomic studies. *Cold Spring Harb Protoc* **2009**(2): pdb emo115.
- Critchley JH, Zeeman SC, Takaha T, Smith AM, Smith SM. 2001.** A critical role for disproportionating enzyme in starch breakdown is revealed by a knock-out mutation in *Arabidopsis*. *Plant J* **26**(1): 89-100.
- Cui H, Levesque MP, Vernoux T, Jung JW, Paquette AJ, Gallagher KL, Wang JY, Blilou I, Scheres B, Benfey PN. 2007.** An evolutionarily conserved mechanism delimiting SHR movement defines a single layer of endodermis in plants. *Science* **316**(5823): 421-425.
- Delatte T, Umhang M, Trevisan M, Eicke S, Thorneycroft D, Smith SM, Zeeman SC. 2006.** Evidence for distinct mechanisms of starch granule breakdown in plants. *J Biol Chem* **281**(17): 12050-12059.
- Di Laurenzio L, Wysocka-Diller J, Malamy JE, Pysh L, Helariutta Y, Freshour G, Hahn MG, Feldmann KA, Benfey PN. 1996.** The *SCARECROW* gene regulates an asymmetric cell division that is essential for generating the radial organization of the *Arabidopsis* root. *Cell* **86**(3): 423-433.
- Diaz C, Lemaitre T, Christ A, Azzopardi M, Kato Y, Sato F, Morot-Gaudry JF, Le Dily F, Masclaux-Daubresse C. 2008.** Nitrogen recycling and remobilization are differentially controlled by leaf senescence and development stage in *Arabidopsis* under low nitrogen nutrition. *Plant Physiol* **147**(3): 1437-1449.

- Doerner P. 2003.** Plant meristems: a merry-go-round of signals. *Curr Biol* **13**(9): R368-R374.
- Dugas DV, Bartel B. 2004.** MicroRNA regulation of gene expression in plants. *Curr Opin Plant Biol* **7**(5): 512-520.
- Edner C, Li J, Albrecht T, Mahlow S, Hejazi M, Hussain H, Kaplan F, Guy C, Smith SM, Steup M, et al. 2007.** Glucan, water dikinase activity stimulates breakdown of starch granules by plastidial beta-amylases. *Plant Physiol* **145**(1): 17-28.
- Edwards G, Walker D. 1983.** Photosynthesis: c3, c4. Mechanisms, and cellular and environmental regulation, of photosynthesis. *Science* **222**(4627): 1009.
- Engstrom EM. 2011.** Phylogenetic analysis of GRAS proteins from moss, lycophyte and vascular plant lineages reveals that *GRAS* genes arose and underwent substantial diversification in the ancestral lineage common to bryophytes and vascular plants. *Plant Signal Behav* **6**(6): 850-854.
- Engstrom EM. 2012.** HAM proteins promote organ indeterminacy: but how? *Plant Signal Behav* **7**(2): 227-234.
- Engstrom EM, Andersen CM, Gumulak-Smith J, Hu J, Orlova E, Sozzani R, Bowman JL. 2011.** *Arabidopsis* homologs of the *Petunia HAIRY MERISTEM* gene are required for maintenance of shoot and root indeterminacy. *Plant Physiol* **155**(2): 735-750.
- Felsenstein J. 1985.** Confidence limits on phylogenies: an approach using the Bootstrap. *Evolution* **39**(4): 783-791.
- Ferreira SJ, Senning M, Fischer-Stettler M, Streb S, Ast M, Neuhaus HE, Zeeman SC, Sonnewald S, Sonnewald U. 2017.** Simultaneous silencing of isoamylases ISA1, ISA2 and ISA3 by multi-target RNAi in potato tubers leads to decreased starch content and an early sprouting phenotype. *PLoS One* **12**(7): e0181444.
- Flores-Perez U, Bedard J, Tanabe N, Lymperopoulos P, Clarke AK, Jarvis P. 2016.** Functional analysis of the Hsp93/ClpCchaperone at the chloroplast envelope. *Plant Physiol* **170**(1): 147-162.
- Frank W, Decker EL, Reski R. 2005.** Molecular tools to study *Physcomitrella patens*. *Plant Biol (Stuttg)* **7**(3): 220-227.
- Fraser NJ, Hashimoto H, Cogdell RJ. 2001.** Carotenoids and bacterial photosynthesis: the story so far ... *Photosynthesis Res* **70**(3): 249-256.
- Fujii H, Chiou TJ, Lin SI, Aung K, Zhu JK. 2005.** A miRNA involved in phosphate-starvation response in *Arabidopsis*. *Curr Biol* **15**(22): 2038-2043.
- Fulton DC, Stettler M, Mettler T, Vaughan CK, Li J, Francisco P, Gil M, Reinhold H, Eicke S, Messerli G, et al. 2008.**  $\beta$ -AMYLASE4, a noncatalytic protein required for starch breakdown, acts upstream of three active  $\beta$ -amylases in *Arabidopsis* chloroplasts. *Plant Cell* **20**(4): 1040-1058.
- Gallagher KL, Benfey PN. 2009.** Both the conserved GRAS domain and nuclear localization are required for SHORT-ROOT movement. *Plant J* **57**(5): 785-797.

- Gan S, Amasino RM. 1995.** Inhibition of leaf senescence by autoregulated production of cytokinin. *Science* **270**(5244): 1986-1988.
- Gan S, Amasino RM. 1997.** Making sense of senescence (molecular genetic regulation and manipulation of leaf senescence). *Plant Physiol* **113**(2): 313-319.
- Greb T, Clarenz O, Schafer E, Muller D, Herrero R, Schmitz G, Theres K. 2003.** Molecular analysis of the *LATERAL SUPPRESSOR* gene in *Arabidopsis* reveals a conserved control mechanism for axillary meristem formation. *Genes Dev* **17**(9): 1175-1187.
- Guan QM, Lu XY, Zeng HT, Zhang YY, Zhu JH. 2013.** Heat stress induction of miR398 triggers a regulatory loop that is critical for thermotolerance in *Arabidopsis*. *Plant J* **74**(5): 840-851.
- Han MH, Goud S, Song L, Fedoroff N. 2004.** The *Arabidopsis* double-stranded RNA-binding protein HYL1 plays a role in microRNA-mediated gene regulation. *Proc Natl Acad Sci U S A* **101**(4): 1093-1098.
- Helariutta Y, Fukaki H, Wsocka-Diller J, Nakajima K, Jung J, Sena G, Hauser MT, Benfey PN. 2000.** The *SHORT-ROOT* gene controls radial patterning of the *Arabidopsis* root through radial signaling. *Cell* **101**(5): 555-567.
- Hendelman A, Kravchik M, Stav R, Frank W, Arazi T. 2016.** Tomato *HAIRY MERISTEM* genes are involved in meristem maintenance and compound leaf morphogenesis. *J Exp Bot* **67**(21): 6187-6200.
- Heo JO, Chang KS, Kim IA, Lee MH, Lee SA, Song SK, Lee MM, Lim J. 2011.** Funneling of gibberellin signaling by the GRAS transcription regulator scarecrow-like 3 in the *Arabidopsis* root. *Proc Natl Acad Sci U S A* **108**(5): 2166-2171.
- Hirano K, Nakajima M, Asano K, Nishiyama T, Sakakibara H, Kojima M, Katoh E, Xiang H, Tanahashi T, Hasebe M, et al. 2007.** The GID1-mediated gibberellin perception mechanism is conserved in the lycophyte *Selaginella moellendorffii* but not in the bryophyte *Physcomitrella patens*. *Plant Cell* **19**(10): 3058-3079.
- Hirsch S, Oldroyd GE. 2009.** GRAS-domain transcription factors that regulate plant development. *Plant Signal Behav* **4**(8): 698-700.
- Hofmann NR. 2016.** A structure for plant-specific transcription factors: the GRAS domain revealed. *Plant Cell* **28**(5): 993-994.
- Huang W, Peng S, Xian Z, Lin D, Hu G, Yang L, Ren M, Li Z. 2017.** Overexpression of a tomato miR171 target gene *SIGRAS24* impacts multiple agronomical traits via regulating gibberellin and auxin homeostasis. *Plant Biotechnol J* **15**(4): 472-488.
- Huang W, Xian ZQ, Kang X, Tang N, Li ZG. 2015.** Genome-wide identification, phylogeny and expression analysis of *GRAS* gene family in tomato. *BMC Plant Biol* **15**.
- Itakura E, Kishi C, Inoue K, Mizushima N. 2008.** Beclin 1 forms two distinct phosphatidylinositol 3-kinase complexes with mammalian Atg14 and UVRAG. *Mol Biol Cell* **19**(12): 5360-5372.
- Kalve S, De Vos D, Beemster GT. 2014.** Leaf development: a cellular perspective. *Front Plant Sci* **5**: 362.

- Kametaka S, Okano T, Ohsumi M, Ohsumi Y. 1998.** APG14P and APG6/VPS30P form a protein complex essential for autophagy in the yeast, *Saccharomyces cerevisiae*. *J Biol Chem* **273**(35): 22284-22291.
- Katagiri Y, Hasegawa J, Fujikura U, Hoshino R, Matsunaga S, Tsukaya H. 2016.** The coordination of ploidy and cell size differs between cell layers in leaves. *Development* **143**(7): 1120-1125.
- Khraiweh B, Ossowski S, Weigel D, Reski R, Frank W. 2008.** Specific gene silencing by artificial microRNAs in *Physcomitrella patens*: An alternative to targeted gene knockouts. *Plant Physiol* **148**(2): 684-693.
- Kim S, Schlicke H, Van Ree K, Karvonen K, Subramaniam A, Richter A, Grimm B, Braam J. 2013.** *Arabidopsis* chlorophyll biosynthesis: An essential balance between the methylerythritol phosphate and tetrapyrrole pathways. *Plant Cell* **25**(12): 4984-4993.
- Kim SH, Kwon C, Lee JH, Chung T. 2012.** Genes for plant autophagy: functions and interactions. *Mol Cells* **34**(5): 413-423.
- Kinoshita A, ten Hove CA, Tabata R, Yamada M, Shimizu N, Ishida T, Yamaguchi K, Shigenobu S, Takebayashi Y, Iuchi S, et al. 2015.** A plant U-box protein, PUB4, regulates asymmetric cell division and cell proliferation in the root meristem. *Development* **142**(3): 444-453.
- Klionsky DJ. 2005.** The molecular machinery of autophagy: unanswered questions. *J Cell Sci* **118**(1): 7-18.
- Kofuji R, Hasebe M. 2014.** Eight types of stem cells in the life cycle of the moss *Physcomitrella patens*. *Curr Opin Plant Biol* **17**: 13-21.
- Kotting O, Pusch K, Tiessen A, Geigenberger P, Steup M, Ritte G. 2005.** Identification of a novel enzyme required for starch metabolism in *Arabidopsis* leaves. The phosphoglucan, water dikinase. *Plant Physiol* **137**(1): 242-252.
- Kotting O, Santelia D, Edner C, Eicke S, Marthaler T, Gentry MS, Comparot-Moss S, Chen J, Smith AM, Steup M, et al. 2009.** STARCH-EXCESS4 is a laforin-like phosphoglucan phosphatase required for starch degradation in *Arabidopsis thaliana*. *Plant Cell* **21**(1): 334-346.
- Kubo M, Imai A, Nishiyama T, Ishikawa M, Sato Y, Kurata T, Hiwatashi Y, Reski R, Hasebe M. 2013a.** System for stable beta-estradiol-inducible gene expression in the moss *Physcomitrella patens*. *PLoS One* **8**(9): e77356.
- Kumar D, Yusuf, M. A., Singh, P., Sardar, M. and Sarin, N. B. 2014.** Histochemical detection of superoxide and H<sub>2</sub>O<sub>2</sub> accumulation in *Brassica juncea* Seedlings. *Bio-protocol* **4**(8).
- Kumar S, Stecher G, Li M, Knyaz C, Tamura K. 2018.** MEGA X: molecular evolutionary genetics analysis across computing platforms. *Mol Biol Evol* **35**(6): 1547-1549.
- Kwon T, Huq E, Herrin DL. 2010.** Microhomology-mediated and nonhomologous repair of a double-strand break in the chloroplast genome of *Arabidopsis*. *Proc Natl Acad Sci U S A* **107**(31): 13954-13959.

- Lamkemeyer P, Laxa M, Collin V, Li W, Finkemeier I, Schottler MA, Holtkamp V, Tognetti VB, Issakidis-Bourguet E, Kandlbinder A, et al. 2006.** Peroxiredoxin Q of *Arabidopsis thaliana* is attached to the thylakoids and functions in context of photosynthesis. *Plant J* **45**(6): 968-981.
- Lang D, Ullrich KK, Murat F, Fuchs J, Jenkins J, Haas FB, Piednoel M, Gundlach H, Van Bel M, Meyberg R, et al. 2018.** The *Physcomitrella patens* chromosome-scale assembly reveals moss genome structure and evolution. *Plant J* **93**(3): 515-533.
- Laux T, Mayer KFX, Berger J, Jurgens G. 1996.** The *WUSCHEL* gene is required for shoot and floral meristem integrity in *Arabidopsis*. *Development* **122**(1): 87-96.
- Lee RC, Feinbaum RL, Ambros V. 1993.** The *C. elegans* heterochronic gene *lin-4* encodes small RNAs with antisense complementarity to *lin-14*. *Cell* **75**(5): 843-854.
- Lee Y, Kim M, Han J, Yeom KH, Lee S, Baek SH, Kim VN. 2004.** MicroRNA genes are transcribed by RNA polymerase II. *EMBO J* **23**(20): 4051-4060.
- Lee ZH, Hirakawa T, Yamaguchi N, Ito T. 2019.** The Roles of Plant Hormones and Their Interactions with Regulatory Genes in Determining Meristem Activity. *Int J Mol Sci* **20**(16): 4065
- Leibfried A, To JP, Busch W, Stehling S, Kehle A, Demar M, Kieber JJ, Lohmann JU. 2005.** WUSCHEL controls meristem function by direct regulation of cytokinin-inducible response regulators. *Nature* **438**(7071): 1172-1175.
- Li J, Francisco P, Zhou W, Edner C, Steup M, Ritte G, Bond CS, Smith SM. 2009.** Catalytically-inactive  $\beta$ -amylase BAM4 required for starch breakdown in *Arabidopsis* leaves is a starch-binding-protein. *Arch Biochem Biophys* **489**(1-2): 92-98.
- Li S, Zhao Y, Zhao Z, Wu X, Sun L, Liu Q, Wu Y. 2016.** Crystal Structure of the GRAS Domain of SCARECROW-LIKE7 in *Oryza sativa*. *Plant Cell* **28**(5): 1025-1034.
- Li XY, Qian Q, Fu ZM, Wang YH, Xiong GS, Zeng DL, Wang XQ, Liu XF, Teng S, Hiroshi F, et al. 2003.** Control of tillering in rice. *Nature* **422**(6932): 618-621.
- Lichtenthaler H WA. 1983.** Determinations of total carotenoids and chlorophylls a and b of leaf extracts in different solvents. *Biochem Soc Trans* **11**(591-592).
- Liu J, Yang HX, Lu QT, Wen XG, Chen F, Peng LW, Zhang LX, Lu CM. 2012.** PSBP-DOMAIN PROTEIN1, a nuclear-encoded thylakoid luminal protein, is essential for photosystem I assembly in *Arabidopsis*. *Plant Cell* **24**(12): 4992-5006.
- Liu XY, Widmer A. 2014.** Genome-wide comparative analysis of the *GRAS* gene family in *Populus*, *Arabidopsis* and rice. *Plant Mol Biol Rep* **32**(6): 1129-1145.
- Liu Y, Bassham DC. 2012.** Autophagy: pathways for self-eating in plant cells. *Annu Rev Plant Biol* **63**: 215-237.
- Liu Z, Miao L, Huo R, Song X, Johnson C, Kong L, Sundaresan V, Yu X. 2018.** *ARF2-ARF4* and *ARF5* are Essential for Female and Male Gametophyte Development in *Arabidopsis*. *Plant Cell Physiol* **59**(1): 179-189.

- Liu ZF, Yan HC, Wang KB, Kuang TY, Zhang JP, Gui LL, An XM, Chang WR. 2004.** Crystal structure of spinach major light-harvesting complex at 2.72 angstrom resolution. *Nature* **428**(6980): 287-292.
- Livak KJ, Schmittgen TD. 2001.** Analysis of relative gene expression data using real-time quantitative PCR and the 2(T)(-Delta Delta C) method. *Methods* **25**(4): 402-408.
- Llave C, Xie Z, Kasschau KD, Carrington JC. 2002.** Cleavage of *Scarecrow-like* mRNA targets directed by a class of *Arabidopsis* miRNA. *Science* **297**(5589): 2053-2056.
- Ma ZX, Hu XP, Cai WJ, Huang WH, Zhou X, Luo Q, Yang HQ, Wang JW, Huang JR. 2014.** *Arabidopsis* miR171-targeted scarecrow-like proteins bind to GT *cis*-elements and mediate gibberellin-regulated chlorophyll biosynthesis under light conditions. *PLoS Genet* **10**(8).
- Mandel T, Moreau F, Kutsher Y, Fletcher JC, Carles CC, Eshed Williams L. 2014.** The ERECTA receptor kinase regulates *Arabidopsis* shoot apical meristem size, phyllotaxy and floral meristem identity. *Development* **141**(4): 830-841.
- Mariotti L, Fambrini M, Scartazza A, Picciarelli P, Pugliesi C. 2018.** Characterization of lingering hope, a new brachytic mutant in sunflower (*Helianthus annuus* L.) with altered salicylic acid metabolism. *J Plant Physiol* **231**: 402-414.
- Marshall RS, Vierstra RD. 2018.** Autophagy: The master of bulk and selective recycling. *Annu Rev Plant Biol* **69**: 173-208.
- Martin A, Lang D, Heckmann J, Zimmer AD, Vervliet-Scheebaum M, Reski R. 2009.** A uniquely high number of *ftsZ* genes in the moss *Physcomitrella patens*. *Plant Biol (Stuttg)* **11**(5): 744-750.
- Martinez DE, Costa ML, Gomez FM, Otegui MS, Guamet JJ. 2008.** 'Senescence-associated vacuoles' are involved in the degradation of chloroplast proteins in tobacco leaves. *Plant J* **56**(2): 196-206.
- Masclaux-Daubresse C, Chardon F. 2011.** Exploring nitrogen remobilization for seed filling using natural variation in *Arabidopsis thaliana*. *J Exp Bot* **62**(6): 2131-2142.
- Mayrose M, Ekengren SK, Melech-Bonfil S, Martin GB, Sessa G. 2006.** A novel link between tomato *GRAS* genes, plant disease resistance and mechanical stress response. *Molecular Plant Pathology* **7**(6): 593-604.
- Mehrpour M, Esclatine A, Beau I, Codogno P. 2010.** Overview of macroautophagy regulation in mammalian cells. *Cell Res* **20**(7): 748-762.
- Menand B, Calder G, Dolan L. 2007.** Both chloronemal and caulonemal cells expand by tip growth in the moss *Physcomitrella patens*. *J Exp Bot* **58**(7): 1843-1849.
- Mikkelsen R, Mutenda KE, Mant A, Schurmann P, Blennow A. 2005.** alpha-Glucan, water dikinase (GWD): A plastidic enzyme with redox-regulated and coordinated catalytic activity and binding affinity. *Proc Natl Acad Sci U S A* **102**(5): 1785-1790.
- Miyazaki S, Nakajima M, Kawaide H. 2015.** Hormonal diterpenoids derived from *ent*-kaurenoic acid are involved in the blue-light avoidance response of *Physcomitrella patens*. *Plant Signal Behav* **10**(2): e989046.

- Mizushima N. 2007.** Autophagy: process and function. *Genes Dev* **21**(22): 2861-2873.
- Moriyasu Y, Ohsumi Y. 1996.** Autophagy in tobacco suspension-cultured cells in response to sucrose starvation. *Plant Physiol* **111**(4): 1233-1241.
- Morohashi K, Minami M, Takase H, Hotta Y, Hiratsuka K. 2003.** Isolation and characterization of a novel *GRAS* gene that regulates meiosis-associated gene expression. *J Biol Chem* **278**(23): 20865-20873.
- Mueller SJ, Lang D, Hoernstein SN, Lang EG, Schuessele C, Schmidt A, Fluck M, Leisibach D, Niegl C, Zimmer AD, et al. 2014.** Quantitative analysis of the mitochondrial and plastid proteomes of the moss *Physcomitrella patens* reveals protein macrocompartmentation and microcompartmentation. *Plant Physiol* **164**(4): 2081-2095.
- Mukae K, Inoue Y, Moriyasu Y. 2015.** ATG5-knockout mutants of *Physcomitrella* provide a platform for analyzing the involvement of autophagy in senescence processes in plant cells. *Plant Signal Behav* **10**(11): e1086859.
- Muller R, Bleckmann A, Simon R. 2008.** The receptor kinase CORYNE of *Arabidopsis* transmits the stem cell-limiting signal CLAVATA3 independently of CLAVATA1. *Plant Cell* **20**(4): 934-946.
- Niittyla T, Comparot-Moss S, Lue WL, Messerli G, Trevisan M, Seymour MDJ, Gatehouse JA, Villadsen D, Smith SM, Chen JC, et al. 2006.** Similar protein phosphatases control starch metabolism in plants and glycogen metabolism in mammals. *J Biol Chem* **281**(17): 11815-11818.
- Nimchuk ZL. 2017.** CLAVATA1 controls distinct signaling outputs that buffer shoot stem cell proliferation through a two-step transcriptional compensation loop. *PLoS Genet* **13**(3).
- Nishiyama T, Sakayama H, de Vries J, Buschmann H, Saint-Marcoux D, Ullrich KK, Haas FB, Vanderstraeten L, Becker D, Lang D, et al. 2018.** The *Chara* genome: secondary complexity and implications for plant terrestrialization. *Cell* **174**(2): 448-464 e424.
- O'Maoileidigh DS, Stewart D, Zheng B, Coupland G, Wellmer F. 2018.** Floral homeotic proteins modulate the genetic program for leaf development to suppress trichome formation in flowers. *Development* **145**(3).
- Ortiz-Ramirez C, Hernandez-Coronado M, Thamm A, Catarino B, Wang M, Dolan L, Feijo JA, Becker JD. 2016.** A transcriptome atlas of *Physcomitrella patens* provides insights into the evolution and development of land plants. *Mol Plant* **9**(2): 205-220.
- Orzechowski S. 2008.** Starch metabolism in leaves. *Acta Biochim Pol* **55**(3): 435-445.
- Overvoorde PJ, Okushima Y, Alonso JM, Chan A, Chang C, Ecker JR, Hughes B, Liu A, Onodera C, Quach H, et al. 2005.** Functional genomic analysis of the AUXIN/INDOLE-3-ACETIC ACID gene family members in *Arabidopsis thaliana*. *Plant Cell* **17**(12): 3282-3300.
- Palatnik JF, Allen E, Wu X, Schommer C, Schwab R, Carrington JC, Weigel D. 2003.** Control of leaf morphogenesis by microRNAs. *Nature* **425**(6955): 257-263.

- Park J, Nguyen KT, Park E, Jeon JS, Choi G. 2013.** DELLA proteins and their interacting RING Finger proteins repress gibberellin responses by binding to the promoters of a subset of gibberellin-responsive genes in *Arabidopsis*. *Plant Cell* **25**(3): 927-943.
- Park W, Li J, Song R, Messing J, Chen X. 2002.** CARPEL FACTORY, a Dicer homolog, and HEN1, a novel protein, act in microRNA metabolism in *Arabidopsis thaliana*. *Curr Biol* **12**(17): 1484-1495.
- Peng J, Carol P, Richards DE, King KE, Cowling RJ, Murphy GP, Harberd NP. 1997.** The *Arabidopsis* *GAI* gene defines a signaling pathway that negatively regulates gibberellin responses. *Genes Dev* **11**(23): 3194-3205.
- Perroud PF, Quatrano RS. 2008.** BRICK1 is required for apical cell growth in filaments of the moss *Physcomitrella patens* but not for gametophore morphology. *Plant Cell* **20**(2): 411-422.
- Pogson B, McDonald KA, Truong M, Britton G, DellaPenna D. 1996.** *Arabidopsis* carotenoid mutants demonstrate that lutein is not essential for photosynthesis in higher plants. *Plant Cell* **8**(9): 1627-1639.
- Potten CS, Loeffler M. 1990.** Stem-Cells - Attributes, Cycles, Spirals, Pitfalls and Uncertainties - Lessons for and from the Crypt. *Development* **110**(4): 1001-1020.
- Pulido P, Toledo-Ortiz G, Phillips MA, Wright LP, Rodriguez-Concepcion M. 2013.** *Arabidopsis* J-Protein J20 delivers the first enzyme of the plastidial isoprenoid pathway to protein quality control. *Plant Cell* **25**: 4183-4194.
- Pysh LD, Wysocka-Diller JW, Camilleri C, Bouchez D, Benfey PN. 1999.** The *GRAS* gene family in *Arabidopsis*: sequence characterization and basic expression analysis of the *SCARECROW-LIKE* genes. *Plant J* **18**(1): 111-119.
- Reiss B. 2003.** Homologous recombination and gene targeting in plant cells. *Int Rev Cytol* **228**: 85-139.
- Rensing SA, Lang D, Zimmer AD, Terry A, Salamov A, Shapiro H, Nishiyama T, Perroud PF, Lindquist EA, Kamisugi Y, et al. 2008.** The *Physcomitrella* genome reveals evolutionary insights into the conquest of land by plants. *Science* **319**(5859): 64-69.
- Reski R, Abel WO. 1985.** Induction of budding on chloronemata and caulonemata of the moss, *Physcomitrella patens*, using isopentenyladenine. *Planta* **165**(3): 354-358.
- Reski R, Frank W. 2005.** Moss (*Physcomitrella patens*) functional genomics-Gene discovery and tool development, with implications for crop plants and human health. *Brief Funct Genomic Proteomic* **4**(1): 48-57.
- Rich MK, Courty PE, Roux C, Reinhardt D. 2017.** Role of the GRAS transcription factor ATA/RAM1 in the transcriptional reprogramming of arbuscular mycorrhiza in *Petunia hybrida*. *BMC Genomics* **18**(1): 589.
- Ripoll JJ, Ferrandiz C, Martinez-Laborda A, Vera A. 2006.** *PEPPER*, a novel K-homology domain gene, regulates vegetative and gynoecium development in *Arabidopsis*. *Dev Biol* **289**(2): 346-359.

- Ritz T, Damjanovic A, Schulten K, Zhang JP, Koyama Y. 2000.** Efficient light harvesting through carotenoids. *Photosynthesis Res* **66**(1-2): 125-144.
- Romera-Branchat M, Ripoll JJ, Yanofsky MF, Pelaz S. 2013.** The *WOX13* homeobox gene promotes replum formation in the *Arabidopsis thaliana* fruit. *Plant J* **73**(1): 37-49.
- Roth O, Alvarez JP, Levy M, Bowman JL, Ori N, Shani E. 2018.** The KNOXI Transcription Factor SHOOT MERISTEMLESS regulates floral fate in *Arabidopsis*. *Plant Cell* **30**(6): 1309-1321.
- Rottmann T, Fritz C, Sauer N, Stadler R. 2018.** Glucose uptake via STP transporters inhibits in vitro pollen tube growth in a HEXOKINASE1-Dependent manner in *Arabidopsis thaliana*. *Plant Cell* **30**(9): 2057-2081.
- Saitou N, Nei M. 1987.** The neighbor-joining method: a new method for reconstructing phylogenetic trees. *Mol Biol Evol* **4**(4): 406-425.
- Sakakibara K, Reisewitz P, Aoyama T, Friedrich T, Ando S, Sato Y, Tamada Y, Nishiyama T, Hiwatashi Y, Kurata T, et al. 2014.** *WOX13-like* genes are required for reprogramming of leaf and protoplast cells into stem cells in the moss *Physcomitrella patens*. *Development* **141**(8): 1660-1670.
- Schaefer D, Zryd JP, Knight CD, Cove DJ. 1991.** Stable transformation of the moss *Physcomitrella patens*. *MGG* **226**: 418-424
- Schaefer DG, Zryd JP. 1997.** Efficient gene targeting in the moss *Physcomitrella patens*. *Plant J* **11**(6): 1195-1206.
- Schlicke H, Hartwig AS, Firtzlaff V, Richter AS, Glasser C, Maier K, Finkemeier I, Grimm B. 2014.** Induced deactivation of genes encoding chlorophyll biosynthesis enzymes disentangles tetrapyrrole-mediated retrograde signaling. *Mol Plant* **7**(7): 1211-1227.
- Schneider A, Hausler RE, Kolukisaoglu U, Kunze R, van der Graaff E, Schwacke R, Catoni E, Desimone M, Flugge UI. 2002.** An *Arabidopsis thaliana* knock-out mutant of the chloroplast triose phosphate/phosphate translocator is severely compromised only when starch synthesis, but not starch mobilisation is abolished. *Plant J* **32**(5): 685-699.
- Schoof H, Lenhard M, Haecker A, Mayer KFX, Jürgens G, Laux, T. 2000.** The stem cell population of *Arabidopsis* shoot meristems is maintained by a regulatory loop between the *CLAVATA* and *WUSCHEL* genes. *Cell* **100**: 635-644.
- Schulze S, Schafer BN, Parizotto EA, Voinnet O, Theres K. 2010.** *LOST MERISTEMS* genes regulate cell differentiation of central zone descendants in *Arabidopsis* shoot meristems. *Plant J* **64**(4): 668-678.
- Schumacher K, Schmitt T, Rossberg M, Schmitz G, Theres K. 1999.** The *LATERAL SUPPRESSOR (Ls)* gene of tomato encodes a new member of the VHIID protein family. *Proc Natl Acad Sci U S A* **96**(1): 290-295.
- Schwab R, Palatnik JF, Riester M, Schommer C, Schmid M, Weigel D. 2005.** Specific effects of microRNAs on the plant transcriptome. *Dev Cell* **8**(4): 517-527.

- Sebastian J, Ryu KH, Zhou J, Tarkowska D, Tarkowski P, Cho YH, Yoo SD, Kim ES, Lee JY. 2015.** PHABULOSA controls the quiescent center-independent root meristem activities in *Arabidopsis thaliana*. *PLoS Genet* **11**(3): e1004973.
- Shin JH, Yoshimoto K, Ohsumi Y, Jeon JS, An G. 2009.** OsATG10b, an autophagosome component, is needed for cell survival against oxidative stresses in rice. *Mol Cells* **27**(1): 67-74.
- Silverstone AL, Ciampaglio CN, Sun T. 1998.** The *Arabidopsis* RGA gene encodes a transcriptional regulator repressing the gibberellin signal transduction pathway. *Plant Cell* **10**(2): 155-169.
- Smith AM, Zeeman SC, Smith SM. 2005.** Starch degradation. *Annu Rev Plant Biol* **56**: 73-98.
- Soubeyrand E, Johnson TS, Latimer S, Block A, Kim J, Colquhoun TA, Butelli E, Martin C, Wilson MA, Basset GJ. 2018.** The peroxidative cleavage of kaempferol contributes to the biosynthesis of the benzenoid moiety of ubiquinone in plants. *Plant Cell* **30**(12): 2910-2921.
- Sowokinos JR. 1981.** Pyrophosphorylases in *Solanum tuberosum*. *Plant Physiol* **68**(4): 924-929.
- Sowokinos JR, Preiss J. 1982.** Pyrophosphorylases in *Solanum tuberosum* *Plant Physiol* **69**(6): 1459-1466.
- Staswick PE, Serban B, Rowe M, Tiriyaki I, Maldonado MT, Maldonado MC, Suza W. 2005.** Characterization of an *Arabidopsis* enzyme family that conjugates amino acids to indole-3-acetic acid. *Plant Cell* **17**(2): 616-627.
- Stettler M, Eicke S, Mettler T, Messerli G, Hortensteiner S, Zeeman SC. 2009.** Blocking the metabolism of starch breakdown products in *Arabidopsis* leaves triggers chloroplast degradation. *Mol Plant* **2**(6): 1233-1246.
- Streb S, Eicke S, Zeeman SC. 2012.** The simultaneous abolition of three starch hydrolases blocks transient starch breakdown in *Arabidopsis*. *J Biol Chem* **287**(50): 41745-41756.
- Strotbek C. 2015.** Vergleichende analyse der miR171-vermittelten genregulation in den landpflanzen *Physcomitrella patens* und *Arabidopsis thaliana*. *Ludwig-Maximilians-Universität München Dissertation*.
- Strotbek C, Krininger S, Frank W. 2013.** The moss *Physcomitrella patens*: methods and tools from cultivation to targeted analysis of gene function. *Int J Dev Biol* **57**(6-8): 553-564.
- Su PH, Li HM. 2008.** *Arabidopsis* stromal 70-kD HEAT SHOCK proteins are essential for plant development and important for thermotolerance of germinating seeds. *Plant Physiol* **146**(3): 1231-1241.
- Sun X, Lin L, Sui N. 2019.** Regulation mechanism of microRNA in plant response to abiotic stress and breeding. *Mol Biol Rep* **46**(1): 1447-1457.
- Sun XD, Ni M. 2011.** HYPOSENSITIVE TO LIGHT, an alpha/beta fold protein, acts downstream of ELONGATED HYPOCOTYL 5 to regulate seedling de-etiolation. *Mol Plant* **4**(1): 116-126.

- Sunkar R, Zhu JK. 2004.** Novel and stress-regulated microRNAs and other small RNAs from *Arabidopsis*. *Plant Cell* **16**(8): 2001-2019.
- Sussex IM. 1952.** Regeneration of the Potato Shoot Apex. *Nature* **170**(4331): 755-757.
- Takehige K, Baba M, Tsuboi S, Noda T, Ohsumi Y. 1992.** Autophagy in yeast demonstrated with proteinase-deficient mutants and conditions for its induction. *J Cell Biol* **119**(2): 301-311.
- Tian CG, Wan P, Sun SH, Li JY, Chen MS. 2004.** Genome-wide analysis of the *GRAS* gene family in rice and *Arabidopsis*. *Plant Mol Biol* **54**(4): 519-532.
- Torres-Galea P, Hirtreiter B, Bolle C. 2013.** Two GRAS proteins, SCARECROW-LIKE21 and PHYTOCHROME A SIGNAL TRANSDUCTION1, function cooperatively in phytochrome A signal transduction. *Plant Physiol* **161**(1): 291-304.
- Torres-Galea P, Huang LF, Chua NH, Bolle C. 2006.** The GRAS protein SCL13 is a positive regulator of phytochrome-dependent red light signaling, but can also modulate phytochrome A responses. *Mol Genet Genomics* **276**(1): 13-30.
- Walters RG, Ibrahim DG, Horton P, Kruger NJ. 2004.** A mutant of *Arabidopsis* lacking the triose-phosphate/phosphate translocator reveals metabolic regulation of starch breakdown in the light. *Plant Physiol* **135**(2): 891-906.
- Wang G, Kong H, Sun Y, Zhang X, Zhang W, Altman N, DePamphilis CW, Ma H. 2004.** Genome-wide analysis of the CYCLIN family in *Arabidopsis* and comparative phylogenetic analysis of plant CYCLIN-LIKE proteins. *Plant Physiol* **135**(2): 1084-1099.
- Wang JW, Wang LJ, Mao YB, Cai WJ, Xue HW, Chen XY. 2005.** Control of root cap formation by MicroRNA-targeted auxin response factors in *Arabidopsis*. *Plant Cell* **17**(8): 2204-2216.
- Wang L, Mai YX, Zhang YC, Luo Q, Yang HQ. 2010.** MicroRNA171c-targeted *SCL6-II*, *SCL6-III*, and *SCL6-IV* genes regulate shoot branching in *Arabidopsis*. *Mol Plant* **3**(5): 794-806.
- Wang ML, Jiang L, Da QG, Liu J, Feng DR, Wang JF, Wang HB, Jin HL. 2016.** DELAYED GREENING 238, a nuclear-encoded chloroplast nucleoid protein, is involved in the regulation of early chloroplast development and plastid gene expression in *Arabidopsis thaliana*. *Plant Cell Physiol* **57**(12): 2586-2599.
- Wang S, Blumwald E. 2014.** Stress-induced chloroplast degradation in *Arabidopsis* is regulated via a process independent of autophagy and senescence-associated vacuoles. *Plant Cell* **26**(12): 4875-4888.
- Wang Y, Deng D. 2014.** Molecular basis and evolutionary pattern of GA-GID1-DELLA regulatory module. *Mol Genet Genomics* **289**(1): 1-9.
- Wattebled F, Dong Y, Dumez S, Delvalle D, Planchot R, Berbezy P, Vyas D, Colonna P, Chatterjee M, Ball S, et al. 2005.** Mutants of *Arabidopsis* lacking a chloroplastic isoamylase accumulate phyto glycogen and an abnormal form of amylopectin. *Plant Physiol* **138**(1): 184-195.

- Whitewoods CD, Cammarata J, Venza ZN, Sang S, Crook AD, Aoyama T, Wang XY, Waller M, Kamisugi Y, Cuming AC, et al. 2108.** CLAVATA Was a Genetic Novelty for the Morphological Innovation of 3D Growth in Land Plants. *Current Biology* 28, 1-12
- Williams L, Grigg SP, Xie M, Christensen S, Fletcher JC. 2005.** Regulation of *Arabidopsis* shoot apical meristem and lateral organ formation by microRNA *miR166g* and its *AtHD-ZIP* target genes. *Development* 132(16): 3657-3668.
- Woo HR, Kim HJ, Nam HG, Lim PO. 2013.** Plant leaf senescence and death - regulation by multiple layers of control and implications for aging in general. *J Cell Sci* 126(21): 4823-4833.
- Wu XM, Qiao Z, Liu HP, Acharya BR, Li CL, Zhang W. 2017.** CML20, an *Arabidopsis* Calmodulin-like Protein, negatively regulates guard cell ABA signaling and drought stress tolerance. *Front Plant Sci* 8.
- Wysocka-Diller JW, Helariutta Y, Fukaki H, Malamy JE, Benfey PN. 2000.** Molecular analysis of SCARECROW function reveals a radial patterning mechanism common to root and shoot. *Development* 127(3): 595-603.
- Xu W, Chen ZX, Ahmed N, Han B, Cui QH, Liu AZ. 2016.** Genome-wide identification, evolutionary analysis, and stress responses of the *GRAS* gene family in castor beans. *Int J Mol* 17(7).
- Xu YH, Liu R, Yan L, Liu ZQ, Jiang SC, Shen YY, Wang XF, Zhang DP. 2012.** Light-harvesting chlorophyll *a/b*-binding proteins are required for stomatal response to abscisic acid in *Arabidopsis*. *J Exp Bot* 63(3): 1095-1106.
- Yadav RK, Perales M, Gruel J, Ohno C, Heisler M, Girke T, Jonsson H, Reddy GV. 2013.** Plant stem cell maintenance involves direct transcriptional repression of differentiation program. *Mol Syst Biol* 9: 654.
- Yang L, Liu ZQ, Lu F, Dong AW, Huang H. 2006.** SERRATE is a novel nuclear regulator in primary microRNA processing in *Arabidopsis*. *Plant J* 47(6): 841-850.
- Yang TW, Xue LG, An LZ. 2007.** Functional diversity of miRNA in plants. *Plant Sci* 172(3): 423-432.
- Yang Z, Ebright YW, Yu B, Chen X. 2006.** HEN1 recognizes 21-24 nt small RNA duplexes and deposits a methyl group onto the 2' OH of the 3' terminal nucleotide. *Nucleic Acids Res* 34(2): 667-675.
- Yang Z, Klionsky DJ. 2010.** Mammalian autophagy: core molecular machinery and signaling regulation. *Curr Opin Cell Biol* 22(2): 124-131.
- Yang ZF, Klionsky DJ. 2009.** An overview of the molecular mechanism of autophagy. *Curr Top Microbiol Immunol* 335: 1-32.
- Yasumura Y, Crumpton-Taylor M, Fuentes S, Harberd NP. 2007.** Step-by-step acquisition of the gibberellin-DELLA growth-regulatory mechanism during land-plant evolution. *Curr Biol* 17(14): 1225-1230.

- Yoshida H, Hirano K, Sato T, Mitsuda N, Nomoto M, Maeo K, Koketsu E, Mitani R, Kawamura M, Ishiguro S, et al. 2014.** DELLA protein functions as a transcriptional activator through the DNA binding of the INDETERMINATE DOMAIN family proteins. *Proc Natl Acad Sci U S A* **111**(21): 7861-7866.
- Yoshida S. 2003.** Molecular regulation of leaf senescence. *Curr Opin Plant Biol* **6**(1): 79-84.
- Yoshimoto K, Hanaoka H, Sato S, Kato T, Tabata S, Noda T, Ohsumi Y. 2004.** Processing of ATG8s, ubiquitin-like proteins, and their deconjugation by ATG4s are essential for plant autophagy. *Plant Cell* **16**(11): 2967-2983.
- Zagari N, Sandoval-Ibañez O, Sandal N, Su J, Rodriguez-Concepcion M, Stougaard J, Pribil M, Leister D, Pulido P. 2017.** SNOWY COTYLEDON 2 promotes chloroplast development and has a role in leaf variegation in both *Lotus japonicus* and *Arabidopsis thaliana*. *Mol Plant* **10**: 721-734.
- Zhang BH, Pan XP, Cobb GP, Anderson TA. 2006.** Plant microRNA: a small regulatory molecule with big impact. *Dev Biol* **289**(1): 3-16.
- Zhang D, Iyer LM, Aravind L. 2012.** Bacterial GRAS domain proteins throw new light on gibberellic acid response mechanisms. *Bioinformatics* **28**(19): 2407-2411.
- Zhang D, Li Y, Zhang X, Zha P, Lin R. 2017.** The SWI2/SNF2 chromatin-remodeling ATPase BRAHMA regulates chlorophyll biosynthesis in *Arabidopsis*. *Mol Plant* **10**(1): 155-167.
- Zhang H, Mi LM, Xu L, Yu CX, Li C, Chen CL. 2019.** Genome-wide identification, characterization, interaction network and expression profile of *GRAS* gene family in sweet orange (*Citrus sinensis*). *Scientific Reports* **9**.
- Zhang HD, Cui YL, Huang C, Yin QQ, Qin XM, Xu T, He XF, Zhang Y, Li ZR, Yang ZN. 2015.** PPR protein PDM1/SEL1 is involved in RNA editing and splicing of plastid genes in *Arabidopsis thaliana*. *Photosynthesis Res* **126**(2-3): 311-321.
- Zhao L, Kim YJ, Dinh TT, Chen XM. 2007.** miR172 regulates stem cell fate and defines the inner boundary of *APETALA3* and *PISTILLATA* expression domain in *Arabidopsis* floral meristems. *Plant J* **51**(5): 840-849.
- Zhou F, Roy B, Dunlap JR, Enganti R, von Arnim AG. 2014.** Translational control of *Arabidopsis* meristem stability and organogenesis by the eukaryotic translation factor eIF3h. *PLoS One* **9**(4): e95396.
- Zhou Y, Liu X, Engstrom EM, Nimchuk ZL, Pruneda-Paz JL, Tarr PT, Yan A, Kay SA, Meyerowitz EM. 2015.** Control of plant stem cell function by conserved interacting transcriptional regulators. *Nature* **517**(7534): 377-380.
- Zhou Y, Yan A, Han H, Li T, Geng Y, Liu X, Meyerowitz EM. 2018.** HAIRY MERISTEM with WUSCHEL confines *CLAVATA3* expression to the outer apical meristem layers. *Science* **361**(6401): 502-+.
- Zhu JK. 2008.** Reconstituting plant miRNA biogenesis. *Proc Natl Acad Sci U S A* **105**(29): 9851-9852.

**Zhuang X, Chung KP, Cui Y, Lin W, Gao C, Kang BH, Jiang L. 2017.** ATG9 regulates autophagosome progression from the endoplasmic reticulum in *Arabidopsis*. *Proc Natl Acad Sci U S A* **114**(3): E426-E435.

**Zhuang XH, Jiang LW. 2019.** Chloroplast degradation: multiple routes into the vacuole. *Front Plant Sci* **10**.

## 6 APPENDIX

**Appendix 1. PCR Primers.** The specificity of primers was confirmed with the Primer-BLAST. Primers were ordered from Sigma-Aldrich (Deisenhofen, Germany).

Gene ID	Accession No	Forward primers (5' → 3')	Reverse primers (5' → 3')	Amplicon Size (bp)	Note
<i>Efla</i>	<i>Pp1s7_445V6</i>	AGCGTGGTATCACAATTGAC	GATCGCTCGATCATGTTATC	412	<i>Efla</i> (cDNA)
<i>Efla</i>	<i>Pp1s7_445V6</i>	AGCGTGGTATCACAATTGAC	GATCGCTCGATCATGTTATC	660	<i>Efla</i> (gDNA)
<i>PpGRAS7</i>	<i>Pp1s130_63V6.1</i>	ggg <b>GGTACC</b> ATGGCAGACGGGG ACTTAGC	ggg <b>GGTACC</b> CGCCCGCCAAGCG CTTGC	1980	GRAS7::C
<i>PpGRAS7</i>	<i>Pp1s130_63V6.1</i>	aggagatcttctagaagat <b>GAATTC</b> TTCG AGACACTGGTTGTTGCTT	ttactagatcgggctcctctcCGGTTTGG ATGATCTTGGTACA	678	KO-c-5'fl
<i>PpGRAS7</i>	<i>Pp1s130_63V6.1</i>	GGGATTACCCGAACCTCATTGTC	gctcagatctttcagaagat <b>GAATTC</b> TGA GGTCCCAGTTTTGATTCT	613	KO-c-3'fl
<i>nptII</i>	<i>MK204379.1</i>	gacaatgagttcggtaatcccATCGGATCC TGTCAAACACTGA	GACAGGAGGCCCGATCTAGTA A	1508	<i>nptII</i> -amp
<i>PpGRAS7</i>	<i>Pp1s130_63V6.1</i>	TCTGGAAGTATCGG TGTCTGGA	AAATTATCGCGCGCGGTGTC	863	KO-5' intg
<i>PpGRAS7</i>	<i>Pp1s130_63V6.1</i>	GCGGCTGAGTGGCTCCTTCA	CCAGTTGCAGAAGTTTGTCTGAT	892	KO-3' intg
<i>PpGRAS7</i>	<i>Pp1s130_63V6.1</i>	TTGAGGGTCATTCAGGCTTTTITA	GTGGTTGTACGATCCTACCTTC G	727	KO-screen
<i>PpGRAS7</i>	<i>Pp1s130_63V6.1</i>	GTCGTTGGAGAGTGGGGTAGTC GTG	CGGCATCTGTTGAAAGTGGGA AAGC	661	KO-RT-PCR
<i>PpGRAS7</i>	<i>Pp1s130_63V6.1</i>	caccATGGCAGACGGGGACTTAG CC	TCACGCCCGCCAAGCGCTTGC	1977	iOE-TOPO <sup>1</sup>
<i>PpGRAS7</i>	<i>Pp1s130_63V6.1</i>	GGAGAGGACACGCTGAAGCTAG	CACGAGCTGTAATCCAGTTGC AGAAG	971	iOE-screen <sup>1</sup>
<i>PpGRAS7</i>	<i>Pp1s130_63V6.1</i>	GCAAAGCCACCTTCAGTTCTCT	GAGGTCCCAGTTTTGATTCTG	443	Probe <sup>1</sup>
<i>PpGRAS12</i>	<i>Pp1s205_1V6.1</i>	ggg <b>GAGCTC</b> GAGCTCTCATTGCC GAGTACCG	ggg <b>GAATTC</b> GCAGATCCACGAG GACGCAGCC	1482	GUS-c-5'fl
<i>GUS</i>	-	ggg <b>GAATTC</b> ATGGTCCGCCGGT AGAAACCC	ggg <b>GTCGACT</b> CATTGTTTGCCT CCCTGCTGC	1812	<i>GUS</i> -amp
<i>PpGRAS12</i>	<i>Pp1s205_1V6.1</i>	ggg <b>GTCGACT</b> TTGATAGTTTAATG TAGGTGCT	ggg <b>GGTACC</b> CATCAAAGTTTCC TTGTTGCAT	1528	GUS-c-3'fl

<i>PpGRAS12</i>	<i>PpIs205_IV6.1</i>	GCTTTCTCAAAGAAATGCTCTCA	CGCCCTGATGCTCCATCACT	2009	GRAS12::GUS-5' intg
<i>PpGRAS12</i>	<i>PpIs205_IV6.1</i>	ATGGTCCGGCCGGTAGAAACCC	AGAGAGCGTCATTTTATAGCTTAGCC	1917	GRAS12::GUS-3' intg
<i>PpGRAS12</i>	<i>PpIs205_IV6.1</i>	TGTCACAGGATCGGGTCCTGCA	CACAATAGTCTAGAGAGCGT	2863	GRAS12::GUS-screen
<i>PpGRAS12</i>	<i>PpIs205_IV6.1</i>	ggg <b>GTCGAC</b> ATGGTGATCACTGCAGGAAGTA	aaa <b>AGATCT</b> GCAGATCCACGAGGACGCAG	2457	GRAS12::C
<i>AtRGA1</i>	<i>At2g01570.1</i>	caccATGAAGAGAGATCATCACCAATTCCA	TCAGTACGCCGCCGTCGAGAGTT	1764	iOE-TOPO <sup>2</sup>
<i>AtRGA1</i>	<i>At2g01570.1</i>	GGAGAGGACACGCTGAAGCTAG	TCAGTACGCCGCCGTCGAGAGTT	1808	iOE-screen <sup>2</sup>
<i>AtRGA1</i>	<i>At2g01570.1</i>	AGAGTACACGTCATTGATTTCTCG	GTCTTGACTATTCGGAACTCCTTC	501	Probe <sup>2</sup>
<i>AtRGL1</i>	<i>At1g66350.1</i>	caccATGAAGAGAGAGCACAAACCACC	TTATTCCACACGATTGATTTCGC	1536	iOE-TOPO <sup>3</sup>
<i>AtRGL1</i>	<i>At1g66350.1</i>	GGAGAGGACACGCTGAAGCTAG	TTATTCCACACGATTGATTTCGC	1580	iOE-screen <sup>3</sup>
<i>AtRGL1</i>	<i>At1g66350.1</i>	GATCTTAAACCGAAATGCTAGAC	CAAACAACCTTCATTCTCTTCCAC	495	Probe <sup>3</sup>
<i>AtSCL6-II</i>	<i>At2g45160.1</i>	caccATGCCCTTATCCTTTGAAAGGTT	CTAACATTTCCAAGCAGAGACAG	1923	iOE-TOPO <sup>4</sup>
<i>AtSCL6-II</i>	<i>At2g45160.1</i>	GGAGAGGACACGCTGAAGCTAG	AGGGAAAACGGGTTGATGAAGA	677	iOE-screen <sup>4</sup>
<i>AtSCL6-II</i>	<i>At2g45160.1</i>	GGGAGGGGGTGTGTTGTTTATC	AGGGAAAACGGGTTGATGAAGA	605	Probe <sup>4</sup>
<i>AtSCL6-III</i>	<i>At3g60630.1</i>	caccATGCCCTGCCCTTTGAGCAAT	TAAACATTTCCAAGCTGAGACAG	1872	iOE-TOPO <sup>5</sup>
<i>AtSCL6-III</i>	<i>At3g60630.1</i>	GGAGAGGACACGCTGAAGCTAG	CTGGTCGATGATTACCGCTGAC	782	iOE-screen <sup>5</sup>
<i>AtSCL6-III</i>	<i>At3g60630.1</i>	ATTTCAAGGGAAGGGGGTTCTG	CTGGTCGATGATTACCGCTGAC	718	Probe <sup>5</sup>
<i>AtSCL6-IV</i>	<i>At4g00150.1</i>	caccATGCCCTTACCCTTTGAAGAGT	TCAGGAGGAGCGACATCTCCATG	1677	iOE-TOPO <sup>6</sup>
<i>AtSCL6-IV</i>	<i>At4g00150.1</i>	GGAGAGGACACGCTGAAGCTAG	TGGTTGATCAGAAGACCGGAAAG	556	iOE-screen <sup>6</sup>
<i>AtSCL6-IV</i>	<i>At4g00150.1</i>	ATGCCCTTACCCTTTGAAGAGT	TGGTTGATCAGAAGACCGGAAAG	512	Probe <sup>6</sup>

**Efla (cDNA)**: amplification of the elongation factor1 $\alpha$  from the cDNA. **Efla (gDNA)**: amplification of the elongation factor1 $\alpha$  from the genomic DNA. **GRAS7::C**: amplification of the full-length *PpGRAS7* coding sequence to generate the PpGRAS7::citrine construct. **KO-c-5'fl**: generation of the 5' flanking part of the knockout construct. Lowercase letters indicate nucleotides, which were used to generate overlaps (see 2.20.1). **KO-c-3'fl**: amplification of the 3' flanking part of the knockout constructs. Lowercase letters indicate nucleotides, which were used to generate overlaps (see 2.20.1). **nptII-amp**: primers were used to amplify *nptII* from the PBSNNNEV vector. Lowercase letters indicate nucleotides, which were used to generate overlaps (see 2.20.1). **KO-5'intg**: confirmation of the 5' integration of *PpGRAS7*-KO lines. **KO-3'intg**: confirmation of the 3' integration of *PpGRAS7*-KO lines. **KO-screen**: screening of knockout lines. **KO-RT-PCR**: confirmation of the absence of transcript in *PpGRAS7*-KO lines via RT-PCR. **iOE-TOPO<sup>1</sup>**: amplification of the full-length *PpGRAS7* coding sequence to generate the *PpGRAS7*-iOE construct. Forward primer contains cacc (small letters) at the 5' end of the primer, which is necessary for TOPO directional cloning\*. **iOE-screen<sup>1</sup>**: screening of the *PpGRAS7*-iOE lines. **Probe<sup>1</sup>**: analysis of *PpGRAS7*-iOE lines via RNA gel blot. **GUS-c-5'fl**: generation of the 5' flanking part of the PpGRAS12::GUS construct. **GUS-amp**: primers were used to amplify *GUS* coding sequence. **GUS-c-3'fl**: generation of the 3' flanking part of the PpGRAS12::GUS construct. **GRAS12::GUS-5'intg**: confirmation of the 5' integration of the PpGRAS12::GUS lines. **GRAS12::GUS-3'intg**: confirmation of the 3' integration of the PpGRAS12::GUS lines. **GRAS12::GUS-screen**: screening of the PpGRAS12::GUS lines. **GRAS12::C**: amplification of the full-length *PpGRAS7* coding sequence to generate the PpGRAS12::citrine construct. **iOE-TOPO<sup>2</sup>**: amplification of the full-length *AtRGAI* coding sequence to generate the *AtRGAI*-iOE construct. **iOE-screen<sup>2</sup>**: screening of the *AtRGAI*-iOE lines. **Probe<sup>2</sup>**: analysis of the *AtRGAI*-iOE lines via RNA gel blot. **iOE-TOPO<sup>3</sup>**: amplification of the full-length *AtRGAI* coding sequence to generate the *AtRGAI*-iOE construct. **iOE-screen<sup>3</sup>**: screening of the *AtRGLI*-iOE lines. **Probe<sup>3</sup>**: analysis of the *AtRGLI*-iOE lines via RNA gel blot. **iOE-TOPO<sup>4</sup>**: amplification of the full-length *AtSCL6-II* coding sequence to generate the *AtSCL6-II*-iOE construct. **iOE-screen<sup>4</sup>**: screening of the *AtSCL6-II*-iOE lines. **Probe<sup>4</sup>**: analysis of the *AtSCL6-II*-iOE lines via RNA gel blot. **iOE-TOPO<sup>5</sup>**: amplification of the full-length *AtSCL6-III* coding sequence to generate the *AtSCL6-III*-iOE construct. **iOE-screen<sup>5</sup>**: screening of the *AtSCL6-III*-iOE lines. **Probe<sup>6</sup>**: analysis of the *AtSCL6-III*-iOE lines via RNA gel blot. **iOE-TOPO<sup>6</sup>**: amplification of the full-length *AtSCL6-IV* coding sequence to generate the *AtSCL6-IV*-iOE construct. **iOE-screen<sup>6</sup>**: screening of the *AtSCL6-IV*-iOE lines. **Probe<sup>6</sup>**: analysis of *AtSCL6-IV*-iOE lines via RNA gel blot.

**GGTACC**: *KpnI* restriction site. **GAATTC**: *EcoRI* restriction site. **GAGCTC**: *SacI* restriction site. **GTCGAC**: *SalI* restriction site. **AGATCT**: *BglII* restriction site. Lowercase letters indicate 3 nucleotides, which were added to the primers to increase the efficiency of restriction enzyme activities.

Probe numbers: Each individual probe's number in the legend describes the corresponding number in the table.

iOE-screen numbers: Each individual iOE-screen's number in the legend describes the corresponding number in the table.

iOE-TOPO numbers: Each individual iOE-TOPO's number in the legend describes the corresponding number in the table.

\*: all iOE-TOPO forward primers contain cacc (lowercase letters) at the 5' end of the primer, which is essential for TOPO directional cloning.

**Appendix 2.** Silent mutations within the *PpGRAS7* miR171 binding site. Yellow box: restriction site for *HpaI*. Red nucleotides indicate silent mutations.

5' ATGTGGTGTGACGCGGCTCAA	3' <i>PpGRAS7</i> DNA-miR171 binding site
5' A <b>CGT</b> A <b>GT</b> G <b>TTA</b> A <b>CT</b> CG <b>A</b> CT <b>G</b> AA	3' <i>PpGRAS7</i> DNA-mutated miR171 binding site ( <i>HpaI</i> )
5' AUGUGGUGUUGACGCGGCUCAA	3' <i>PpGRAS7</i> mRNA-miR171 binding site
:   :       X	
3' UACACUAUAACCGCGCCGAGU	5' Pp-miR171a
3'   ACACUAUAACCGCGCCGAGUU	5' Pp-miR171b
X     X :   :     XX   X     X     X	
5' ACGUAGUGUUAACUCGACUGAA	3' <i>PpGRAS7</i> mRNA-mutated miR171 binding site

**Appendix 3.** Silent mutations within the *PpGRAS12* miR171 binding site. Yellow box: restriction site for *pauI*. Red nucleotides indicate silent mutations.

5' AAGCGATATTGGCGCGGCTCAA	3' <i>PpGRAS12</i> DNA-miR171 binding site
5' AAGCGAT <b>TCTA</b> G <b>CGCG</b> <b>CTT</b> AAA	3' <i>PpGRAS12</i> DNA-mutated miR171 binding site ( <i>PauI</i> )
5' AAGCGAUUUGGCGCGGCUCAA	3' <i>PpGRAS12</i> mRNA-miR171 binding site
X   X	
3' UACACUAUAACCGCGCCGAGU	5' Pp-miR171a
3'   ACACUAUAACCGCGCCGAGUU	5' Pp-miR171b
X   X       XX   X           X :   X	
5' AAGCGAUUCUAGCGCGCUUAAA	3' <i>PpGRAS12</i> mRNA-mutated miR171 binding site

**Appendix 4.** *P. patens* homologs of *AtPWD*, *AtGWD*, *AtMEX1*, *AtBAM3*, *AtISA3*, *AtSEX4*, and *AtDPE*.

<i>A. thaliana</i>	<i>P. patens</i> homologs
<i>AtPWD: at5g26570</i> (Kotting <i>et al.</i> , 2005)	<i>PpPWDa: Pp1s3_320V6.1</i>
	<i>PpPWDb: Pp1s34_54V6.1</i>
<i>AtGWD: at1g10760</i> (Kotting <i>et al.</i> , 2005)	<i>PpGWDa: Pp1s8_70V6.1</i>
	<i>PpGWDb: Pp1s74_185V6.1</i>
<i>AtMEX1: at5g17520</i> (Stettler <i>et al.</i> , 2009)	<i>PpMEX1a: Pp1s14_134V6.1</i>
	<i>PpMEX1b: Pp1s268_86V6.1</i>
<i>AtBAM3: at4g17090</i> (Li <i>et al.</i> , 2009)	<i>PpBAM3a: Pp1s317_42V6.1</i>
	<i>PpBAM3b: Pp1s23_21V6.1</i>
	<i>PpBAM3c: Pp1s233_4V6.1</i>
	<i>PpBAM3d: Pp1s106_57V6.1</i>
<i>AtISA3: at4g09020</i> (Ferreira <i>et al.</i> , 2017)	<i>PpISA3: Pp1s25_63V6.1</i>
<i>AtSEX4: at3g52180</i> (Kotting <i>et al.</i> , 2009)	<i>PpSEX4a: Pp1s144_24V6.1</i>
	<i>PpSEX4b: Pp1s14_180V6.1</i>
<i>AtDPE1: at5g64860</i> (Stettler <i>et al.</i> , 2009)	<i>PpDPE1a: Pp1s44_268V6.1</i>
	<i>PpDPE1b: Pp1s8_30V6.1</i>

**Appendix 5.** The subset of genes involved in photosynthesis, cell growth, cell division, and stress response.

<i>A. thaliana</i>	<i>P. patens</i> homologs	Involvement
<i>AtAGL1: at3g58780</i> (O'Maoileidigh <i>et al.</i> , 2018)	* <i>PpAGL1: Pp1s118_209V6.2</i>	Cell division
<i>AtARF5: at1g19850</i> (Liu <i>et al.</i> , 2018)	<i>PpARF5: Pp1s65_227V6.1</i>	Response to auxin-meristem development
<i>AtARR15: at1g74890</i> (Leibfried <i>et al.</i> , 2005)	<i>PpARR15: Pp1s94_88V2.1</i>	Response to cytokinin
<i>AtATML1: at4g21750</i> (Katagiri <i>et al.</i> , 2016)	<i>PpATML1: Pp1s209_10V6.1</i>	Cell growth and differentiation
<i>AtAtpA: atcg00120</i> (Lamkemeyer <i>et al.</i> , 2006)	<i>PpAtpA: NC_005087.1:c63541-6201</i>	Photosynthesis
<i>AtBRK1: at2g22640</i> (Perroud & Quatrano, 2008)	<i>PpBRK1: Pp1s35_157V6.1</i>	Cell morphogenesis
<i>AtCYCD1: at1g70210</i> (Wang <i>et al.</i> , 2004)	* <i>PpCYCD1: Pp1s359_22V6.1</i>	Cell cycle control
<i>AtChIL: at5g05270</i> (Soubeyrand <i>et al.</i> , 2018)	<i>PpChIL: NC_005087.1: c113204-112317</i>	Photosynthesis
<i>AtCLV1: at1g75820</i> (Nimchuk, 2017)	* <i>PpCLV1a: Pp1s5_68V6.1</i>	Cell differentiation
<i>AtCLV1: at1g75820</i> (Nimchuk, 2017)	* <i>PpCLV1b: Pp1s14_447V6.1</i>	Cell differentiation
<i>AtCOR47: at1g20440</i> (Wu <i>et al.</i> , 2017)	<i>PpCOR47: Pp1s421_9V2.1</i>	Stress response
<i>AtCRN: at5g13290</i> (Muller <i>et al.</i> , 2008)	<i>PpCRN: Pp1s145_89V6.1</i>	Meristem maintenance
<i>AtGH3.5: at4g27260</i> (Staswick <i>et al.</i> , 2005)	<i>PpGH3: Pp1s323_82V6.1</i>	Cell differentiation

<i>AtGRP23: at1g10270</i> (Busch <i>et al.</i> , 2010)	<i>PpGRP23: Pp1s219_51V6.1</i>	Cell division
<i>AtHSF3: at5g16820</i> (Guan <i>et al.</i> , 2013)	* <i>PpHSF3: Pp1s249_84V6.1</i>	Stress response
<i>AtHXX1: at4g29130</i> (Rottmann <i>et al.</i> , 2018)	<i>PpHXX1: Pp1s150_124V6.1</i>	Cellular glucose homeostasis, programmed cell death
<i>AtIAA27: at4g29080</i> (Overvoorde <i>et al.</i> , 2005)	<i>PpIAA27: Pp1s184_21V6.1</i>	Response to auxin
<i>AtJAZ5: at1g17380</i> (Busch <i>et al.</i> , 2010)	<i>PpJAZ5: Pp1s15_170V6.1</i>	Regulation of defense response
<i>AtLHCb1: at1g29910</i> (Sun & Ni, 2011)	<i>PpLHCb1: AW126861</i>	Photosynthesis
<i>AtLHCb2: at2g05070</i> (Xu <i>et al.</i> , 2012)	* <i>PpLHCb2: AW126861</i>	Photosynthesis
<i>AtNCED: at1g04010</i> (Bouvier-Nave <i>et al.</i> , 2010)	* <i>PpNCED: Pp1s69_201V6.1</i>	Leaf senescence
<i>AtNdhA: atcg01100</i> (Zhang <i>et al.</i> , 2015)	<i>PpNdhA: Pp3c11_850.v3.1</i>	Photosynthesis
<i>AtPEP: at4g26000</i> (Ripoll <i>et al.</i> , 2006)	<i>PpPEP: Pp1s275_2V6.1</i>	Shoot system development
<i>AtPetA: atcg00540</i> (Liu <i>et al.</i> , 2012)	<i>PpPetA: NC_005087.1: c20179-19220</i>	Photosynthesis
<i>AtPpPHABULOSA: at2g34710</i> (Sebastian <i>et al.</i> , 2015)	<i>PpPHABULOSA: Pp1s188_95V6.1</i>	Meristem initiation
<i>AtPORA: at5g54190</i> (Zhang <i>et al.</i> , 2017)	* <i>PpPORAa: Pp1s146_112V6.1</i>	Chlorophyll biosynthesis
<i>AtPORA: at5g54190e</i> (Zhang <i>et al.</i> , 2017)	* <i>PpPORA b: Pp1s108_171V6.1</i>	Chlorophyll biosynthesis
<i>AtPsaA: atcg00350</i> (Wang <i>et al.</i> , 2016)	* <i>PpPsaA: NC_005087.1: 35758-38010</i>	Photosynthesis
<i>AtPsaB: atcg00340</i>	* <i>PpPsaB: NC_005087.1: 38036-40240</i>	Photosynthesis

(Liu <i>et al.</i> , 2012)		
<i>AtPsaC: atcg01060</i> (Liu <i>et al.</i> , 2012)	<i>*PpPsaC: NC_005087.1: c100617100372</i>	Photosynthesis
<i>AtPsbA: atcg00020</i> (Wang <i>et al.</i> , 2016)	<i>*PpPsbA: NC_005087.1: c54280-53219</i>	Photosynthesis
<i>AtPsbD: atcg00270</i> (Liu <i>et al.</i> , 2012)	<i>*PpPsbD: PpapaCp044</i>	Photosynthesis
<i>AtPsbM: atcg00220</i> (Cho <i>et al.</i> , 2009)	<i>*PpPsbM: NC_005087.1: 4306-4410</i>	Photosynthesis
<i>AtPUB4: at2g23140</i> (Kinoshita <i>et al.</i> , 2015)	<i>PpPUB4: Pp1s307_2V6.2</i>	Cell division
<i>Atprbc1a: at1g67090</i> (Kwon <i>et al.</i> , 2010)	<i>*Pprbcs: Pp1s459_1V6.1</i>	Photosynthesis
<i>AtSTM: at1g62360</i> (Roth <i>et al.</i> , 2018)	<i>PpSTM: Pp1s235_27V6.1</i>	The stem cell population maintenance
<i>AtTCP9: at2g45680</i> (Zhou <i>et al.</i> , 2015)	<i>PpTCP9a: Pp1s446_21V6.1</i>	Cell division
<i>AtTCP9: at245680</i> (Zhou <i>et al.</i> , 2015)	<i>PpTCP9b: Pp1s356_40V6.1</i>	Cell division
<i>AtTIC110: at1g06950</i> (Flores-Perez <i>et al.</i> , 2016)	<i>PpTIC110: Pp1s509_22V6.2</i>	Chloroplast organization
<i>AtTIP2;2: at4g17340</i> (Zhou <i>et al.</i> , 2015)	<i>*PpTIP2;2a: Pp1s101_226V6.1</i>	Stress response
<i>AtTIP2;2: at4g17340</i> (Zhou <i>et al.</i> , 2015)	<i>*PpTIP2;2b: Pp1s156_153V6.1</i>	Stress response
<i>AtTOC75: at3g46740</i> (Baldwin <i>et al.</i> , 2005)	<i>PpTOC75: Pp1s2_62V6.1</i>	Chloroplast organization
<i>AtTPL: at1g15750</i> (Busch <i>et al.</i> , 2010)	<i>PpTPLa: Pp1s99_260V6.1</i>	Shoot apical meristem specification
<i>AtTPL: at1g15750</i> (Busch <i>et al.</i> , 2010)	<i>PpTPLb: Pp1s316_34V6.1</i>	Shoot apical meristem specification

<i>AtWOX13: at4g35550</i> (Romera-Branchat <i>et al.</i> , 2013)	<i>PpWOX13: Pp1s224_106V6.1</i>	Cell division
<i>AtHSC70-1: at4g24280</i> (Su & Li, 2008)	<i>PpHSP70a: Pp1s6_146V6.1</i>	Stress response
<i>AtHSC70-1: at4g24280</i> (Su & Li, 2008)	<i>PpHSP70b: Pp1s153_153V6.1</i>	Stress response
<i>AtHSC70-1: at4g24280</i> (Su & Li, 2008)	<i>PpHSP70c: Pp1s115_168V6.1</i>	Stress response

The Asterisk (\*) shows differentially regulated genes in response to an elevated level of *PpGRAS7* (Fig. 14a). No differences in expression levels between genes without asterisk and WT were observed in response to an elevated level of *PpGRAS7*.

**Appendix 6.** qRT-PCR primers. The specificity of primers was confirmed with the Primer-BLAST. Primers were ordered from Sigma-Aldrich (Deisenhofen, Germany).

Gene ID	Accession No	Forward primers	Reverse primers	Amplicon Size (bp)
<i>PpAGL1+</i>	<i>Pp1s118_209V6.2</i>	GCGCAGGAGCTGTCTGGTGG	CCCACCCCTTCGCCGTGTCG	123
<i>PpAGO1a+</i>	<i>Pp1s28_182V6.1</i>	CGAGCAGATTTGCATCATCTTG GGC	GTCACCTCCACTTTGACTCCGCGGA	389
<i>PpAGO1b+</i>	<i>Pp1s7_194V6.1</i>	CCGAGCAGATTTGGATCATCTC AGACG	AGCATCGGATAGACCACGTGTCAC G	340
<i>PpAGO1c+</i>	<i>Pp1s173_134V6.1</i>	TTCACCCGATCTGGGCACGC	TCCACCTTCACCCCACGGAGG	246
<i>PpARF5+</i>	<i>Pp1s65_227V6.1</i>	GGCCGAACCTCACCTTGGGTGC	CACCTGAGGCTCGTGGCCAAT	129
<i>PpARR15+</i>	<i>Pp1s94_88V2.1</i>	GCCGGGGATGACTGGATATGAC CT	TCAGCACCTCTGCAAGGCAA	135
<i>PpATG5</i>	<i>Pp1s227_54V6.1</i>	ATGGTTACCTACCGTTGTTG	TTCCAAGGTCTTTCAAATTC	169
<i>PpATG7</i>	<i>Pp1s73_159V6.1</i>	CTGATGGCAGTATAAAATCACA A	CGGAAGATTGAAGGATCATAAA	148
<i>PpATML1+</i>	<i>Pp1s209_10V6.1</i>	AGGGCGTGTGGGCAGTGGTA	CCACGCACGTCACCTTCGCA	141
<i>PpAtpA+</i>	<i>NC_005087.1:c635 41-6201</i>	GCGCCTGGTATTATTTCAAGAC GTT	ACTCACGTTGACCACGTCCAA	100
<i>PpBAM3a</i>	<i>Pp1s317_42V6.1</i>	CGGATTAGAGGACTTCGCCGT	ACTATTGCCCTCGTTCGCTGT	132
<i>PpBAM3b</i>	<i>Pp1s23_21V6.1</i>	GCCACATGGAGGAAGGACGA	ACACGCTTACGGATCAGTGGT	132
<i>PpBAM3c</i>	<i>Pp1s233_4V6.1</i>	GCGGCAATGTTCTGACGGAC	CTGCGAGCATGATACGCCCTG	110
<i>PpBAM3d</i>	<i>Pp1s106_57V6.1</i>	CGTCACATGGAGGAGGGTCG	ACCAAGGGTCCAGTGGCTTT	89
<i>PpBRK1+</i>	<i>Pp1s35_157V6.1</i>	AGACGGGCTCGCCAACATGG	CCGGACGTTTCAGCGACAGGG	118
<i>PpCYCD1+</i>	<i>Pp1s359_22V6.1</i>	GCCCTTTGCTCCTCGTCCACTC	GTCAACAGGCTCGGGCAGC	147
<i>PpChIL+</i>	<i>NC_005087.1:c113 204-112317</i>	CCGGAGCTGGTTGTGGAGGC	AATGGAGCAGCAAACCCACCA	136
<i>PpCLV1a+</i>	<i>Pp1s5_68V6.1</i>	TGGTTTGTGTATGAGATGGTCTG GA	TCGGCTGGAGGTGCAAAACGC	127
<i>PpCLV1b+</i>	<i>Pp1s14_447V6.1</i>	GCTCCTACGGTTACATCGCGCC	CCCCGTCGCCAAACTCGCTC	138
<i>PpCOR47+</i>	<i>Pp1s421_9V2.1</i>	CGCCCTGATGTGCCTTCGAGC	AGCCAGTCAGCCGCTCAGGA	118

<i>PpCRN+</i>	<i>Pp1s145_89V6.1</i>	GACCCTCAGCAACGCCCAA	TTCTGCGGGAACAGGGTCGG	81
<i>PpDPE1a</i>	<i>Pp1s44_268V6.1</i>	CCATGCACGGTAAGTGGCAG	TTCTTGCGAAGCGAGACGAC	133
<i>PpDPE1b</i>	<i>Pp1s8_30V6.1</i>	ATACTGGGCTGTTCGATGCGG	CGCCAACACGTCAGGGGTTA	154
<i>PpE3UL+</i>	<i>Pp1s116_97V6.1</i>	AGGAAGGGCAGAAGGAGAACC A	TTGACAAAGGTTGAAGCCACAAAC A	94
<i>PpEfla</i>	<i>Pp1s7_445V6</i>	GTACCTCCCAGGCTGACTGC	GTGCTCACGGGTCTGTCCAT	95
<i>PpGH3.5+</i>	<i>Pp1s323_82V6.1</i>	CACCATCACGCCGAACCCCG	TGCCACGAGGGATGGGTTCGG	90
<i>PpGRAS12</i>	<i>Pp1s205_1V6.1</i>	TGGTCTTCCTTCCAGCAGCG	ACGAGTCCACGCCAGCCTCA	98
<i>PpGRAS7</i>	<i>Pp1s130_63V6.1</i>	CGTCCCGCAGCACCAAGCTTT	GCGGCGACAATGAGTTCGGGT	98
<i>PpGRP23+</i>	<i>Pp1s219_51V6.1</i>	TGGACGATGCCTGTGGGCTACT	TGCTTCGTCCACGTTGCCCC	116
<i>PpGWDa</i>	<i>Pp1s8_70V6.1</i>	GCGGAGGTAGCTAGTGCAT	GCGCCGACCATATCTGGAGT	131
<i>PpGWDb</i>	<i>Pp1s74_185V6.1</i>	CAGGCCGTGCCCTTAGTTTTG	AAGACCAGCTCCTGCATAGCC	161
<i>PpH3FS+</i>	<i>Pp1s249_84V6.1</i>	CGCGAGCCGACAATCAGGTGT	AGGCGAGGGTATGTGCATGTCAG	124
<i>PpHSP70a +</i>	<i>Pp1s6_146V6.1</i>	GGGAAGCAGCACTGGCCCTG	TCGGTCGAAGGGGAACGTGGT	119
<i>PpHXK1+</i>	<i>Pp1s150_124V6.1</i>	GGGTGATGGAGCTGGGCGTCT	AAGGATGGAAGAGAGAAAGCGCG TC	104
<i>PpIAA27+</i>	<i>Pp1s184_21V6.1</i>	AAGCCGCATGGTCCACGTCA	GGGCGCTGCAATCTTCGGTG	126
<i>PpISA3</i>	<i>Pp1s25_63V6.1</i>	AACAGCTGGAGTCGAAGCGT	CGGCTCTCTGGATTTCGACCA	151
<i>PpJAZ5+</i>	<i>Pp1s15_170V6.1</i>	GCGACGAGCACCAACAGCCA	AGGACCACTAAAATCCGCACCCA	119
<i>PpLHCb1+</i>	<i>AW126856</i>	ATGCGCGTCTACTGCCCTGG	CGGTCTTGCGCATGGTGACG	104
<i>PpLHCb2+</i>	<i>AW126861</i>	CCCGGAGGCTCATTCGACCC	ACATGGCCAATCGCCCGTTCT	81
<i>PpMEX1a</i>	<i>Pp1s14_134V6.1</i>	CTCCCAGGCACCGTTTTTGG	GCGCTACAGGACCCACATA	145
<i>PpMEX1b</i>	<i>Pp1s268_86V6.1</i>	TGCCTCATGGTTTGGTTCGGT	TCCAATAGCACTTCGGGTTCT	121
<i>PpMIR171a+</i>	-	CGTGGTGGACGGGCAGGATT	CGGCACTCCTGGTACTTCAGGC	147
<i>PpMIR171b+</i>	-	ACGAACAGCAGGAATCGCCTAA GT	TTATTGGGCCCGCTCAATCAGATG T	130
<i>PpNCED+</i>	<i>Pp1s69_201V6.1</i>	TTCTCGTGGGAGAGGGAGCA	TGCAAGGCTCTCATTGCGACT	133
<i>PpNdhA+</i>	<i>Pp3c11_850.V3.1</i>	AGGTGGTCTTCGAGCGGCAG	CCATCCCCAAAAGCCATATTTTGC C	145
<i>PpPEP+</i>	<i>Pp1s275_2V6.1</i>	GTCAGGGGCGGGAGAGGTGT	TGCCGCTCCCAATCATGCGG	129

<i>PpPetA+</i>	<i>NC_005087.1: c20179-19220</i>	ATTGTACCGCAGGACCAGAAC TT	ACCAAAGCCACCCACATTAGGGTT A	96
<i>PpPHABULOSA+</i>	<i>PpIs188_95V6.1</i>	CTGTACTCTCTGGGTGGCGGC	CCGCCACTCTGACCGATGT	112
<i>PpPORAa+</i>	<i>PpIs146_112V6.1</i>	ACAGGGCTCTCCCGAGCA	TGCGCCAGTCTCCTGCCAGA	113
<i>PpPORA b+</i>	<i>PpIs108_171V6.1</i>	TCCCAGGAAGCTAGCGATGCG	CAAGTCGGCAACTGGGGCCAA	112
<i>PpPsaA+</i>	<i>NC_005087.1: 35758-38010</i>	TCTTTAGCTTGGGCAGGACACC A	TCTTTAGGATCCACCCGGCATCT	80
<i>PpPsaB+</i>	<i>NC_005087.1: 38036-40240</i>	TGGCTGACTGATATGGCTCATC ACC	CCCACGGCCTAAACGACCTCCT	150
<i>PpPsaC+</i>	<i>NC_005087.1:c100 617100372</i>	AATGGTACCTGGGATGGATGC	GCAGATTCACATCTTTTGCAGCCT	90
<i>PpPsbA+</i>	<i>NC_005087.1: c54280-53219</i>	GCTTGCTACATGGGTCTGTGAGT GGG	AGCAGTAGCAGCCGCAACAGGA	99
<i>PpPsbD+</i>	<i>PhpapaCp044</i>	TGGGGTCCAGAAGCACAAGGA	AGCAAGCTCAAATTGGCGCAACA	123
<i>PpPsbM+</i>	<i>NC_005087.1: 4306-4410</i>	GCATTGTTCAATTTAATCCCCAC AGCT	TTAACTACCCTGACTAGCTGTTTGT A	72
<i>PpPUB4+</i>	<i>PpIs307_2V6.2</i>	ACGAATAGCCACAGGCACCGC	CCACCGTGTCGTTGCTCCCG	143
<i>PpPWDa</i>	<i>PpIs3_320V6.1</i>	GGTGAAACGCTGGCTTCTGG	GGCTCCACCCTTGACCATCA	126
<i>PpPWDb</i>	<i>PpIs34_54V6.1</i>	CCGCTAGAAGGTGGGGCATT	CTCGCACTCGACCGGACTAT	146
<i>Pprbc s+</i>	<i>PpIs459_1V6.1</i>	GACCTTCTCGTACCTGCCCCC	GCACCGACTTACCGTGTGAA	112
<i>PpSAG12</i>	<i>PpIs19_362V6.1</i>	ATCTGTTGAGGGTATCACG	AGAATGAAATCGAAGGCGTA	128
<i>PpSAG13</i>	<i>PpIs457_13V6.1</i>	CTCTCGACATCCTTGTC AAT	ACTCCAAATTGGTTGACATC	102
<i>PpSAG18</i>	<i>PpIs74_138V6.1</i>	TTTCGGGTCAGCATACTQATC	ATTCGCTCGATGATAAACAC	114
<i>PpSEN1</i>	<i>PpIs81_135V6.1</i>	CTTCATTTCTGTAAGAAGTGAC C	CTGTAATATATAACCTCGTGGGC	153
<i>PpSEX4a</i>	<i>PpIs144_24V6.1</i>	TGTCGTAGACGGCGTTTGG A	TCCCGCAATGTTCTGGTCTGT	129
<i>PpSEX4b</i>	<i>PpIs14_180V6.1</i>	CCTCTCCAGACCACGCAGAT	TCATCCCCAGTTCATGCCTGT	154
<i>PpSIR2+</i>	<i>PpIs145_60V6.1</i>	AGCAATCGGACAACCTCCAAGGC CA	TGCTGCAGCCATGGCCCTT	136
<i>PpSTM+</i>	<i>PpIs235_27V6.1</i>	TGGCACCGACCCTGCACTCG	AGTGGCCGCAGATGCCTTCCA	146
<i>PpTCP9a+</i>	<i>PpIs446_21V6.1</i>	GGGGGTGAGTGACAGCAGAGC	TGCTGGAACCCGGCCATCAG	102
<i>PpTCP9b+</i>	<i>PpIs356_40V6.1</i>	AGCTGGTGTGGGGTAAGCACGG	ACAAGCAGGACTTCAACACGCGG	92

<b><i>PpTIC110+</i></b>	<i>Pp1s509_22V6.2</i>	CCCAAGCAAAGAGCCTACAGGA GA	ACCTCCTCCGGTTCTGTCCCC	147
<b><i>PpTIP2;2a+</i></b>	<i>Pp1s101_226V6.1</i>	TCCCATGTCTGCGGTGCTGA	CGGTGAAGCCGATGGCCAAG	128
<b><i>PpTIP2;2b+</i></b>	<i>Pp1s156_153V6.1</i>	CCGTGGTGGCCTGGGATTTC	GCCGGGGACATGAATACGCC	106
<b><i>PpTOC75+</i></b>	<i>Pp1s2_62V6.1</i>	AGCCGAGTATGCCAGGGACTG	TGCCCCACCCCACGCATGTA	145
<b><i>PpTPLa+</i></b>	<i>Pp1s99_260V6.1</i>	TGCAAGACAGTGGAGATGGGTC	GCTACACGGCCTTTCCTCC	135
<b><i>PpTPLb+</i></b>	<i>Pp1s316_34V6.1</i>	TGCTTGCTGTCACTACCTCGGAT	TGCATTTCCGACTGGCGGCT	149
<b><i>PpTPTa+</i></b>	<i>Pp1s450_17V6.1</i>	TCTTTTCCAGGCGTGGTGGT	GTTCTCAGGCACACTGTTTCACA	138
<b><i>PpWOX13+</i></b>	<i>Pp1s224_106V6.1</i>	TGCTCCGATGTGGTGTGCC	ACACCCAAGAGAGCAGCGCAA	95
<b><i>Cytokinin related+</i></b>	<i>Pp1s536_11V6.1</i>	CGCCGCTAGTGC GACTTGCT	TGTCGCCTCAATTTTGTGTCGCGC	144
<b><i>Cytokinin related+</i></b>	<i>Pp1s69_95V6.1</i>	ACCGCACCATGAGCACTCCA	CGCCCCATCCCGTAGTCTGC	99
<b><i>ABA related+</i></b>	<i>Pp1s234_91V2.1</i>	AGCGACGTGACCGCCAAAC	CACCTTGTCACCACGCCCG	141
<b><i>PpHSB70b+</i></b>	<i>Pp1s153_153V6.1</i>	CAGCACGCGCAGGAATGCGT	CACCGGACTTGGCCCTCAGC	86
<b><i>PpHSB70c+</i></b>	<i>Pp1s115_168V6.1</i>	GCAGGACAGGGAGTGTCT	TCCCTCCGAAGAAGGCTCT	101

Genes with a red plus were used for the expression analysis by qRT-PCR (see 3.1.6). Only 19 genes (Fig. 14a) were differentially regulated in response to an elevated level of *PpGRAS7*. Genes, which were not differentially regulated (not present in Fig. 14a) in response to an elevated level of *PpGRAS7* have not been mentioned in the main text.

#### Gene's abbreviations:

<b><i>AGL1</i></b>	<i>AGAMOUS-LIKE 1</i>
<b><i>AGO1</i></b>	<i>ARGONAUTE PROTEIN 1</i>
<b><i>ARF5</i></b>	<i>AUXIN RESPONSE FACTOR 5</i>
<b><i>ARR15</i></b>	<i>RESPONSE REGULATOR 15</i>
<b><i>ATG5</i></b>	<i>AUTOPHAGY PROTEIN 5</i>
<b><i>ATG7</i></b>	<i>AUTOPHAGY PROTEIN 7</i>
<b><i>ATML1</i></b>	Homeobox-leucine zipper protein, <i>MERISTEM LAYER 1</i>
<b><i>AtpA</i></b>	<i>ATP synthase subunit alpha</i>
<b><i>BAM</i></b>	<i>β-AMYLASE</i>
<b><i>CYCD1</i></b>	<i>CYCLIN-D1</i>
<b><i>CLV</i></b>	<i>CLAVATA</i>
<b><i>DPE1</i></b>	<i>DISPROPORTIONATING ENZYME 1</i>
<b><i>Ef1α</i></b>	<i>ELONGATION FACTOR 1α</i>
<b><i>GRAS12</i></b>	<i>GRAS domain transcription factor gene in P. patens (Pp1s205_1V6.1)</i>
<b><i>GRAS7</i></b>	<i>GRAS domain transcription factor gene in P. patens (Pp1S130_63V6.1)</i>
<b><i>GRP23</i></b>	<i>GLUTAMINE-RICH PROTEIN 23</i>
<b><i>HSF3</i></b>	<i>HEAT SHOCK FACTOR PROTEIN 3</i>
<b><i>HSP70</i></b>	<i>HEAT SHOCK PROTEIN 70</i>
<b><i>HXK1</i></b>	<i>HEXOKINASE 1</i>
<b><i>ISA3</i></b>	<i>ISOAMYLASE 3</i>
<b><i>JAZ5</i></b>	<i>JASMONATE-ZIM-DOMAIN PROTEIN 5</i>

<b>LHCA</b>	<i>LIGHT HARVESTING COMPLEX A</i>
<b>LHCB</b>	<i>LIGHT HARVESTING COMPLEX B</i>
<b>MEX1</b>	<i>MALTOSE EXCESS PROTEIN 1</i>
<b>NCED</b>	<i>9-CIS-EPOXYCAROTENOID DIOXYGENASE</i>
<b>PetA</b>	<i>Photosynthetic electron transfer A</i>
<b>POR</b>	<i>PROTOCHLOROPHYLLIDE OXIDOREDUCTASE</i>
<b>PsaA</b>	<i>Photosystem I P700 chlorophyll a apoprotein A1</i>
<b>PsaB</b>	<i>Photosystem I P700 chlorophyll a apoprotein A2</i>
<b>PsaC</b>	<i>Photosystem I iron-sulfur center</i>
<b>PsbA</b>	<i>Photosystem II protein D1</i>
<b>PsbD</b>	<i>Photosystem II protein D2</i>
<b>PsbM</b>	<i>Photosystem II reaction center protein M</i>
<b>PUB4</b>	<i>U-box domain-containing protein 4</i>
<b>PWD</b>	<i>PHOSPHOGLUCAN WATER DIKINASE</i>
<b>rbcS</b>	<i>ribulose biphosphate carboxylase small chain</i>
<b>SAG</b>	<i>SENESCENCE ASSOCIATED GENE</i>
<b>SEX4</b>	<i>STARCH-EXCESS 4</i>
<b>SIN1</b>	<i>SENESCENCE 1</i>
<b>SIR2</b>	<i>NAD-dependent histone deacetylase, SIR2</i>
<b>STM</b>	<i>SHOOT MERISTEMLESS</i>
<b>TCP9</b>	<i>TCP DOMAIN PROTEIN 9</i>
<b>TIC110</b>	<i>TRANSLOCON AT THE INNER ENVELOPE MEMBRANE OF CHLOROPLASTS 110</i>
<b>TIP2;2</b>	<i>TONOPLAST INTRINSIC PROTEIN 2;2</i>
<b>TOC75</b>	<i>TRANSLOCON AT THE OUTER ENVELOPE MEMBRANE OF CHLOROPLASTS 75</i>
<b>TPL</b>	<i>TOPLESS PROTEIN</i>
<b>TPT</b>	<i>TRIOSE PHOSPHATE/PHOSPHATE TRANSLOCATOR</i>
<b>WOX</b>	<i>WUSCHEL-RELATED HOMEODOMAIN</i>
<b>GH3</b>	<i>Auxin-responsive GH3</i>
<b>E3UL</b>	<i>E3 UBIQUITIN LIGASE</i>
<b>CRN</b>	<i>CORYNE</i>
<b>COR47</b>	<i>COLD-REGULATED 47</i>
<b>BRK1</b>	<i>BRICK1</i>
<b>PHABULOSA</b>	<i>A. thaliana HOMEODOMAIN PROTEIN 14</i>
<b>IAA27</b>	<i>Auxin-responsive protein IAA27</i>
<b>PEP</b>	<i>PEPPER</i>
<b>NdhA</b>	<i>NADH dehydrogenase subunit 1</i>

## Appendix 7. Lines specifications.

Lines were used in this study:

$\Delta PpGRAS12$  # 34 = Line 1 (was generated by Christoph Strotbek)

$\Delta PpGRAS12$  # 60 = Line 2 (was generated by Christoph Strotbek)

$\Delta PpGRAS7$  # 15 = Line 1 (was generated by M. Asif Arif)

$\Delta PpGRAS7$  # 19 = Line 2 (was generated by M. Asif Arif)

$PpGRAS7$ -iOE # 17 = Line 1

$PpGRAS7$ -iOE # 19 = Line 2

$PpGRAS12$ -iOE # 82 = Line 1 (was generated by Christoph Strotbek)

$PpGRAS12$ -iOE # 98 = Line 2 (was generated by Christoph Strotbek)

$PpGRAS12::GUS$  # 3 = Line 1

$PpGRAS12::GUS$  # 61 = Line 2

$mPpGRAS12::GUS$  # 5 = Line 1

$mPpGRAS12::GUS$  # 40 = Line 2

$AtRGAI$ -iOE # 8 = Line 1

$AtRGAI$ -iOE # 15 = Line 2

$AtRGL1$ -iOE # 10 = Line 1

$AtRGL1$ -iOE # 12 = Line 2

$AtSCL6-II$ -iOE # 106 = Line 1

$AtSCL6-II$ -iOE # 107 = Line 2

$AtSCL6-III$ -iOE # 11 = Line 1

$AtSCL6-III$ -iOE # 21 = Line 2

$AtSCL6-IV$ -iOE # 5 = Line 1

$AtSCL6-IV$ -iOE # 12 = Line 2